GENETIC DETERMINANTS OF GENOME STABILITY AND CROSSOVER DISTRIBUTION IN THE NEMATODE *CAENORHABDITIS ELEGANS*

by

George Chih Hsuen Chung

B.Sc., Simon Fraser University, 2008 (Honours)

A THESIS SUBMITTED IN PARTIAL FULFILLMENT OF

THE REQUIREMENTS FOR THE DEGREE OF

DOCTOR OF PHILOSOPHY

in

THE FACULTY OF GRADUATE AND POSTDOCTORAL STUDIES

(Medical Genetics)

THE UNIVERSITY OF BRITISH COLUMBIA

(Vancouver)

January 2016

Abstract

Guanine-rich DNA sequences can form secondary structures *in vitro*. *In vivo*, helicases are responsible for undoing these structures during DNA replication. In the absence of helicase function, these structures may be unrepaired and undergo mutagenic end-joining processes that generate DNA sequence deletions. In *Caenrhabditis elegans*, a majority of these guanine-rich structures are resolved by the helicase DOG-1. This report presents genetic evidence that a related helicase, CHL-1, acts as a backup mechanism through which guanine-rich structures may be bypassed or resolved in the absence of DOG-1 function.

In the absence of CHL-1 function, DNA double-strand breaks accumulate and are repaired inefficiently in the meiotic germline. In an attempt to generate a translational fusion tag for *chl-1* in order to characterize the localization of the CHL-1 helicase in the germline, I generated an unexpected knock-out allele of *chl-1* using the emerging CRISPR-Cas9 technology adapted for *C. elegans*. Taking lessons learned from this approach, I used the CRISPR-Cas9 reagents to generate new alleles of *y18h1a.7*, a candidate coding sequence for the *rec-1* gene.

Classical genetic studies showed that a mutation in *rec-1* altered the meiotic recombination pattern across the autosomes in *C. elegans*. The new alleles of *y18h1a.7* enabled complementation testing and confirmed that the coding sequence for *rec-1* is *y18h1a.7* on Chromosome I. Through a synteny analysis of six other *Caenorhabditis* genomes in the region surrounding *rec-1*, I identified putative *rec-1* orthologues which have limited sequence similarity to *rec-1*. Furthermore, the similarity of these *rec-1* orthologues to *C. elegans him-5* suggests that *him-5* is a paralogue of *rec-1*. By genetic analysis, I show that *rec-1* and *him-5* function in partial redundancy to initiate meiotic recombination events. Thus, *rec-1* and *him-5* define a new class of early meiosis genes in several *Caenorhabditis* species.

In summary, this thesis brings together the findings on *chl-1* and *rec-1* by highlighting their respective roles in the meiotic germline of *Caneorhabditis elegans*.

Preface

A version of Chapter 2 has been published in *DNA Repair* (Chung et al. 2011). I designed and carried out all the experiments in the report.

A version of Chapter 4 has been published in *Genes and Development* (Chung et al. 2015). This version was the result of the collaboration among four research groups – the lab of Ann M. Rose, the lab of Judith Yanowitz (Magee-Women's Institute), the lab of Chris P. Ponting (Oxford) and the lab of Simon J. Boulton (Crick Institute). I am responsible for drafting the manuscript for this report. Contribution in the writing and the revision of the *Genes and Development* version also came from Ann M. Rose, Judith Yanowitz, Chris P. Ponting and Simon J. Boulton, but for this thesis, the text has been altered to include only experimental contributions from me. Experimentally, I was responsible for the cloning of *rec-1*, the generation of new alleles of *rec-1* by CRISPR-Cas9, the analysis of double-strand break formation in *rec-1* and *him-5* mutants, and the construction of several *rec-1* and *him-5* double/triple mutant strains. The biochemical characterization of the REC-1 recombinant protein (presented in *Genes and Development*) was carried out in the Boulton laboratory and thus are not presented in this thesis. This includes the assays for phosphorylation on the recombinant REC-1 protein and the peptide array mapping of putative phosphorylation sites; however, recombination assays on the potential phosphomutant and phosphomimic alleles of *rec-1* were done in the Rose lab, so these results are presented in this thesis.

Additionally for Chapter 4, I was responsible for the phylogenetic analysis of *rec-1* and the syntenic region, and through this I identified the conserved residues of the REC-1 orthologues in other *Caenorhabditis* species. The Ponting lab was responsible for identifying *him-5* as a putative paralogue of *rec-1*. As this paralogy links *rec-1* to *him-5*, I have chosen to

retain this portion of the *Genes and Development* report in this thesis. Results from the viability assays of *rec-1; him-5* double mutants from the *Genes and Development* report, including irradiation experiments, were done by the Yanowitz lab, so these are not presented here.

Table of contents

List of tables

List of figures

List of abbreviations

BRC-2: orthologue of mammalian BRCA2

BRD-1: orthologue of mammalian BARD1

ChIP: chromatin immunoprecipitation

chl-1: orthologue of budding yeast *CHL1*

CO: crossover

COM-1: orthologue of budding yeast Com1, also known as Sae2

COSA-1: gene product of a crossover site associated gene

CRISPR: clustered regularly-interspaced short palindromic repeats

Cas9: CRISPR-associated protein 9

D-loop: displacement loop

DNA: deoxyribonucleic acid

dog-1: gene, mutant phenotype = deletion of guanine-rich DNA

DSB: double-strand break

FANCJ: Fanconi anemia complementation group J

FCD-2: orthologue of human FANCD2

GEN-1: orthologue of human GEN1

G-quadruplex: guanine-quadruplex (DNA)

G-tract: guanine-rich tract (of DNA)

H3K4: histone H3 lysine 4

H3K9: histone H3 lysine 9

HA: haemagglutinin

him: gene class, mutant phenotype = high incidence of males, some gene products listed below

HIM-1: a cohesin subunit

HIM-5: a meiotic protein

HIM-6: orthologue of mammalian BLM

HIM-8: a zinc finger required for X chromosome pairing

HIM-9/XPF-1: orthologue of mammalian XPF

HIM-18/SLX-4: orthologue of budding yeast Slx4

HJ/dHJ: Holliday junction/double Holliday junction

HORMA: protein domain defined by Hop1, Rev7 and Mad2

LEM-2: lamina-associated polypeptide–emerin–MAN1 domain protein 2

modENCODE: model organism encyclopedia of DNA elements database

MRE-11*:* orthologue of budding yeast Mre11

MSH-4/5: MutS homologue 4/5

MUS-81: orthologue of budding yeast Mus81

NCO: non-crossover

NHEJ: non-homologous end-joining

PCR: polymerase chain reaction

POLH-1, POLK-1 and POLQ-1: orthologues of DNA polymerases η, κ and θ

PRDM9/Prdm9 - mammalian PR domain protein 9

rad: gene class, mutant phenotype = radiation sensitivity, some gene products listed below

RAD-50, RAD-51 and RAD-54: orthologues of budding yeast Rad50, Rad51 and Rad54

rec-1: gene, mutant phenotype = recombination abnormal

RFS-1: rad fifty-one (RAD-51)-like, short

RTEL-1: orthologue of mammalian regulator of telomere length (RTEL1)

SC: synaptonemal complex

SLX-1: orthologue of budding yeast Slx1

*smc-3/*SMC-3: orthologue of budding yeast *SMC3/*Smc3

*spo-11/*SPO-11: orthologue of budding yeast *SPO11/*Spo11

syp: gene class, mutant phenotype = synapsis abnormal

SYP-1, SYP-2, SYP-3, and SYP-4 are synaptonemal complex components

TMEJ: theta-mediated end-joining

xnd-1: gene, mutant phenotype = X chromosome non-disjunction

ZHP-3: budding yeast Zip-homologous protein ZIP3/CST9

zim: gene class, encoding zinc fingers in meiosis, required for homologue pairing (*i.e.* ZIM-1, ZIM-2 and ZIM-3)

Acknowledgements

I would like to thank Dr. Ann M. Rose for her guidance and support; my supervisory committee members Drs. Donald G. Moerman, Philip Hieter and Peter M. Lansdorp for their constructive feedback on my work; and Dr. David L. Baillie for discussions during my graduate studies.

I would like to acknowledge the past members of the Rose laboratory for their work leading up to the molecular characterization of *rec-1* in *Caenorhabditis elegans*. In particular, single-nucleotide variation association studies by Dr. Nigel J. O'Neil and Aleeza H. T. Tam were crucial in defining the genome region in which *rec-1* would eventually be identified. Genetic studies of *rec-1* with *lin-35* by Zoe Lohn reinforced the idea REC-1 may be functioning at the level of double-strand break formation. Finally, bioinformatic analyses by Dr. Jeffrey Chu, further refinement in genetic mapping by Dr. Ann M. Rose, RNAi experiments by Dr. Martin Jones and Jason Luce, and the characterization of several point mutants by Dr. Ann Marie Davison, ultimately led to the selection of *y18h1a.7* as a candidate coding sequence for *rec-1*. Help from and discussions with Shir Hazhir and Annie S. Tam are appreciated. Additionally, I would like to acknowledge the ongoing work on *rec-1* and *him-5* by the laboratories led by Drs. Simon J. Boulton (Crick Institute), Judith Yanowitz (Magee-Womens Institute) and Chris P. Ponting (University of Oxford).

The encouragement from the Vancouver *C. elegans* research groups (VanWoRM) cannot be understated. This is a forum for sharing reagents, techniques and unpublished results freely. I would like to thank the principal investigators and the students in VanWoRM for fostering a sense of research community. Also, I would like to thank the hard work by Cheryl Bishop in the Department of Medical Genetics for her role as a liaison between the University, the Department

and the students. Finally, I would like to thank Drs. Robert M. Brosh Jr. (National Institute on Aging, NIH), Francesca Cole (MD Anderson), Neil Hunter (UC Davis) and Scott Keeney (Memorial Sloan-Kettering) for discussions on helicases and meiotic recombination in model systems outside *C. elegans.*

In addition to the operational funding to Dr. Ann M. Rose from NSERC, the work presented here was funded by NSERC, CIHR, and UBC fellowships awarded to me throughout my graduate studies.

Chapter 1: Introduction

The roundworm *Caenorhabditis elegans* is a genetically tractable organism. This work describes two main research objectives for which *C. elegans* presents an attractive model to use. The first research objective concerns DNA replication through guanine-rich regions, where several factors are required for the bypass or the repair of secondary structures impeding replication (van Kregten and Tijsterman 2014). Indeed, the first demonstrated guanine-specific mutator phenotype was discovered in *C. elegans* mutant *dog-1*, where heritable and non-heritable mutations could be detected by a simple PCR reaction spanning a guanine-rich tract (Cheung et al. 2002; Youds et al. 2006). A similar phenotype has since been described for the human orthologue *FANCJ* (London et al. 2008); however, the availability of genetic mutants in different repair pathways in *C. elegans* has allowed the extensive analysis of DNA repair components which can act on guanine-rich DNA structures (Youds et al. 2006; Ward et al. 2007; Youds et al. 2008; Koole et al. 2014). An extensive search for non-essential (*i.e.* viable) mutations that maintain the integrity of guanine-rich sequences has only isolated mutations in *dog-1* (Kruisselbrink et al. 2008), so the question remains if there are any *essential* genes involved in the maintenance or the repair of guanine-rich sequences in *C. elegans*. The *chl-1* gene in *C. elegans* is an essential, helicase-encoding gene related to *dog-1*. My first research objective is to determine if *chl-1* also has a role in the resolution of guanine-rich secondary structures in *C. elegans.*

The second main research objective of this work exploits the short generation time and the high fecundity of *C. elegans* to examine how the positioning of meiotic recombination events is genetically determined. The large numbers of progeny per generation, as short as 3 days, allows for the quick recovery of many products of meioses. Additionally, the high density of

molecular markers in the *C. elegans* genome enables the generation of meiotic recombination maps at a high resolution across the entire genome (Barnes et al. 1995; Rockman and Kruglyak 2009; Kaur and Rockman 2014). These properties have allowed the discovery of a phenomenon known as the meiotic recombination pattern, where crossover events preferentially, but not exclusively, occur in certain regions of the chromosomes.

The *rec-1* locus is one genetic determinant of this patterning. Prior to this work, only a single recessive mutant allele of *rec-1* was known, but its sequence identity was not known (Rose and Baillie 1979; Zetka and Rose 1995; Rose et al. 2010). Recently, the adaptation of the CRISPR-Cas9 technology in *C. elegans* has paved the way for directed mutagenesis, a previously difficult task in *C. elegans* (Friedland et al. 2013). Additionally, whole-genome sequencing combined with detailed annotation of the *C. elegans* genome allowed the identification of candidate coding regions for *rec-1* (Rose et al. 2010). My second research objective is to determine the molecular identity of *rec-1* in order to clarify the role of REC-1 in the establishment of the meiotic recombination pattern.

1.1 Response to DNA damage in *C. elegans*

DNA damage under different circumstances determines the types of cellular response and DNA repair that follow (Clejan et al. 2006; Holway et al. 2006; Garcia-Muse and Boulton 2005). A comprehensive summary on the response to base damage, replication fork stalling, double-strand breaks in the context of germ cells, somatic cells and embryonic cells can be found elsewhere (Lans and Vermeulen 2015). For this work, I will focus on DNA damage caused by the hypothesized replication block at guanine-rich sequences. Replication blocks are particularly dangerous lesions for proliferating cells undergoing DNA replication.

1.2 Guanine-rich sequences are sources of replication blocks which require helicase activity or DNA repair machinery for faithful transmission

The hypothesis that guanine-rich DNA sequences capable of forming guanine quadruplexes *in vitro* (Sen and Gilbert 1988) could cause problems during replication came about from a curious phenotype observed in *C. elegans dog-1(gk10)* mutants. Visible and heritable mutant traits appeared at predictable frequencies due to spontaneous genomic deletions initiating at guanine-rich sequences ('G-tracts') (Cheung et al. 2002). A model put forth to explain this unique DNA repair signature depended on DNA replication, as DNA replication allowed for a transient single-stranded state to favour the Hoogstein interactions among four guanine residues over the usual Watson-and-Crick pairing between guanine and cytosine residues. Normally, these guanine-rich secondary structures would be unwound efficiently by DOG-1 and its orthologues [*e.g.* FANCJ (Bharti et al. 2013; Wu et al. 2008)]; however, without DOG-1, these structures could impede the replication machinery (Figure 1.1a-b). This prediction is supported by stalled replication intermediates observed in *Xenopus* extracts lacking the activity of FANCJ, a DOG-1 orthologue (Castillo Bosch et al. 2014). Genetic evidence suggests that this blocked replication fork is then turned into a substrate for repair directed by the homologous recombination (HR) machinery (Figure 1.1c) and not by the classical non-homologous end-joining (NHEJ) machinery (Youds et al. 2006; Ward et al. 2007; Youds et al. 2008). If this HR-mediated repair cannot cope with the blocked structure, then repair may be directed to a POLQ-1/Polymerase θ-dependent pathway, whose repair signatures include small deletions consistent with the lesions seen in *dog-1(gk10)* mutants (Koole et al. 2014) (Figure 1.1d).

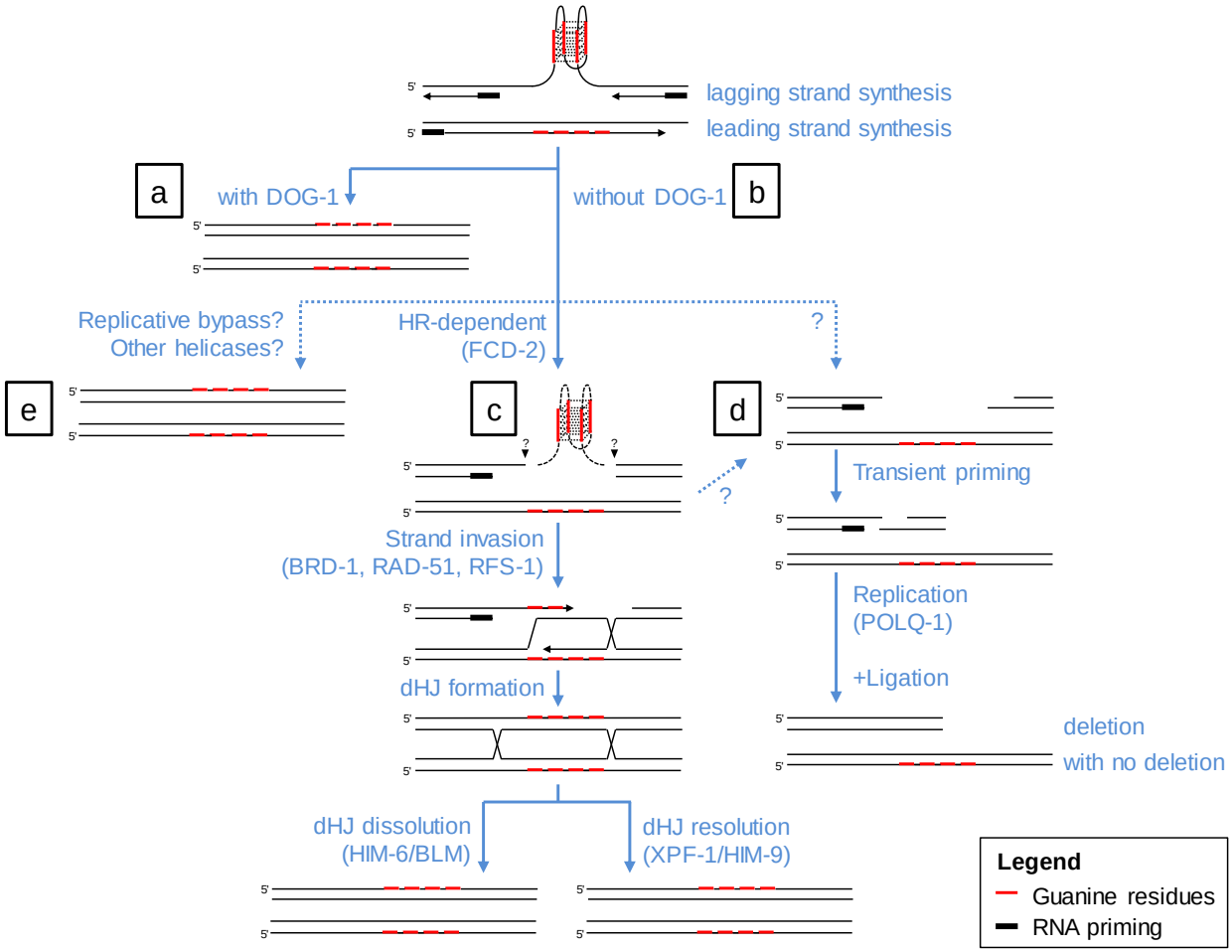

Figure 1.1: Faithful replication of guanine-rich DNA requires the action of DOG-1.
a) Functional DOG-1 is required for the normal, faithful replication of guanine-rich sequences. b) Without functional DOG-1, the replication block may become substrates for a number of processes, of which faithful repair dependent on homologous recombination (HR-dependent, c) is the best characterized genetically. c) In double mutant analyses with *dog-1*, additionally abolishing FCD-2 function (which likely promotes repair by homologous recombination), strand invasion, double Holliday junction dissolution (dHJ dissolution) and double Holliday junction resolution (dHJ resolution) all increase the instability of guanine-rich sequences (Youds et al. 2006; Ward et al. 2007; Youds et al. 2008). With any part of this HR-dependent pathway non-functional, or if fully functional HR cannot repair the replication block formed by guanine-rich sequences, the block structure may instead become a substrate for POLQ-1-dependent repair (d), which is error-prone. In double mutant analysis with *dog-1*, additionally knocking out *polq-1* suppresses the formation of small deletions characteristic of *dog-1(gk10)* single mutants (Koole et al. 2014). Factors that lead to or promote this POLQ-1-depedent repair are not known (marked with dotted arrows and '?'). e) Replicative bypass through the block by other polymerases (POLH-1 and POLK-1) is possible, but genetic results so far appear contradictory (Youds et al. 2006; Koole et al. 2014). Involvement by another helicase, CHL-1, will be explored in Chapter

2. In parentheses: factors whose encoding genes have been analyzed in double mutant assays with *dog-1(gk10)*.

Forward genetic screens for mutants with G-tract instability have so far isolated only loss-of-function alleles of *dog-1*, indicating that *dog-1* is likely the only non-essential gene with a role in maintaining the integrity of guanine-rich DNA sequences (Kruisselbrink et al. 2008). This may seem surprising, as several closely related helicase genes are present in the *C. elegans* genome, including *xpd-1, chl-1* and *rtel-1* (Chung et al. 2011). Also, orthologues of several other helicase genes have been shown to encode proteins with G-quadruplex unwinding activity [such as BLM and WRN helicases (Mohaghegh et al. 2001)]. In Chapter 2, I will explore how CHL-1, a helicase closely related to DOG-1, is involved in maintaining the integrity of guanine-rich sequences.

1.3 Meiotic recombination events (crossovers) in the germline

Meiosis is a programme involving one round of DNA replication followed by two rounds of specialized cell division, thus halving the original ploidy (Page and Hawley 2003). With several notable exceptions in model systems (such as males in *Drosophila*), the first meiotic division involves a physical link, or a crossover, between the homologous DNA molecules. Our current understanding of meiotic recombination by crossing over came from observations made throughout the last century. The hypothesis that chiasmata were cytological manifestations of an exchange between paternal and maternal chromatids was first proposed by Janssens based on observations in *Batrachoseps attenuatus* (California slender salamander) (Janssens 1909). Soon after, the concept of genetic linkage was formulated to explain co-inherited traits in *Drosophila melanogaster* (Sturtevant 1913a, 1913b). The correlation between genetic linkage and physical

linkage was shown definitively by Creighton and McClintock from experiments in maize (Creighton and McClintock 1931). The molecular details of how chromatid exchanges came about were slowly revealed through advances in genetics and molecular biology.

The double helical structure of DNA (Watson and Crick 1953) informed Robin Holliday's model of strand exchange, which involved two singly-nicked and homologous DNA molecules (Holliday 1964). The current model of meiotic recombination, the double-strand break repair model, improves upon Holliday's original by removing the need for two perfectly symmetric nicks and simply breaking one DNA double helix while leaving the other intact (Szostak et al. 1983). Confirmation of this double Holliday junction (dHJ) theoretical structure soon followed from studies in yeast (Sun et al. 1989; Cao et al. 1990; Schwacha and Kleckner 1994, 1995). Thus, the double-strand break repair model is the current paradigm for understanding homologous recombination in meiosis. Since meiotic chromosomes are actively broken to initiate recombination, control over double-strand break formation and the subsequent repair is essential to ensure that the chromosomes segregate properly at the end of meiosis I and stay intact after meiotic recombination.

1.3.1 A hierarchy of factors govern the processes from DSB to meiotic recombination

In the meiotic prophase, this double-strand break (DSB) is generated by the orthologues of the budding yeast Spo11 protein (Keeney et al. 1997). In *C. elegans*, meiotic recombination initiates by the phosphodiesterase action of the orthologous SPO-11 protein, without which meiotic DSBs are not made and chromosomes fail to segregate properly at the end of meiosis I (Dernburg et al. 1998). Remarkably, only a single DSB per homologue pair is required to ensure the accurate segregation of chromosomes at the end of meiosis I in *C. elegans* (Rosu et al. 2011);

however, the SPO-11 protein is able to generate up to a dozen DSBs per homologue pair in some genetic backgrounds (Mets and Meyer 2009; Nottke et al. 2011; Rosu et al. 2011; Saito et al. 2012). As meiotic crossovers use DSBs as substrates, DSB formation is the topmost level of control that influences the eventual formation of crossovers.

How the meiosis programme encourages or limits the activity of SPO-11 is the subject of ongoing research, based on a paradigm where the concepts of 'assurance' and 'homeostasis' act in opposite directions to control meiotic processes. 'Assurance' means that a homologue pair will undergo at least one instance of a particular meiotic process (*e.g.* DSB formation or crossover formation). 'Homeostasis' means a particular meiotic process is self-limiting. Applied to meiotic DSB formation, DSB assurance is achieved as every homologue pair receives at least one DSB during the normal meiotic programme in *C. elegans*. DSB homeostasis is achieved as every homologue pair receives at most a dozen DSBs in *C. elegans*, and no more.

Examination of early meiotic events surrounding DSB formation in *C. elegans* is hampered by a lack of antisera against SPO-11 or an epitope-tagged SPO-11. In other model organisms, antisera or tagged constructs exist to allow a thorough characterization of the DSB formation dynamics by co-immunoprecipitating DNA bound to Spo11 orthologues (see Pan et al. 2011; Fowler et al. 2014). A lack of antisera against *C. elegans* SPO-11 means that the number and the frequency of DNA cleavage mediated by SPO-11 cannot be determined directly, and thus the control of DSB formation in *C. elegans* is not very well understood.

Independent from the DSBs generated by SPO-11 (Dernburg et al. 1998), replicated and homologous chromosomes in the meiotic programme must be brought into close proximity to allow DNA strand exchange between them. This is achieved through homologue pairing (Figure 1.2a; see references contained therein) and the formation of the synaptonemal complex (SC)

between the homologues (Figure 1.2b; see references contained therein). Once the homologues are brought close together (*i.e.* they are 'synapsed'), the DSBs generated by SPO-11 use a core set of largely conserved factors for their repair and eventual resolution as crossovers (COs) or non-crossovers (NCOs) (Figure 1.2d-k) (reviewed by Lui and Colaiácovo 2013). The decision to resolve a double Holliday junction (dHJ, see Figure 1.2g) as a crossover or a non-crossover represents a second layer of control influencing the formation of meiotic crossovers. Here, the CO-versus-NCO decision could be made by putative Holliday junction resolvases such as SLX-1, MUS-81, XPF-1/HIM-9 and GEN-1, as well as the BLM/Sgs1 orthologue HIM-6 (Figure 1.2h, j and k).

Again, the paradigm of assurance-versus-homeostasis frames the current interpretation of the CO-versus-NCO decision. Crossover assurance is the idea that every homologue pair must receive one crossover event – the so-called 'obligate crossover' – to ensure the homologue pair is held together before segregation at the end of meiosis I. Pro-crossover factors such as ZHP-3, MSH-4/5 and COSA-1 are absolutely required for the maturation of a DSB into this obligate crossover and the accurate segregation of chromosomes at the end of meiosis I (Figure 1.2h). These factors can be detected as six discrete cytological foci in mid-pachytene, corresponding to their localization to the six homologue pairs (Zalevsky et al. 1999; Kelly et al. 2000; Jantsch et al. 2004; Bhalla et al. 2008; Yokoo et al. 2012; Libuda et al. 2013). On the other hand, crossover homeostasis is the idea that every homologue pair under normal circumstances in *C. elegans* is limited to *exactly* one crossover event (and rarely two, if ever); this concept, arrived from a different angle, is known from genetic studies as 'crossover interference' (Figure 1.2i) (Hodgkin et al. 1979; Zetka and Rose 1995; Meneely et al. 2002; Hillers and Villeneuve 2003; Nabeshima et al. 2004; Lim et al. 2008; Gabdank and Fire 2014), inferred from genetic maps of roughly 50

map units per chromosome and the absence (or extremely low frequencies) of gametes with double crossovers. Crossover homeostasis/interference may be relaxed if RTEL-1 function is compromised (Youds et al. 2010), if chromosome lengths are increased substantially (Yokoo et al. 2012; Libuda et al. 2013), or if the synaptonemal complex is perturbed (Libuda et al. 2013).

1.3.2 The distribution of meiotic crossovers is not even across the autosomes

While the assurance-versus-homeostasis paradigm frames our understanding of the *number* of DSBs and COs, it does not address the *location* of the crossover events. Because each homologue pair receives only one CO event per meiosis in *C. elegans*, this effect is better understood in terms of CO events over *many* meioses.

It has long been known that in *C. elegans*, crossover events on the autosomes occur preferentially (although not exclusively) on roughly the terminal thirds of the autosomes, regions known as 'autosomal arms'. Over many meioses, CO events would be mapped more frequently to the terminal thirds of the autosomes than the middle third. This also means that the genetic map does not scale linearly to the physical map (see Figure 1.3) (Barnes et al. 1995; Zetka and Rose 1995; Rockman and Kruglyak 2009). This skewed distribution of meiotic COs does not apply to the X chromosome, where the CO distribution appears relatively invariant throughout the length of the chromosome (Barnes et al. 1995; Rockman and Kruglyak 2009). Hence, in addition to the numerical constraints on DSB and CO *numbers*, or *frequency*, described earlier, there appears to be an additional layer of control over the CO *location*, or *distribution*.

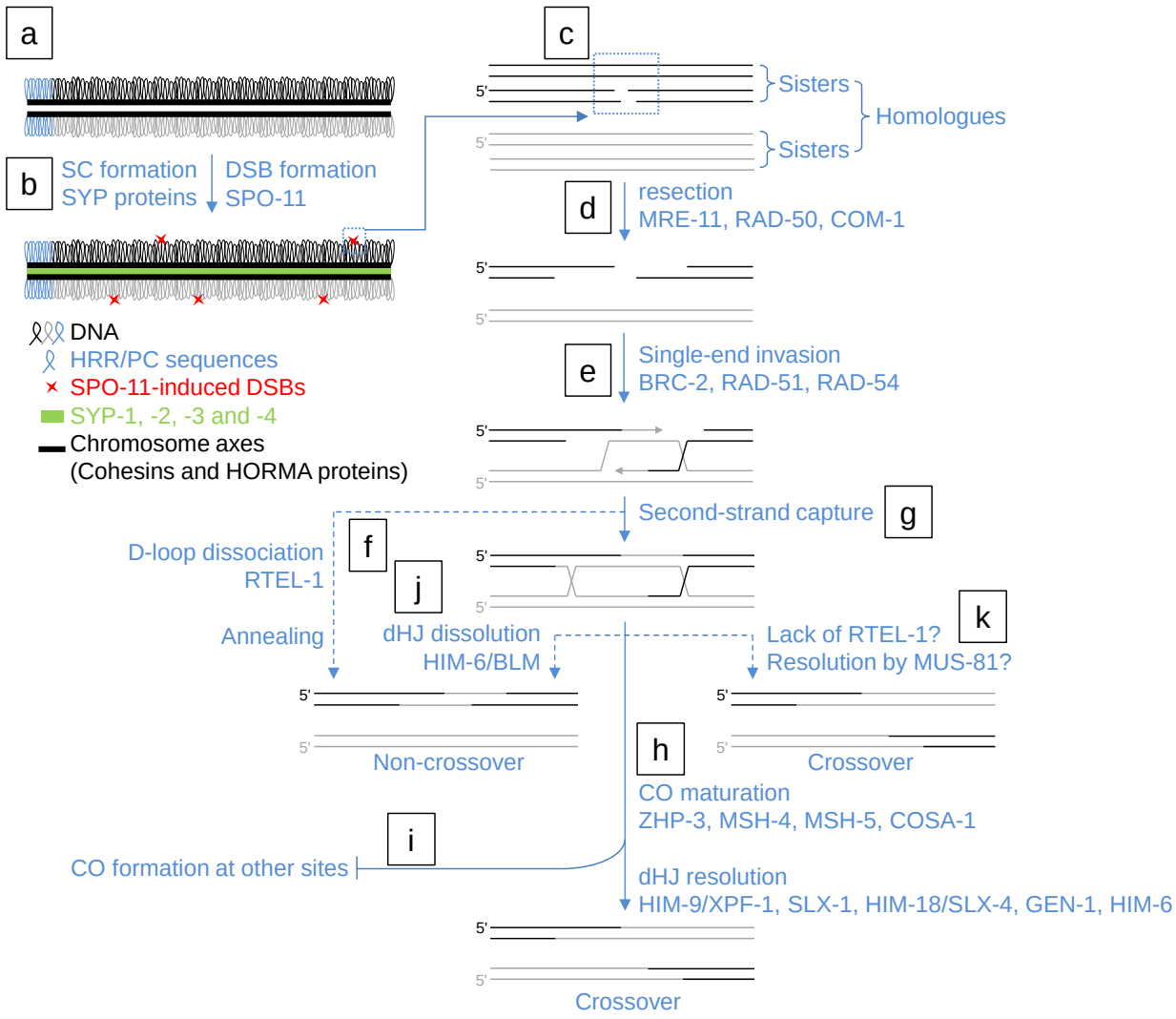

Figure 1.2: Major events leading up to crossover formation in *C. elegans*
The homologous chromosomes are shown here immediately before synapsis. Schematic based on transmission electron microscopy images (Smolikov et al. 2008) and currently accepted models of synaptonemal complex (SC) structure from other models, where the sister chromatids form loops. a) Axis proteins (thickened lines, also known as axial/lateral elements) – which include cohesins and HORMA-domain-containing proteins – hold together the replicated sister chromatids (Pasierbek et al. 2001, 2003; Severson et al. 2009), promote inter-homologue recombination (Zetka et al. 1999), and may act to prevent inter-sister recombination (Couteau et al. 2004). Homologous chromosomes associate by the action of HIM-8, ZIM-1, ZIM-2 and ZIM-3 proteins on pairing centre (PC) sequences (Sanford and Perry 2001; Phillips et al. 2005; Phillips and Dernburg 2006) inside the homologue recognition region (HRR) (Rosenbluth and Baillie 1981; Herman et al. 1982; Rose et al. 1984; McKim et al. 1988, 1993; Villeneuve 1994). b) Formation of the synaptomenal complex (SC), with the association of SYP-1, -2, -3 and -4 (in green), brings the homologous chromosomes into close proximity. Without the SC, inter-homologue recombination could not take place (Colaiácovo et al. 2003; Smolikov et al. 2007a,

2007b). Proper SC formation in *C. elegans*, unlike in many other organisms, does not depend on SPO-11-induced double-strand breaks (red) (Dernburg et al. 1998), shown here occurring in parallel to SC formation. c) A zoomed-in schematic of the homologous chromosomes at the site of a DSB – the sister chromatids not involved in inter-homologue recombination will be omitted from the schematic in the later steps. The homologous chromosome without the DSB is coloured grey throughout. Many aspects of homologous recombination here resemble Figure 1.1c, as the core homologous recombination machinery are the same for both the repair of stalled replication forks and meiotic DSBs. d) The DSBs are processed to have single-stranded 3' overhangs to allow for strand invasion, dependent on the action of MRE-11, RAD-50 and COM-1 (Chin and Villeneuve 2001; Hayashi et al. 2007; Penkner et al. 2007). e) Single-end strand invasion, forming a displacement loop (D-loop), is dependent on the strand exchange activity of RAD-51. BRC-2 stabilizes the RAD-51 interaction with DNA (Petalcorin et al. 2006, 2007), while the removal of RAD-51 is dependent on RAD-54 (Mets and Meyer 2009). f) Dissolution of the D-loop by RTEL-1 can result in non-crossover. Such dissolution may be required for aberrant recombination between non-homologous sequences (Barber et al. 2008; Youds et al. 2010). g) Second-strand capture forms a double Holliday junction (dHJ). h) Recruitment ZHP-3, MSH-4, MSH-5 and COSA-1 to the eventual site of the obligate crossover to promote crossover (CO) resolution. Without any of these factors, obligate COs do not form (Zalevsky et al. 1999; Kelly et al. 2000; Jantsch et al. 2004; Bhalla et al. 2008; Yokoo et al. 2012; Libuda et al. 2013). Structure-specific endonucleases (SLX-1, XPF-1/HIM-9, HIM-18, MUS-81 and GEN-1) act on dHJs to ensure proper resolution (Agostinho et al. 2013; Saito et al. 2013; O'Neil et al. 2013), although they are not restricted to acting on the obligate crossovers. Additionally, HIM-6 promotes dHJ resolution as a CO (Agostinho et al. 2013; Schvarzstein et al. 2014), as evidenced by the reduced number of CO events in *him-6* mutants (Zetka and Rose 1995). i) The maturation of the obligate crossover suppresses the formation of another crossover throughout the entire chromosome (Rosu et al. 2011), a phenomenon known as interference (Hodgkin et al. 1979; Zetka and Rose 1995; Meneely et al. 2002; Hillers and Villeneuve 2003; Nabeshima et al. 2004; Lim et al. 2008; Gabdank and Fire 2014). Effective suppression of additional crossovers (interference) may require an intact synaptonemal complex (Libuda et al. 2013). j) Without pro-CO factors such as MSH-5, dHJ junction may dissolve or resolve as a non-crossover (Rosu et al. 2011). Genetic studies in *C. elegans* suggest that HIM-6, the BLM/Sgs1 orthologue in *C. elegans*, plays a role (Schvarzstein et al. 2014). The role of structure-specific endonucleases in resolving dHJs as non-crossovers is not well defined. k) In cases where aberrant or excess dHJs are found, such as when RTEL-1 function is compromised, MUS-81 may act to resolve dHJs (Youds et al. 2010), leading to additional crossover events which can be detected genetically but are not associated with the obligate crossover cytological markers (Yokoo et al. 2012).

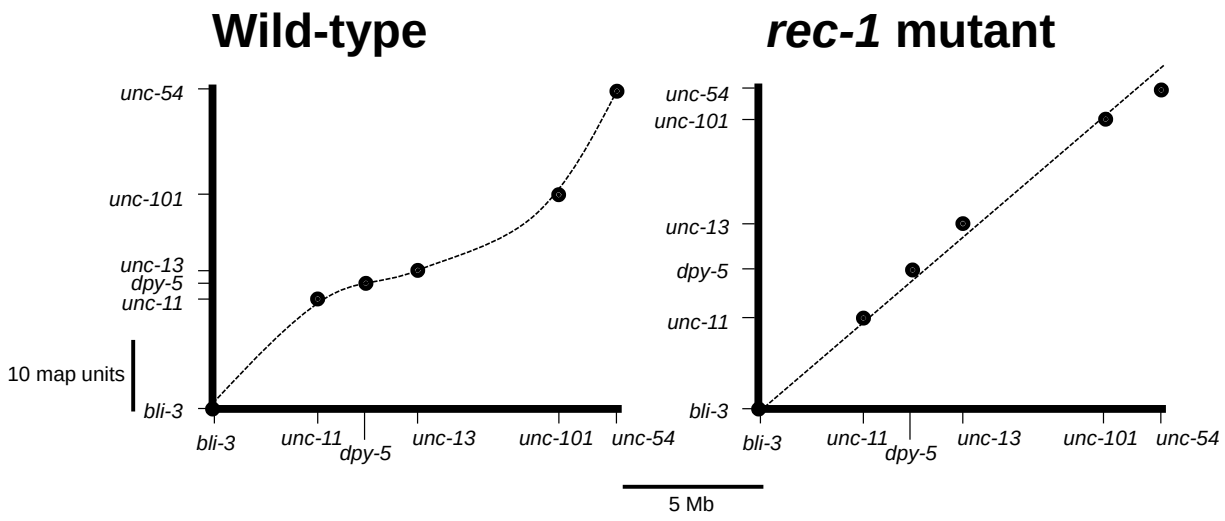

Figure 1.3: A 'Marey map' representation of the correspondence between genetic distances and physical distances on Chromosome I in *C. elegans*.
Based on the data from the work of Zetka and Rose (1995). The slope of the fitted curve represents the recombination frequency per unit physical distance (in base-pairs). Whereas *rec-1(+)* animals show higher recombination on the chromosome arms and lower recombination in the chromosome centre (figure left), such pattern is eliminated in the *rec-1(s180)* mutant (figure right).

The meiotic recombination pattern – one where COs are found preferentially on the autosomal arms – is under genetic control. The first mutation found to disrupt this pattern was at the *rec-1* (recombination abnormal) locus. In *rec-1* mutants, the CO distribution appears randomized, thus the genetic map appears to scale linearly with the physical map. CO assurance appears to hold for autosomes as there is no detectable autosomal aneuploidy, and CO homeostasis/interference also appears to hold as the genetic map of Chromosome I was still roughly 50 map units (Zetka and Rose 1995). There is a small, however significant, increase of X chromosome non-disjunction in *rec-1* mutants (Rattray and Rose 1988). Since the description of *rec-1*, several mutants have also been described to have a randomized CO distribution, including *xnd-1* (Wagner et al. 2010), *him-5* (Meneely et al. 2012) and *slx-1* (Saito et al. 2012)

mutants. While the Holliday junction resolvase activity of the SLX-1 protein could explain the altered distribution phenotype in the mutant (Saito et al. 2012), the molecular functions of the XND-1, HIM-5 and REC-1 gene products are not known. I will present the coding sequence of *rec-1* in Chapter 4 and discuss possible mechanisms for REC-1 function in Chapters 4 and 5.

1.3.3 The meiotic recombination pattern may be controlled by biased DSB distribution, biased crossover/non-crossover resolution, or a combination of the two

Just as the control over DSB formation and CO-versus-NCO resolution is useful in framing our understanding of the number (frequency) of crossovers, it is also useful for framing our understanding of the location (distribution) of crossovers. Is the meiotic recombination established due to a biased DSB distribution on the autosomal arms, a bias toward crossover resolution on the autosomal arms (or non-crossover resolution in the autosomal centres), or a combination of both?

The 'biased resolution' for CO or for NCO shapes the meiotic recombination pattern in other organisms to varying extents. In humans and mice, where sperm genotyping allows the identification of crossover or gene conversion (non-crossover) meiotic products from large pools of sperm DNA, the CO/NCO ratio is variable from one chromosome location to another (Holloway et al. 2006; Cole et al. 2010; de Boer et al. 2015), which partly contributes to the meiotic recombination pattern in addition to the biased DSB formation in humans and mice. A notable case of biased resolution is found in fission yeast in a phenomenon known as 'crossover invariance' (Hyppa and Smith 2010). Here, DSBs at preferred DSB sites resolve as NCOs, while DSBs at other sites resolve as COs. The net effect is that the crossover frequency appears

invariant across the length of a chromosome (Young et al. 2002; Hyppa and Smith 2010; Fowler et al. 2014).

'Biased DSB distribution' also contributes to the meiotic recombination pattern in several organisms. DSB distribution can be mapped at very high resolutions where the deep-sequencing of meiotic DSB ends is possible – Spo11-oligo sequencing in *S. cerevisiae* (Pan et al. 2011) and single-stranded DNA sequencing in mice (Khil et al. 2012). The *S. cerevisiae* DSB distribution patterns are largely concordant with its CO patterns, with far more DSBs mapping to intergenic regions than to genic regions; furthermore, correlations could be drawn between DSB formation patterns and nucleosome occupancy, histone modifications or DNA sequence content (Pan et al. 2011). Analogous analyses have also been carried out in mice where DSB formation has been mapped to sites bound by Prdm9 (Brick et al. 2012).

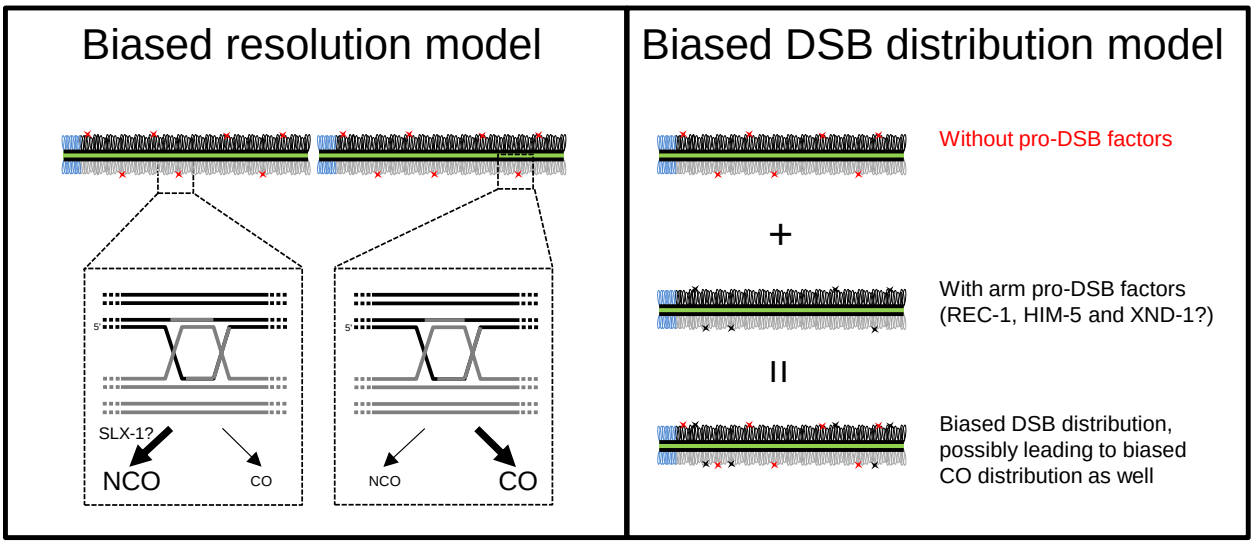

Figure 1.4: Biased resolution and biased DSB distribution could be shaping the *C. elegans* recombination pattern.

1.3.4 Testing for biased DSB distribution and biased CO-vs-NCO resolution in *C. elegans*

Unfortunately in *C. elegans*, neither scenario (nor the combination of the two) has been tested extensively. CO versus NCO resolution could be determined using closely-spaced genetic markers and a transposase-induced DSB. This technique has been exploited at the *unc-5* locus, where the crossover-to-non-crossover ratio (CO/NCO ratio) was estimated to be 1:8. In other words, for all DSBs formed at the *unc-5* locus, around 11% resolved as COs while 89% resolved as NCOs (gene conversion events) (Rosu et al. 2011). This technique has not been applied to multiple sites across a chromosome. Conceivably, a variable CO/NCO ratio across the chromosome could contribute to the meiotic recombination pattern, perhaps by promoting CO resolution in the autosome arms and promoting NCO resolution in the autosomal centers.

On the other hand, testing for biased DSB distribution remains a challenge, at least at the level of base-pair resolution that was achieved in budding yeast and mice. As noted earlier, neither SPO-11 antibodies nor tagged SPO-11 constructs exist. However, antibodies against RAD-51 are available, which mark sites of double-strand breaks (Alpi et al. 2003). Cytologically, RAD-51 foci appear to be evenly distributed across the chromosome, leading to a proposal that meiotic recombination pattern in *C. elegans* is shaped primarily by promoting non-crossover resolution in the autosomal centers (Saito et al. 2012).

The most convincing evidence for the 'biased resolution' model in *C. elegans* (Figure 1.4 left) comes from an altered recombination pattern in the oocytes from *slx-1* mutants (Saito et al. 2012, 2013), where increased recombination frequencies in autosome centers are accompanied by decreased recombination frequencies in the autosome arms. Since *slx-1* encodes a structure-specific endonuclease which can cleave recombination substrates *in vitro* (Saito et al. 2012), in this 'biased resolution' model, SLX-1 specifically targets recombination intermediates in the

autosome centers for non-crossover resolution. At least two issues for this model remain. First, the SLX-1-resolvase machinery needs to cleave double Holliday junctions in a manner consistent with *non*-crossovers. This specificity for non-crossovers over crossovers has not been shown *in vitro* for SLX-1, so additional factors may be involved. Second, the SLX-1-resolvase machinery needs to localize to the autosomal centers by an unknown mechanism; this mechanism may very well depend upon tethering or associating with chromatin marks that are associated with these regions (Liu et al. 2011).

In apparent contradiction with the cytological results where RAD-51 foci appear to distribute evenly along the chromosome (Saito et al. 2012), unpublished RAD-51 chromatin immunoprecipitation data from modENCODE (Celniker et al. 2009) deposited by the Lieb lab (University of Chicago) indicate that RAD-51 binding sites are positioned preferentially on the autosomal arms (Figure 1.5). Crucially, there appears to be fewer RAD-51 binding sites, distributed almost evenly, on the X chromosome. This corroborates with cytological results (Gao et al. 2015) (Figure 1.5). An important caveat for this set of modENCODE chromatin observations is that these binding patterns were not derived purely from meiotic cells for practical reasons. Nonetheless, SPO-11-induced DSBs in the germline would be expected to constitute a major source of DSBs in whole adult animals. Furthermore, these RAD-51 binding patterns correlate with the known patterns of meiotic crossovers on the autosomes and the X chromosome (Barnes et al. 1995; Rockman and Kruglyak 2009), which suggests that the meiotic recombination pattern in *C. elegans* may be linked to the distribution of double-strand breaks.

This ‘biased DSB distribution’ model, unlike the ‘biased resolution’ model, is attractive as it eliminates the mechanistic need for a resolvase to decide between CO versus NCO cleavage. Here, it is the double-strand break machinery that preferentially associates with autosomal arm

DNA. As SPO-11 by itself is unlikely to confer the sequence specificity required for the biased DSB distribution [based on analyses from the *S. cerevisiae* orthologue (Pan et al. 2011)], additional factors are likely involved.

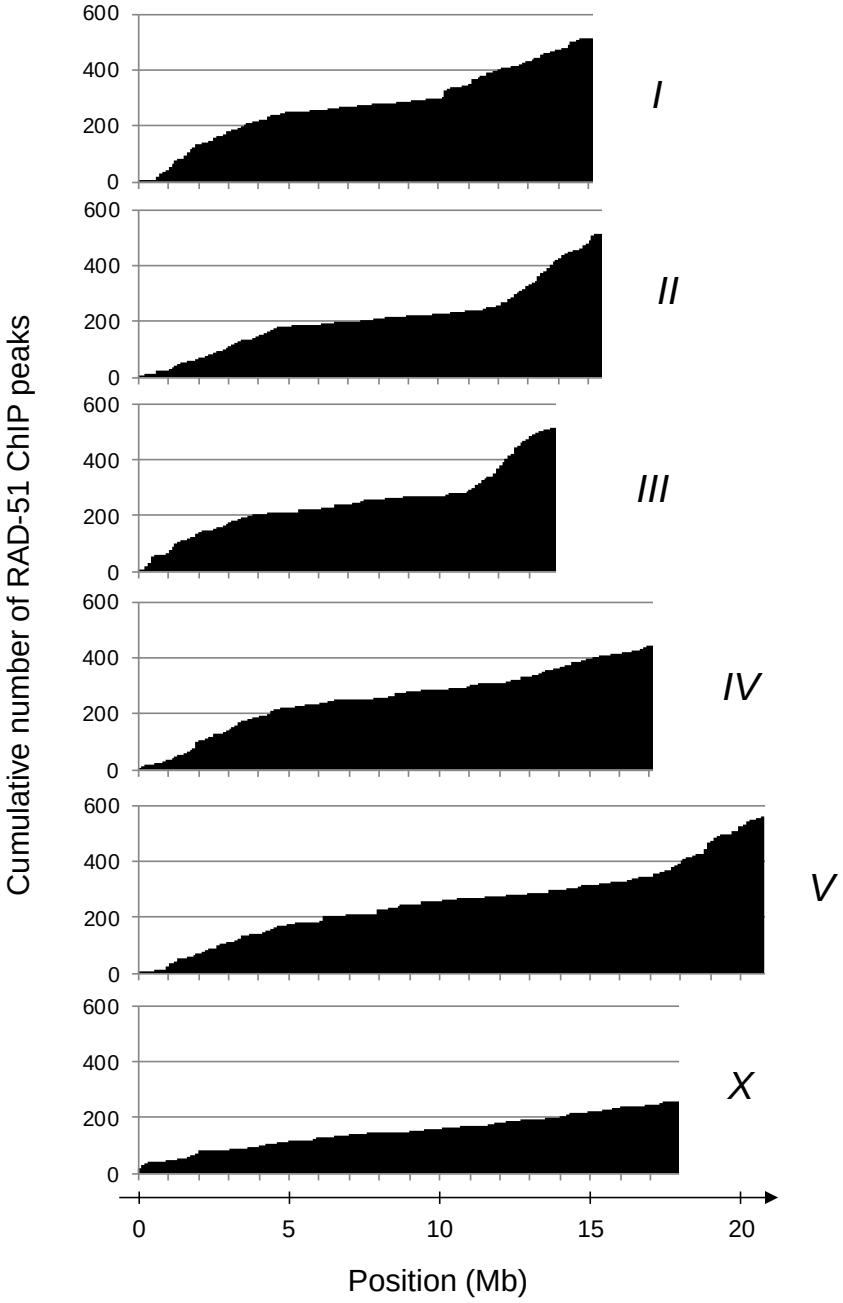

Figure 1.5: Cumulative counts of RAD-51 binding sites in young adult *C. elegans*.

RAD-51 binding profiles prepared from whole animals with a *fem-2* mutation from the modENCODE database (Celniker et al. 2009), deposited by the Lieb lab (University of Chicago). As somatic tissue is not expected to have a large number of DSBs and RAD-51 binding, these patterns may represent the RAD-51 binding profile in the germline. These binding profiles resemble the meiotic recombination patterns generated from comparing genetic and physical maps (see Figure 1.3) (Barnes et al. 1995; Rockman and Kruglyak 2009).

In this 'biased DSB distribution' framework, mutants with a crossover re-distribution phenotype may illuminate the mechanism that targets SPO-11 activity to the autosomal arms. The phenotypes of *xnd-1*, *him-5* and *rec-1* fall under this category. A possible mechanism for the 'biased DSB distribution' model is illustrated in Figure 1.4. Here, SPO-11 is responsible for a baseline, non-biased distribution of DSBs throughout the autosomes. The proteins REC-1, HIM-5 and XND-1 act, perhaps through one or multiple pathways, to additionally target SPO-11 to the autosomal arms. This model makes two testable predictions on the double-strand break dynamics in *rec-1*, *him-5* and *xnd-1* mutants.

1) A lack of REC-1, HIM-5 or XND-1 function will lead to fewer numbers of DSBs on the autosomes.
2) In addition to fewer total number of DSBs, the DSB distribution will be even across the autosomes.

The first prediction has been shown to be true in *him-5* mutants (Meneely et al. 2012). This work will aim to clarify the role of REC-1 in the formation of double-strand breaks by testing the first prediction. Testing the second prediction at a high resolution across the genome requires the use of chromatin immunoprecipitation in *rec-1* mutants with anti-RAD-51 and is outside the scope of this work.

1.3.5 Large-scale chromosomal/chromatin domains in *C. elegans* correlate with recombination distribution patterns, but a causal link between them has so far been missing

Meiotic crossover patterns are known to correlate well with the histone H3K4 trimethylation sites in budding yeast, made by the Set1 methyltransferase (Borde et al. 2009), and this histone modification physically associates with the DSB formation machinery (Acquaviva et al. 2013; Sommermeyer et al. 2013). In mice, higher levels of DSB formation are specifically linked to sites of H3K4 trimethylation catalyzed by the Prdm9 protein and not other H3K4 trimethylation sites (Brick et al. 2012). This suggests that Prdm9 recruits factors of the DSB formation machinery to the chromatin.

Despite a lack of an obvious orthologue to PRDM9/Prdm9 in *C. elegans* and a lack of a clear correlation between H3K4 trimethylation and increases in meiotic recombination in *C. elegans* (Liu et al. 2011), several other large-scale chromosome/chromatin features in *C. elegans* have been identified on autosomal arms. Autosomal arms are enriched in several classes of repetitive elements but not others (Surzycki and Belknap 2000). In addition, histone H3K9 methylation is enriched on the autosomal arms (Liu et al. 2011). More recently, nuclear attachment sites mediated by LEM-2 have been found to demarcate a single autosomal arm-and-centre boundary precise to the detection limit of the recombination assays (Liu et al. 2011; Kaur and Rockman 2014). These findings point to a possibility that histone modifications and LEM-2 binding sites could act as ‘docking sites’ for the DSB formation or the meiotic recombination machinery, analogous to the situation in budding yeast; however, several challenges remain in the attempts to link large-scale chromosome/chromatin features to crossover patterns. First, it is difficult to isolate an exclusively synchronous population of cells undergoing meiosis in *C.*

elegans, thus for practical purposes, ChIP data are derived from a mixture of somatic and germ nuclei. One instance of a reported correlation between meiotic recombination and chromatin marks (Liu et al. 2011) included chromatin-immunoprecipitation data from embryos and juvenile animals – two life stages with no active meiotic processes. Thus, these histone marks or LEM-2 attachment sites may not reflect the true nature of the meiotic chromosomes. Second, it is difficult to draw a causal link between the distribution of repetitive elements and the distribution of meiotic recombination. It may simply be that autosomal arms are more accessible to the meiotic DSB formation machinery by some means (see Figure 1.5); if so, the autosomal arms might also be more accessible to the transposase machinery by a similar means. Taken altogether, a definitive causal link between large-scale chromosomal/chromatin structures and the meiotic recombination pattern has yet to be established.

1.4 The molecular identity of *rec-1* – a thirty-five-year journey

It has long been known that *C. elegans* genetic map distances do not scale linearly to physical map distances across the autosomes (Brenner 1974; Barnes et al. 1995; Rockman and Kruglyak 2009). Even though every homologue pair normally receives one crossover event every meiosis, over many meioses, gene-poor, near-terminal regions of the autosomes (loosely defined as the 'autosomal arms') receive a far greater share of meiotic crossover events than the gene-rich autosomal centres ('the autosomal gene cluster' or 'the autosomal center') per unit of physical distance. To this day, it remains to be resolved if this is due to the bias in the DSB machinery or a bias in the resolvase machinery, or a combination of these two possibilities.

Based on an important observation that several lines of *C. elegans* yielded increased recombination at different genetic intervals, Rose and Baillie proposed that meiotic

recombination *C. elegans* is under the genetic control of the *rec-1* locus, the mutation of which may have spontaneously arisen during the repeated passaging of superficially wild-type stocks (Rose and Baillie 1979; Rose et al. 2010). With normal brood sizes, near-normal non-disjunction frequencies and a mutant recombination phenotype that was only apparent after counting thousands of F_2 animals, identifying the coding sequence for *rec-1* remained a challenge for many years (Rattray and Rose 1988). After all, *rec-1* is unique in that it remains the only locus identified in *C. elegans* based on its effect on recombination (the *rec* gene class) and not from either a visible phenotype or an *a priori* understanding of the function or orthology of the gene product.

Zetka and Rose recognized that in mutant *rec-1* animals, not only did recombination frequencies increase in the autosomal central clusters as previously reported, they decreased in the autosomal arms while each homologue pair appeared to maintain one crossover event (Zetka and Rose 1995). The resulting genetic map of Chromosome I from mutant *rec-1* animals is one that still retains 50 cM of recombination and that appears to scale linearly to the physical map (Figure 1.3). Duplication mapping at the time placed *rec-1* at the right end of Chromosome I (Zetka and Rose 1995). In retrospect, this result may have been confounded by the unpredictable recombination behaviour of chromosomes in the presence of unattached chromosomal duplications. The *rec-1* gene, whose coding sequence is identified in this work, is now known to be on the left end of Chromosome I.

The Rose lab proceeded to find several candidate genes on the right end of Chromosome I, one of which, now known as *dog-1* (**d**eletion **o**f **g**uanine-rich sequences 1), encoded a helicase, which might be expected to alter the dynamics of meiotic recombination. The RTEL-1 helicase is one such example (see Figure 1.2f) (Barber et al. 2008; Youds et al. 2010). A screen isolated

an out-of-frame deletion in *dog-1* which, while it failed to confer a mutant meiotic recombination phenotype, led to spontaneous deletions that map to guanine-rich regions of the genome (Cheung et al. 2002). This was the first known instance of a loss of helicase function conferring a mutator phenotype that is highly sequence-specific (Cheung et al. 2002; Kruisselbrink et al. 2008). As guanine-rich sequences may form guanine quadruplexes *in vivo* (van Kregten and Tijsterman 2014), DOG-1 and other repair factors likely function to resolve such DNA secondary structures and structures formed in the presence of inter-strand crosslinks (Cheung et al. 2002; Youds et al. 2006, 2008; Jones and Rose 2012). The helicase gene described in this work, *chl-1*, is related to *dog-1*, and the role of CHL-1 in guanine-rich sequences has not been explored in *C. elegans* prior to the work presented in this thesis.

As whole-genome sequencing technologies matured, the Rose lab continued its efforts to identify the *rec-1* gene by sequencing the strain which contained the *rec-1(s180)* mutation. A total of 441 single-nucleotide variants were identified in this strain compared to the wild-type isolate N2 (strain VC2010), with most variants mapping to Chromosome I, which confirmed the linkage of *rec-1* to this chromosome (Rose et al. 2010). In turn, O'Neil, Tam and Rose were able to determine that the altered recombination phenotype was associated more frequently with sequence variants on the *left* end of Chromosome I (N. O'Neil, A. H. T. Tam and A. M. Rose, unpublished data). RNAi against a candidate gene identified in this region only partly recapitulated the abnormal recombination phenotype (J. Chu, J. Luce, M. R. Jones and A. M. Rose, unpublished data), and this coding sequence, *y18h1a.7*, was selected by me as a candidate for targeted knockout using the emerging CRISPR-Cas9 technologies adapted for *C. elegans* (Friedland et al. 2013).

This thesis brings together several long-standing streams of research initiated by the Rose lab. First, it attempts to clarify the function of the iron-sulfur helicase CHL-1 in the context of genome instability and in relation to another iron-sulfur helicase, DOG-1. It then describes the meiotic double-strand break repair defect due to the loss of CHL-1 function in the *C. elegans* germline. Lastly, it wraps up the thirty-five-year hunt for the coding sequence of *rec-1*, a genetic determinant of double-strand break number and meiotic crossover distribution in *C. elegans.*

Chapter 2: CHL-1 provides an essential function affecting cell proliferation and chromosome stability in *Caenorhabditis elegans*

[A version of this chapter has been published in *DNA Repair* (Chung et al. 2011).]

2.1 Introduction

The stability of the genome is essential for normal development and survival in all organisms. Among the many factors that contribute to genome stability are several related helicases defined by the presence of an iron-sulfur domain (Fairman-Williams et al. 2010). There are four core members in this family: the XPD/RAD3 and CHL1/DDX11 helicases in metazoans and yeast, and the FANCJ/DOG-1 and RTEL1 helicases in metazoans (Fairman-Williams et al. 2010).

The XPD helicase (xeroderma pigmentosum D) functions in nucleotide excision repair and is a subunit in the $TF_{II}H$ complex. Patients with mutations in the encoding gene present with extreme sensitivity to ultraviolet exposure known as xeroderma pigmentosum, stemming from defects in the nucleotide excision repair pathway (Cleaver et al. 2009). Another well-studied member of this helicase family is the human FANCJ helicase (Fanconi anemia J) and its orthologue in *Caenorhabditis elegans*, DOG-1 (deletion of guanine-rich DNA). Defects in these helicases lead to heightened sensitivity to DNA interstrand crosslinks and the spontaneous deletion of guanine-rich DNA (Cantor et al. 2001; Cheung et al. 2002; Levitus et al. 2005; Levran et al. 2005; Litman et al. 2005; Youds et al. 2006; London et al. 2008; Youds et al. 2008; Kruisselbrink et al. 2008; Wu et al. 2008). Based on the directionality of these deletions, FANCJ/DOG-1 has been proposed to unwind secondary guanine structures during the replication of the lagging strand (Cheung et al. 2002). The mouse Rtel1 helicase (regulator of telomere

length) and its orthologues in humans (RTEL1) and *C. elegans* (RTEL-1) represent a third member of this helicase family. They control homologous recombination by disassembling recombination intermediates, and defects in their function result in shortened telomeres and increased meiotic recombination frequency (Ding et al. 2004; Barber et al. 2008; Youds et al. 2010; Uringa et al. 2011).

While much is known about the functions of these three helicases in the family, less is known about the biological function of CHL-1. The *CHL1* gene was first identified in yeast in a screen for mutants with decreased fidelity of chromosome transmission (Haber 1974; Gerring et al. 1990) and later shown to be required for sister chromatid cohesion (Skibbens 2004; Mayer et al. 2004; Petronczki et al. 2004; Xu et al. 2007) and the repair of methylmethane sulfonate-induced DNA lesions (Laha et al. 2006; Ogiwara et al. 2007). Impaired function in the mammalian orthologue ChlR1 (CHL1-related 1)/DDX11 (DEAD/H box polypeptide 11) led to defects in sister chromatid cohesion in mouse embryos (Inoue et al. 2007) and human cell cultures (Parish et al. 2006). Recently, it was shown that biallelic mutations in the human gene resulted in Warsaw breakage syndrome (WABS), a newly described genetic condition characterized by congenital abnormalities, abnormal skin pigmentation and severe growth retardation (van der Lelij et al. 2010; Capo-Chichi et al. 2013; Bailey et al. 2015). At the chromosomal level, this syndrome exhibited sister chromatid cohesion defects similar to the cohesinopathy observed in Roberts syndrome. In addition, *DDX11* mutant cells were sensitive to mitomycin C (MMC), a DNA interstrand crosslinking agent and camptothecin (CPT), a topoisomerase inhibitor. This sensitivity to replicative stress is similar to that observed in cell lines derived from Fanconi anemia patients (van der Lelij et al. 2010).

In biochemical assays, the human ChlR1/DDX11 ATPase-helicase co-immunoprecipitated with cohesin subunits (Parish et al. 2006). Furthermore, it has been found to possess directional specificity in its helicase function (Farina et al. 2008). Its function is also required for the efficient activity of the flap endonuclease Fen1, thus implicating ChlR1/DDX11 in the processing of the lagging strand during replication (Farina et al. 2008).

Beyond the characterization of *chl1*/*ChlR1/DDX11* mutant phenotypes and the biochemical characterization of the human ChlR1/DDX11 helicase, little is known about the function of this gene in a multi-cellular organism. *C. elegans* provides an excellent system for investigating the biological role of CHL-1. The genetic amenability of *C. elegans* allows me to explore its interaction with DOG-1, with which it shares homology and possible lagging-strand specificity. Here, I characterize the mutant phenotype of *chl-1* and describe a functional interaction with *dog-1* in maintaining genome stability.

2.2 Materials and methods

2.2.1 Bioinformatic analyses of iron-sulfur helicases

The amino acid sequences of the following helicases were obtained from the National Center for Biotechnology Information: from *Caenorhabditis elegans*, CHL-1 (accession number NP_499295.1), DOG-1 (accession number NP_493618.1) and RTEL-1 (accession number NP_492769.1); from humans, DDX11 (accession number NP_004390.3), FANCJ/BRIP1 (accession number NP_114432.2), RTEL1 (accession number CAC16223.1) and XPD/ERCC2 (accession number AAL48323.1); from *Mus musculus*, Ddx11 (accession number NP_001003919.1), Fancj (accession number NP_840094.1), Rtel1 (accession number AAI45659.1) and Ercc2 (accession number NP_031975.2); and from *Saccharomyces cerevisiae,*

CHL1 (accession number CAA39922.1) and RAD3 (accession number AAB64698.1). The *C. elegans* XPD-1 sequence was generated by Genewise 2.2.0 (Birney et al. 2004) using the human ERCC2/XPD amino acid sequence as the protein query and the genomic DNA sequence encompassing gene models *Y50D7A.11* and *Y50D7A.2* as the DNA query.

The helicase amino acid sequences were subject to multiple sequence alignment by Clustal using default parameters (Chenna et al. 2003). Using the Clustal alignment, a phylogenetic tree was inferred by the Maximum Likelihood method based on the JTT matrix-based model in the MEGA5 package (Jones et al. 1992; Tamura et al. 2011). The reliability of this phylogenetic tree was tested with 100 bootstrap replications (Felsenstein 1985).

The percentage similarity and identity between *C. elegans* CHL-1 and its orthologues were determined using the Needleman-Wunsch global pair-wise alignment algorithm with default parameters applied to the corresponding domains of each protein (Needleman and Wunsch 1970). The alignment program was run on the European Bioinformatics Institute server using the interface provided at the URL http://www.ebi.ac.uk/Tools/psa/emboss_needle/.

2.2.2 Strains and maintenance

Strains were maintained on *Escherichia coli* strain OP-50 as described by Brenner (Brenner 1974) or in liquid nitrogen frozen culture between experiments. The *chl-1(tm2188)* heterozygote was obtained from Shohei Mitani of the Japan National Bioresource Project. Several strains were obtained from the Caenorhabditis Genetics Center: JR667, which contains a seam-cell-specific green fluorescent protein transgene *wIs51[SCM::gfp, unc-119(+)] (V)* (Clucas et al. 2002); EG1285, containing a D-neuron-specific green fluorescent protein transgene *oxIs12[unc-47::gfp lin-15(+)]lin-15(n765ts)(X)* (McIntire et al. 1993b); CB879 *him-1(e879)*;

VC1245 with the genotype *+/hT2 (I); smc-3(ok1703)/ hT2[bli-4(e937) let(q782) qIs48(myo-2::gfp; pes-10::gfp; ges-1::gfp)]*; and MT5491 (genotype *nDf40 dpy-18(e364)/eT1[unc-36] (III); +/eT1 (V))*, with a deletion (*nDf40*) known to span the *m03c11.2* region. We generated strains KR5114 *chl-1(tm2188)/eT1 (III); wIs51/eT1 (V)*, strain KR5115 *+/hT2 (I); chl-1(tm2188)/ hT2[bli-4(e937) let(q782) qIs48] (III); wIs51 (V)*, strain KR4677 *chl-1(tm2188)/eT1 (III); +/eT1 (V); oxIs12 (X)*, strain KR5116 *+/hT2 (I); chl-1(tm2188)/ hT2[bli-4(e937) let (q782) qIs48] (III); oxIs12 (X)*, strain KR5117 *him-1(e879) dog-1(gk10)*, KR4681 *dog-1(gk10) (I); chl-1(tm2188)/eT1 (III); +/eT1 (V)*, and strain KR5118 *dog-1(gk10) (I); smc-3(ok1703)/eT1 (III); +/eT1 (V).* Additional *dog-1(gk10)*-containing double mutants were constructed and described previously by Youds *et al.* (2006) (Youds et al. 2006), using diagnostic PCR to determine the presence of the *dog-1(gk10)* allele.

Outcrossing of *tm2188* to VC2010 wild-type animals was done as follows. Initially, a spontaneous male with the genotype *chl-1/+* was crossed to a VC2010 hermaphrodite, and for 9 subsequent generations, the *chl-1* heterozygous male was mated with a VC2010 hermaphrodite. After 10 generations the *chl-1* heterozygous males were mated with an *eT1* translocation homozygote to balance the lethal. The strain, KR4676, has the genotype *chl-1(tm2188)/eT1[unc-36] (III); +/eT1 (V)*.

2.2.3 RNA isolation, cDNA synthesis and sequencing of the cDNA

Animals were grown on agar plates seeded with OP50 at 20°C for four days. Animals were then washed with M9 (22mM KH_2PO_4, 22mM Na_2HPO_4, 85mM NaCl, 1mM $MgSO_4$ at pH 6.0) and suspended in 4 mL of TRIzol® (Invitrogen) per 1 mL worms. Total RNA was extracted following the manufacturer's instructions.

The first-strand cDNA was synthesized from the total RNA with RevertAid™ H Minus M-MuLV Reverse Transcriptase (Fermentas), using the supplied oligo$(dT)_{18}$ as the primer and following the manufacturer's protocol. A portion of the *chl-1* cDNA was amplified using primers gsp4 (AAGAAGCGGAGCCTGAGC) and gsp5 (CTTGACTTGAGTGCGATCTCC) (see Figure 2.2a). The primers span the region known to be deleted by *tm2188*. The PCR amplification used 0.4 mM of each primer, with 1X PCR buffer (50mM Tris pH 8.3, 50mM KCl, 35µM Na_2HPO_4, 0.05% Tween-20), 2.0mM $MgCl_2$, 0.25 mM of each dNTP, and 1 unit of Taq polymerase (Applied Biological Materials). The PCR product was agarose-gel-purified using a QIAquick Gel Extraction Kit following the manufacturer's instructions and sent for sequencing at the NAPS facility at the University of British Columbia, Vancouver campus.

2.2.4 Visualization of cell nuclei

Staged one-day-old adults were picked into 10 µL of M9 buffer (22mM KH_2PO_4, 22mM Na_2HPO_4, 85mM NaCl, 1mM $MgSO_4$ at pH 6.0) and 200µl of 150 nM 4',6-diamidino-2-phenylindole dihydrochloride (DAPI, Sigma) dissolved in ethanol was added for 2 hours in a dark chamber. These animals were de-stained by soaking in M9 overnight at 4°C in a humid chamber. Stained animals were mounted on microscope slides. and visualized with a 20X objective on a Zeiss Axioplan 2 microscope fitted with a CoolSNAP HQ charge-coupled device (Photometrics). Image capture was done using Metamorph v6.1r6 software (Universal Imaging Corporation) and the merging of multiple microscopy images was done using Adobe Photoshop CS2 to accommodate objects larger than the field-of-view.

2.2.5 Visualization of GFP-labeled cells in live animals

Staged L1, L4 or adult animals were picked into in 20 µL of 20 mM levamisole on a microscope slide. A cover slip was applied after the animals became immobilized by the levamisole. Animals were then visualized with a 20X objective on a Zeiss Axioplan 2 microscope fitted with a CoolSNAP HQ charge-coupled device (Photometrics). Image capture was done using Metamorph v6.1r6 software (Universal Imaging Corporation) and the merging of multiple microscopy images was done using Adobe Photoshop CS2 to accommodate objects larger than the field-of-view.

2.2.6 Measurement of guanine tract deletions

The PCR-based detection of genomic deletions that originate from *vab-1* guanine tract was described previously (Youds et al. 2006). I followed this protocol, with the exception that I used ethidium bromide to stain the PCR products in the agarose gel in place of SYBR Green (Molecular Probes, Eugene, OR).

2.3 Results

2.3.1 *m03c11.2* is the *C. elegans* orthologue of *S. cerevisiae CHL1* and human *DDX11*

I identified *m03c11.2* as a gene whose conceptual translation had a high degree of similarity to the *Saccharomyces cerevisiae* Chl1 and the *Homo sapiens* DDX11 amino acid sequences (Figure 2.1a). Chl1 and DDX11 are DEAH-box helicases belonging to a subset of superfamily 2 (SF2) helicases defined by an iron-sulfur domain (Fairman-Williams et al. 2010). The predicted cysteine residues in the iron-sulfur domain and the conserved SF2 helicase motifs are shown in Figure 2.1a. The conceptual translation of *m03c11.2* is more similar to human

DDX11, mouse Ddx11 and yeast Chl1 than it is to other *C. elegans* iron-sulfur helicases or their orthologues (Figure 2.1b). I conclude that *m03c11.2* is the *chl-1* gene in *C. elegans*, orthologous to yeast *CHL1* and human *DDX11*.

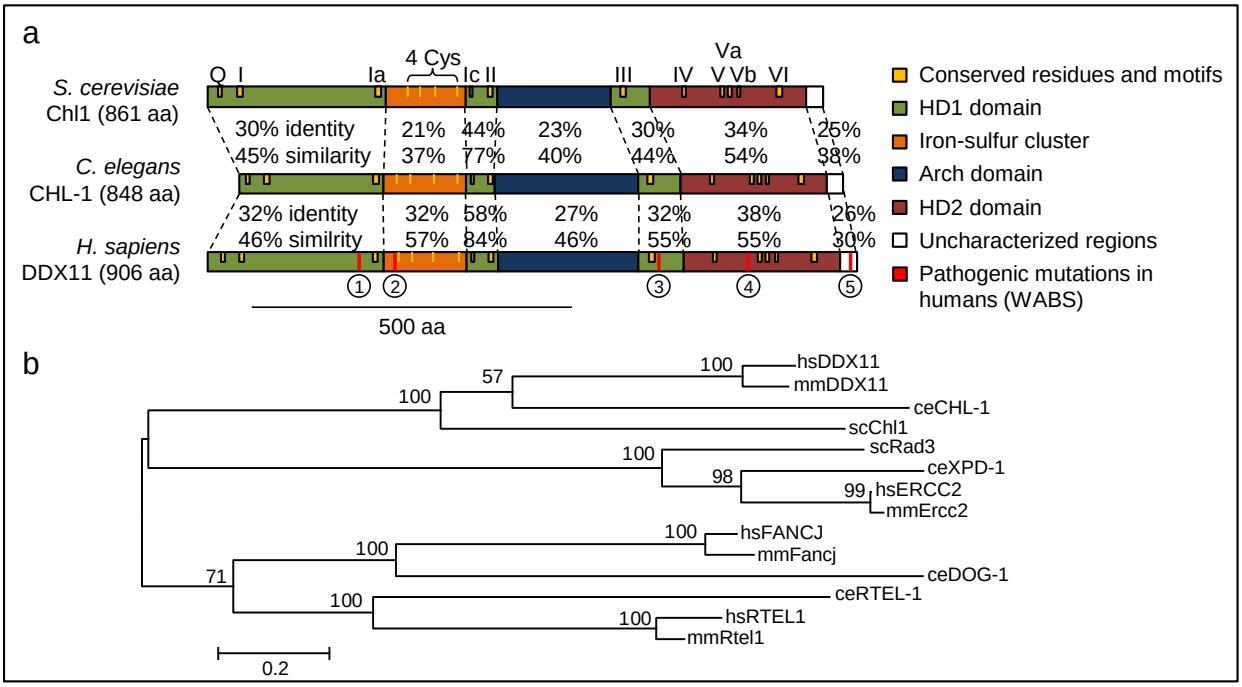

Figure 2.1: CHL-1 is the orthologue of the human DDX11 and *S. cerevisiae* Chl1.
a) The *C. elegans* CHL-1 has high sequence identity and similarity with Chl1 in *S. cerevisiae* and *H. sapiens* DDX11. Pathogenic alleles in Warsaw breakage syndrome (WABS) are numbered and indicated in red. 1) and 3) Missense mutation and frameshift deletion (Bailey et al. 2015). 2) Missense mutation (Capo-Chichi et al. 2013). 4) and 5) Frameshift due to splice site mutation, and in-frame deletion (van der Lelij et al. 2010). b) A bootstrapped phylogenetic tree representing the evolutionary histories of 14 iron-sulfur helicases from *C. elegans*, *S. cerevisiae* and *H. sapiens* based on Clustal multiple sequence alignment analysis. The tree is drawn to scale with the branch lengths measured in the number of substitutions per site.

2.3.2 *chl-1(tm2188)* homozygotes have germ-line abnormalities and are sterile

A deletion within the *chl-1* gene, *tm2188*, removes 845 base pairs from exon 7, exon 8 and the intervening intron (Figure 2.2a). Cloning and sequencing of the *chl-1* cDNA revealed that the *tm2188* deletion produces an mRNA transcript with exon 6 spliced to exon 9 (Figure 2.2b), leading to several missense codons and a premature stop codon. This resulting translation

is missing the entire HD2 domain and motif III in the HD1 domain. The missing motifs are known to aid in ATP binding and hydrolysis, in coordination between nucleic acids and ATP binding sites, and in nucleic acid binding (Fairman-Williams et al. 2010).

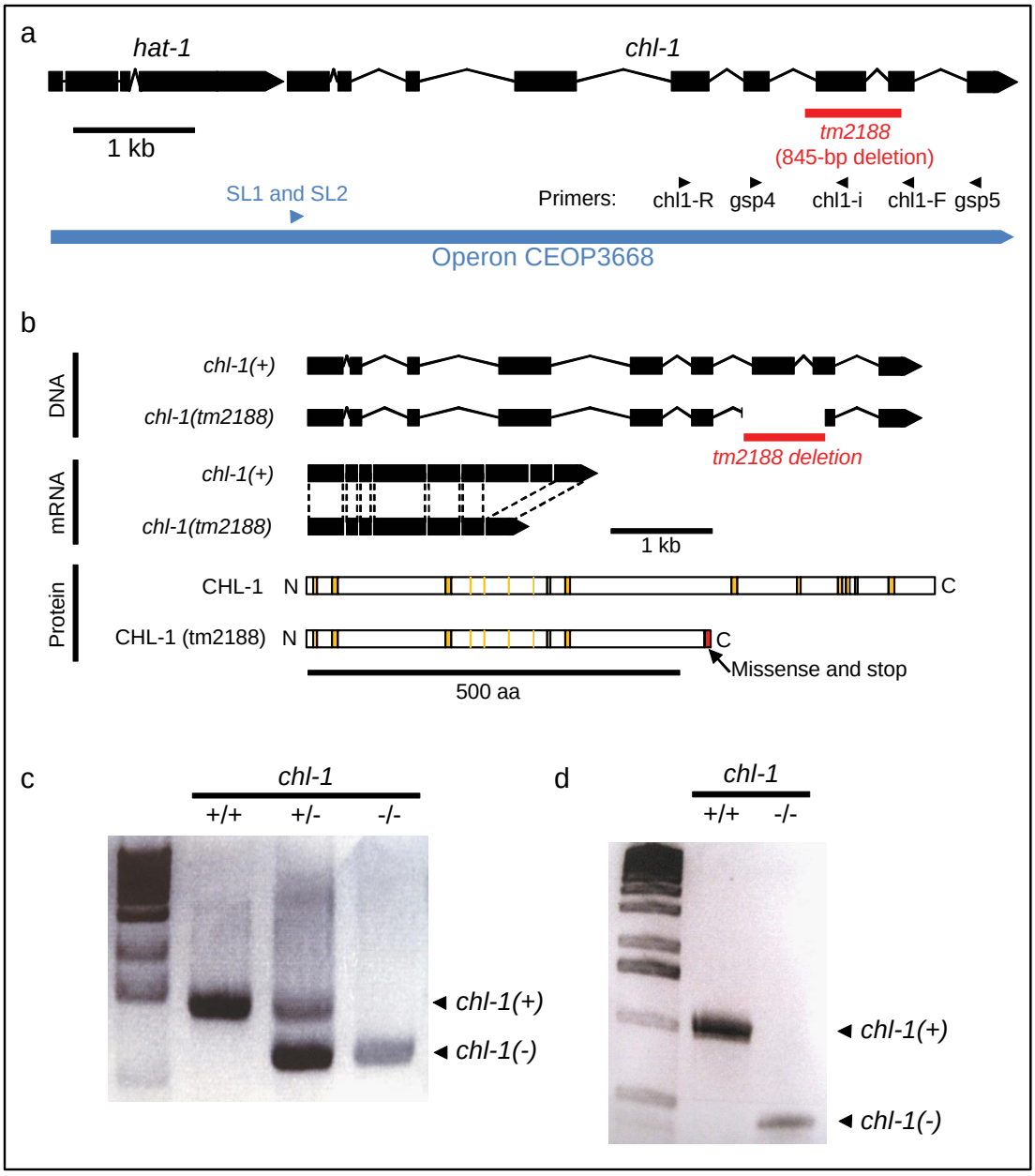

Figure 2.2: Molecular characterization of *chl-1*.
a) Genomic environs around the gene *chl-1* in *C. elegans*. The extent of the *tm2188* is shown. The gene *chl-1* is transcribed in an operon with *hat-1* (operon CEOP3668), with the transcript trans-spliced to SL1 and SL2 splice leaders. Primers chl1-R, chl1-i and chl1-F were used to

detect the presence of the *tm2188* deletion (see panel c), and primers gsp4 and gsp5 were used amplify cDNA to see the effects of *tm2188* (see panel d). b) Comparison of the wild-type *chl-1*, its transcript and its translation to *chl-1(tm2188)*. In yellow are conserved motifs, shown also in yellow in Figure 2.1a. c) The *tm2188* deletion can be detected by PCR using primers chl1-R, chl1-i and chl1-F. d) The *tm2188* deletion can be detected in the transcript by using primers gsp4 and gsp5. '-' indicates *tm2188* allele.

In order to characterize the phenotypes associated with *chl-1(tm2188)*, I used an outcrossed strain (KR4676) carrying the *tm2188* allele to eliminate confounding mutations generated in the mutagenesis (Gengyo-Ando and Mitani 2000). The strain is heterozygous for *chl-1(tm2188)* and segregates *chl-1(tm2188)* homozygotes, which are sterile and uncoordinated. Sterile-uncoordinated animals also appear in the F_1 when KR4676 is crossed with animals carrying *nDf 40,* a chromosomal rearrangement deleting *chl-1* (data not shown). Based on the analysis of the *tm2188* transcript and our genetic observations, I conclude that *tm2188* is a loss-of-function allele of *chl-1*.

All *chl-1(tm2188)* animals assayed are sterile and produce no embryos, consistent with the embryonic lethality observed by Piano *et al.* (Piano et al. 2002) after injection of dsRNA for the *m03c11.2* gene sequences. To determine the cause of sterility, we visualized germ-line nuclei after staining with 4',6-diamidino-2-phenylindole (DAPI). The *chl-1(tm2188)* gonad appears to have fewer cells, which suggests a proliferation defect in the gonad (Figure 2.3b). 13% of the homozygotes have only one gonad arm (Figure 2.3e). Most of the mutants (72%) have sperm (Figure 2.3b, arrowheads), but only 20% of the animals contain oocytes that developed as far as diakinesis. Despite having the limited ability to make mature sperm and oocytes that progress as far as diakinesis, all *chl-1* mutants assayed are sterile. This sterility is not rescued by crossing with wild-type males (data not shown). This suggests that the sterility of *chl-1* homozygotes is not limited to a problem intrinsic to the *chl-1* sperm.

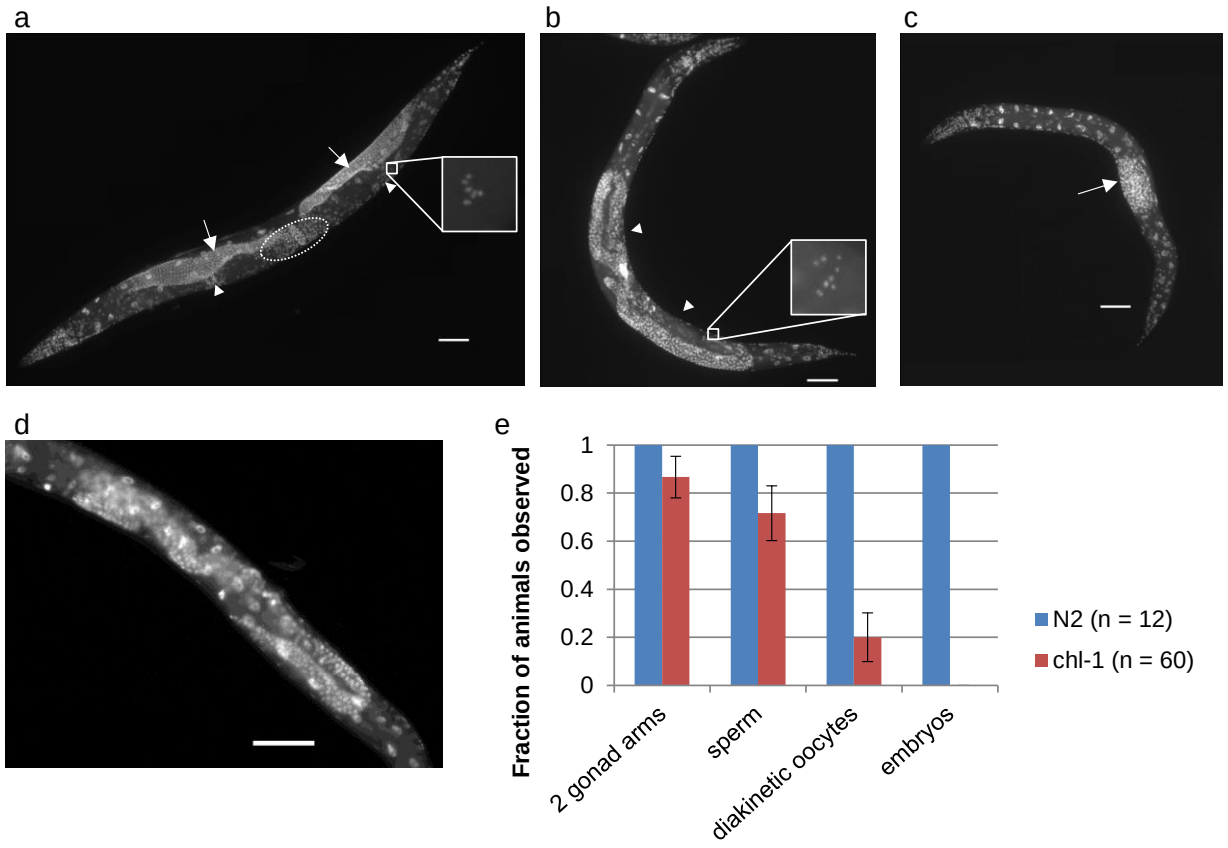

Figure 2.3: DAPI staining of the gonad reveals germline abnormalities in *chl-1* mutants. a) Wild-type gravid hermaphrodites have two gonad arms (arrows), six clearly visible DAPI spots per diakinetic oocyte (boxed, enlarged inset), sperm (arrowheads) and embryos (dotted circle). Embryos have never been observed in *chl-1* animals (b, c and d). b) A *chl-1* animal with more than six DAPI spots in a diakinetic oocyte (boxed, enlarged inset) and sperm (arrowheads). c) A *chl-1* animal with only one gonad arm, grossly deformed (arrow). d) Germline of a *chl-1* animal with no observable sperm, which usually show up as small, bright DAPI dots (see A and B arrowheads). Scale bar = 50 µm for A-D. e) A summary of the range of germline phenotypes associated with *chl-1(tm2188).* Error bars denote the 95% confidence intervals ($\mu \pm 1.96\ SE$).

The few diakinetic oocytes that are produced exhibit abnormal karyotypes (average 7.2 DAPI-staining bodies, ranging from 5 to 9, $n = 11$) that differ from the wild-type number of six DAPI-staining bodies (Figure 2.3b, boxed). The data are consistent with *C. elegans* mutants exhibiting chromosomal instability (CIN) as was originally observed for the chromosome-loss mutants in *S. cerevisiae*.

2.3.3 *chl-1(tm2188)* homozygotes have somatic cell loss

To determine if the uncoordinated (Unc) phenotype of *chl-1(tm2188)* mutants was due to cell proliferation defects, I examined the GABAergic D motor neurons (McIntire et al. 1993a, 1993b). Newly hatched larvae have 6 GABAergic D motor neurons posterior to the pharyngeal bulb and the number increases to 19 by the end of larval development (McIntire et al. 1993b). Using an integrated transgenic array *oxIs12* carrying a D-neuron-specific promoter fused to the coding sequence of green fluorescent protein, we scored the number of D neurons in *tm2188* homozygotes. Upon hatching, *chl-1(tm2188)* homozygotes have the same number of D neurons as wild-type animals (Figure 2.4a and c). By the adult stage, however, *chl-1* mutants have significantly fewer GFP-marked D neurons: 12 in the mutant, compared to 19 in wild-type animals ($p = 2.4 \times 10^{-13}$, Student's *t*-test; see Figure 2.4b and c).

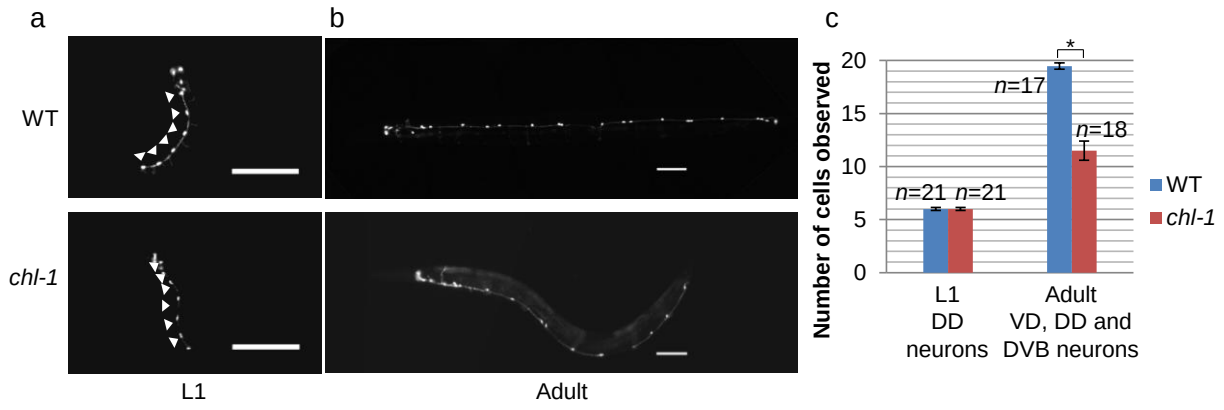

Figure 2.4: CHL-1 function is required for the proliferation of the D-neurons
a) The six DD neurons (arrowheads) can be seen in both wild-type and *chl-1* animals at L1. b) Some D neurons are missing in the adult *chl-1* animal (scale bar = 50 µm). c) A summary of the number of D neurons at various stages in the development of wild-type and *chl-1(tm2188)* animals. Error bars represent the 95% confidence intervals ($\mu \pm 1.96\ SE$). The number of D neurons in the adult *chl-1(tm2188)* animals is significantly fewer than the number of D neurons in adult wild-type animals ($p = 2.4 \times 10^{-13}$, Student's *t*-test).

To determine if the observed cell number reduction was lineage-specific, I examined the proliferation of seam cells using a seam-cell-specific GFP transgenic array *wIs51*. Early in development, wild-type animals and *chl-1* homozygotes had the same number of seam cells (10 cells per row). Later in development, *chl-1* homozygotes had an average of 13 seam cells per row compared to 16 in wild-type animals ($p = 8.6 \times 10^{-7}$, Student's *t*-test; see Figure 2.5b and c). Thus, the proliferation defects observed in *chl-1* mutants are not specific to only one cell type.

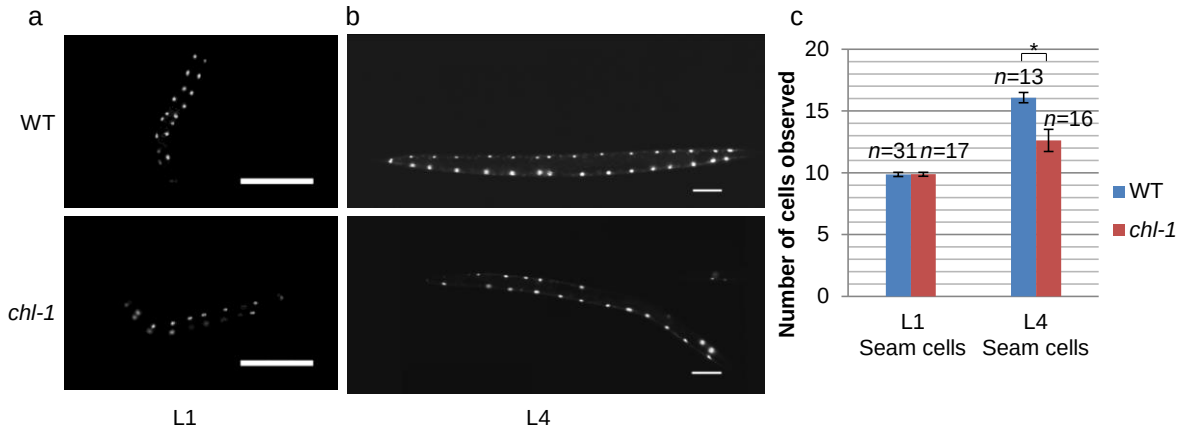

Figure 2.5: CHL-1 function is required for the proliferation of the seam cells
a) The 10 seam cells (one row of seam cells on each side of the worm) are visible in both wild-type and *chl-1* animals. b) Several seam cells are clearly missing in the L4 *chl-1* animal (scale bar = 50 µm). c) A summary of the number of seam cells per row at various stages in the development of wild-type and *chl-1(tm2188)* animals. Error bars represent the 95% confidence intervals $\mu \pm 1.96\ SE$. The number of seam cells in the L4 *chl-1* animals is significantly fewer than the number of seam cells in L4 wild-type animals ($p = 8.6 \times 10^{-7}$, Student's *t*-test).

The gonadal abnormalities and the reduction of germ-line nuclei (Figure 2.3) show that there are cell proliferation defects in both the germ line and the soma. In the soma, the cells affected are those that divide later in larval development (Sulston and Horvitz 1977). I interpret this result as a need for CHL-1 after hatching when the maternal contribution of *chl-1(+)* transcripts has been depleted.

2.3.4 The *tm2188* mutation increased G-tract instability in the absence of DOG-1

To further investigate the role of CHL-1 in *C. elegans*, I considered what was known about the mutant phenotypes of CHL-1 orthologues in other species. The human orthologue ChlR1/DDX11 appears to have a role in the lagging strand processing during replication (Farina et al. 2008), and the yeast *chl1* mutant is sensitive to methyl methanesulfonate-induced DNA damage (Laha et al. 2006; Ogiwara et al. 2007). Furthermore, it has been proposed that the related helicase in *C. elegans*, DOG-1, functions during lagging strand synthesis (Cheung et al. 2002), and in the absence of DOG-1 function, homologous recombination is required to suppress additional deletions originating from poly-guanine sites (G-tracts) (Youds et al. 2006). In this context, and considering the shared homology between *C. elegans* CHL-1 and DOG-1, I tested the possibility of functional overlap between these two helicases.

The DOG-1 helicase prevents spontaneous deletion of poly-guanine/poly-cytosine tracts (G-tracts) (Cheung et al. 2002). Using a PCR-based assay to detect deletions that originate from a poly-guanine tract in *vab-1*, I found that in 188 *dog-1* homozygotes tested, 13% had a detectable genomic deletion. I investigated if CHL-1 helicase function is redundant with DOG-1. Unlike in *dog-1(gk10)* mutants, I saw no guanine tract deletions in the 55 *chl-1(tm2188)* homozygotes (Figure 2.6) tested. The data indicate that CHL-1 function is not required for poly-guanine tract integrity when DOG-1 function is present and CHL-1 is not functionally redundant with DOG-1.

Next, we tested if CHL-1 contributed to genome stability in the absence of DOG-1. I observed an increase in the deletion frequency of the *dog-1(gk10); chl-1(tm2188)* double mutant. In 113 double mutants tested, 32% of the animals had a deletion, a two- to three-fold increase from *dog-1(gk10)* single mutants ($p = 0.0004$ with χ^2-test; Figure 2.6) compared to animals

heterozygous for *chl-1(tm2188)* and homozygous for *dog-1(gk10),* in which the deletion frequency was not significantly increased (p = 0.44 with χ^2-test; see Figure 2.6). The increase in guanine-tract deletions for *chl-1* homozygotes is similar to the increases observed for homologous recombination (HR) repair mutants [(Youds et al. 2006) and data not shown]. In this previous study, Youds *et al.* (Youds et al. 2006) showed that the deletion frequency increased with defects in HR and translesion-synthesis (TLS), but not non-homologous end-joining in a *dog-1(gk10)* mutant background. Based on the double mutant results, I observed that, similar to HR repair and translesion synthesis, CHL-1 functions to reduce the number of G-tract deletions generated in the absence of DOG-1.

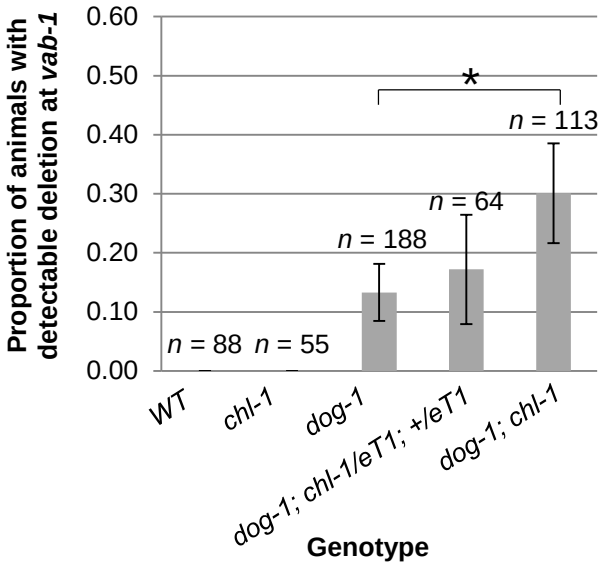

Figure 2.6: CHL-1 function is required for G-tract stability in the absence of DOG-1 function.
chl-1(tm2188) enhances the deletion frequency of *vab-1* in the *dog-1(gk10)* background (p = 0.0004 with χ^2-test). Error bars represent the 95% confidence intervals ($\mu \pm 1.96\ SE$).

2.3.5 Cohesin mutants enhanced the guanine tract instability

Given that yeast and mammalian Chl1 affect cohesion (Skibbens 2004; Mayer et al. 2004; Petronczki et al. 2004; Xu et al. 2007; Inoue et al. 2007; Parish et al. 2006; van der Lelij et al. 2010), I asked whether or not defects in cohesins would have an effect similar to *chl-1(tm2188)* on the guanine tract stability. One of the cohesin mutations we tested was the *e879* hypomorphic allele of *him-1*, which encodes an orthologue of the cohesin SMC1 (Chan et al. 2003). Although most alleles of *him-1* are lethal (Howell et al. 1987), the *e879* mutation, which maps near the 3' end of the gene (Chan et al. 2003), is not lethal but produces a high incidence of males (Him), an indicator of X-chromosome missegregation. Homozygous *him-1(e879)* animals did not produce detectable guanine tract deletions; however, 39% of the 132 *him-1(e879) dog-1(gk10)* double mutants tested had detectable deletions, a three-fold increase from 13% in *dog-1* single mutants ($p = 7 \times 10^{-8}$ with χ^2-test; Figure 2.7a).

A mutant in the related cohesin SMC-3, *smc-3(ok1703)*, was tested. Animals homozygous for the *ok1703* deletion allele are sterile and uncoordinated. In the *dog-1; smc-3* double homozygote, no increase in the guanine tract deletion frequency was observed over that in *dog-1* mutants (88 *dog-1; smc-3* animals tested; $p = 0.94$ with χ^2-test against *dog-1* single mutants). In animals homozygous for *dog-1(gk10)* but heterozygous for *smc-3(ok1703)*, 29% of 133 animals tested had deletions, a significant increase when compared with the *dog-1; dpy-18/eT1; unc-46/eT1* control ($p = 0.0005$ with χ^2-test; Figure 2.7b). In the *dog-1(gk10)* genetic background, the enhancement by *smc-3(ok1703)* heterozygotes was comparable to the hypomorphic allele of *him-1*. The *smc-3* heterozygotes were fertile with normal movement, but generated males at a higher incidence than normal, suggesting a semi-dominant phenotype (data not shown). The Him phenotype in the heterozygote may be a result of cohesion defects that

result in X-chromosome mis-segregation, as is the case for the *e879* allele of *him-1*. I conclude that defects in these cohesin components, like defects in the CHL-1 helicase, and HR and TLS repair functions, enhance G-tract deletion frequency in the absence of DOG-1.

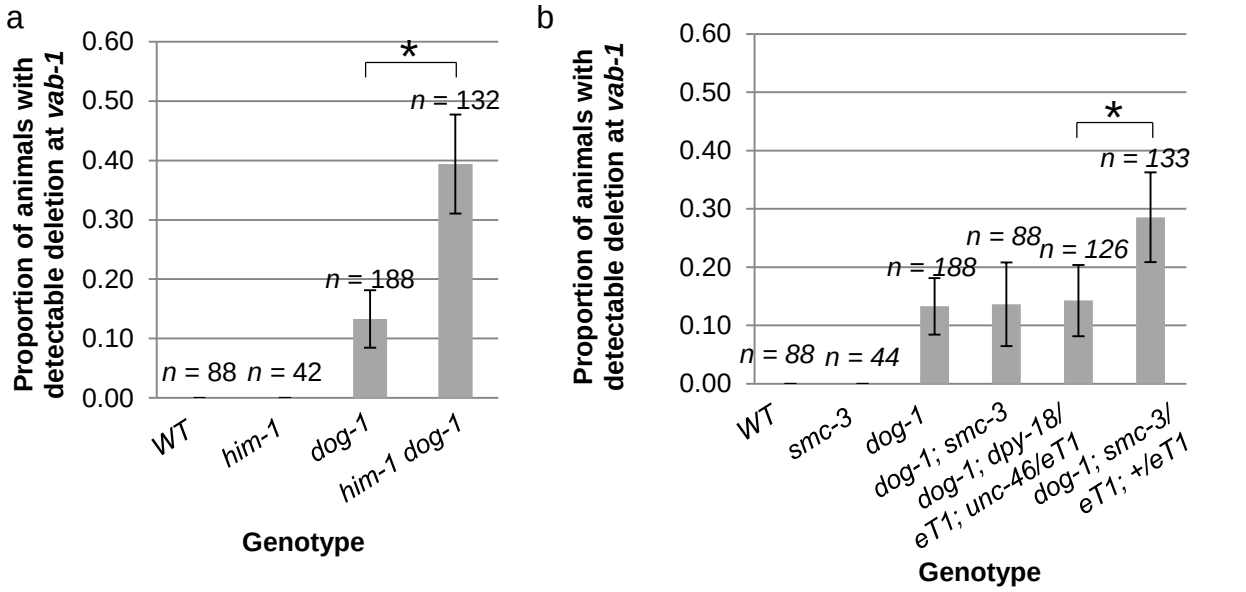

Figure 2.7: Cohesin genes interact with *dog-1*.
a) *him-1(e879)* enhances the deletion frequency of *vab-1* in the *dog-1(gk10)* background ($p = 7 \times 10^{-8}$ with χ^2-test). b) *smc-3(ok1703)*, in a heterozygous state, enhances the deletion frequency of *vab-1* in the *dog-1(gk10)* background ($p = 0.0005$ with χ^2-test). Error bars represent the 95% confidence intervals ($\mu \pm 1.96\ SE$).

2.4 Discussion

In this work, I have characterized the *Caenorhabditis elegans chl-1* gene and its loss-of-function phenotype. Without CHL-1 function, animals have proliferation defects in the soma and the germline. Chromosome instability can be observed in *chl-1* animals that have diakinetic oocytes. I have also shown that CHL-1 function is involved in preventing guanine tract deletions in the absence of DOG-1 function, which establishes *C. elegans* CHL-1 as an important player in the response to DNA secondary structures that perturb the replication machinery.

The *chl-1* mutant defects demonstrated by an abnormal number of DAPI spots during diakinesis are comparable to the chromosome instability originally described for yeast *chl1* mutants (Haber 1974; Gerring et al. 1990). In my DAPI staining assay, an excess number of DAPI signals at diakinesis may indicate meiotic pairing defects (Colaiácovo et al. 2003), sister chromatid cohesion defects (Pasierbek et al. 2003, 2001; Chan et al. 2003), or chromosome fragmentation (Adamo et al. 2008). A reduction in the number of DAPI signals could indicate chromosomal fusions (Ahmed and Hodgkin 2000) or the loss of both homologues of a homologous pair, possibly due to sister chromatid cohesion failure leading to missegregation events occurring over successive cell divisions. Taking into consideration what is known about the function of CHL-1 and its orthologues, I favour sister chromatid cohesion failure as the cause of the abnormal number of DAPI signals, even though I cannot fully exclude the possibilities that the loss of CHL-1 function may lead to meiotic defects, chromosome fragmentation, or chromosome fusion events.

I found that defects in both CHL-1 and cohesins affected guanine tract stability in the absence of DOG-1 function. CHL-1 and DOG-1 have been proposed to be involved in lagging strand functions during replication (Farina et al. 2008; Cheung et al. 2002). For DOG-1, the invariant directionality of the deletions originating from the guanine tract makes a strong case for a lagging-strand-dependent defect and Cheung *et al.* have proposed that guanine-rich DNA form secondary structures akin to guanine quadruplexes that hinder replication on the lagging strand (Cheung et al. 2002). For CHL-1, biochemical assays have shown that its human orthologue ChlR1/DDX11 enhances the activity of the flap endonuclease Fen1, which operates on the lagging strand (Farina et al. 2008). The genetic interaction results presented in this chapter

indicate that in the absence of DOG-1 function, CHL-1 and cohesins play a role the repair or the error-free bypass of DNA secondary structures at guanine-rich sequences.

Replication blocks can arise from DNA-altering agents such as methyl methanesulfonate (MMS), and these replication blocks require homologous recombination to resolve (Lundin et al. 2005). As yeast *chl1* mutants are defective in homologous recombination and thus sensitive to MMS (Laha et al. 2006; Ogiwara et al. 2007), it may be possible that *C. elegans chl-1* mutants are defective in a mechanism that resolves replication blocks posed by guanine secondary structures. It was previously shown that homologous recombination repair and translesion synthesis are required to repair an appreciable proportion of lesions left by the lack of DOG-1 function (Youds et al. 2006). Here, I propose the additional involvement of CHL-1 and the core cohesins in this process.

Species-specific phenotypes have been observed in different genetic models. The *C. elegans chl-1(tm2188)* mutants exhibit sterility unlike *Saccharomyces cerevisiae chl1* mutants, which are viable (Gerring et al. 1990). This difference can be reconciled in the following way. The cell cycle progression delay exhibited by *chl1* yeast cells (Gerring et al. 1990) can be compensated by slowing down the cell cycle, while a similar delay in the multi-cellular *C. elegans* is not tolerated due to the tight control of cell divisions and cell fate in development (Sulston et al. 1983; Sulston and Horvitz 1977). Thus, *chl1* yeast cells exhibit a less dramatic phenotype. The *C. elegans chl-1* mutant phenotype is more similar to other multicellular animals such as mouse, where *ChlR1/Ddx11*$^{-/-}$ mutants are inviable (Inoue et al. 2007). The *C. elegans* phenotypes provide insight into the consequence of replicative defects that persist over multiple cell divisions in a multi-cellular organism.

Similarities between DDX11/CHL-1 function in humans and *C. elegans* make *C. elegans* a useful model system. In humans, mutation in the orthologous gene results in the severe condition of Warsaw breakage syndrome. In one case of bi-allelic mutation, the paternal allele resulted in deletion of a lysine residue near the C terminus resulting in an unstable protein and the maternal allele caused a frameshift. Cell lines derived from this individual were sensitive to intrastrand crosslinks (ICLs), the topoisomerase inhibitor camptothecin and had sister chromatid cohesion defects. ICL repair involves coordination of nucleotide excision, homologous recombination and translesion synthesis repair [reviewed in (Deans and West 2011)]. Genes in both systems appear to respond to DNA damage during replication. *C. elegans* guanine tracts are likely to form secondary structures similar to guanine quadruplexes (G4) in humans and may act in an analogous fashion to ICLs in hindering the progression of the replication fork as proposed by Youds *et al.* (Youds et al. 2006). In the absence of secondary structure resolution by the DOG-1/FANCJ helicase, repair pathways such as homologous recombination and translesion synthesis are required to prevent additional problems that may occur either as small intrachromosomal deletions or as larger interchromosomal rearrangements (Zhao et al. 2008). Evidence from yeast (Skibbens 2004) and humans (van der Lelij et al. 2010) and now *C. elegans* indicate that in addition to the known HR and TLS repair components, cohesins and CHL-1 are required. Investigation of CHL-1 function in *C. elegans* provides an opportunity to study its role in a living animal model amenable to experimental manipulation.

Chapter 3: The function of CHL-1 helicase in the meiotic germline of *C. elegans*

3.1 Introduction

CHL1 was initially described by Haber and Hieter groups as a gene required for proper mitotic chromosome transmission in the budding yeast *Saccharomyces cerevisiae* (Haber 1974; Gerring et al. 1990). In addition to mitotic chromosome loss phenotypes in yeast, (Skibbens 2004; Mayer et al. 2004; Petronczki et al. 2004; Xu et al. 2007; Rudra and Skibbens 2013), mitotic chromosome loss has also been observed in the soma of mice (Inoue et al. 2007) and humans (van der Lelij et al. 2010; Capo-Chichi et al. 2013) lacking the function of Chl1. Furthermore, factors that co-immunoprecipitate with the Chl1 orthologues are generally associated with DNA replication: factors such as Fen1 (Farina et al. 2008), RPA (Farina et al. 2008), PCNA (Farina et al. 2008), the Ctf18-RFC complex (Farina et al. 2008), Timeless (Leman et al. 2010) and Tipin (Leman et al. 2010). Although current models have not been able to explain precisely how the helicase activity is required for proper chromatid cohesion, the emerging models suggest that orthologues of Chl1 unravel secondary structures at or near the replication fork (Bharti et al. 2014), interacting with cohesins directly (Parish et al. 2006) and perhaps influencing their loading and acetylation (Rudra and Skibbens 2013). This appears to be the role of Chl1 and its orthologues in actively replicating, mitotic cells.

In contrast to their well-established mitotic functions, Chl1 and its orthologues have not been extensively tested for any meiotic functions. In *Caenorhabditis elegans*, mRNA-based expression data support a role for CHL-1 in the gonad: *chl-1* mRNA can be detected by *in situ* hybridization (with probes derived from clone ‘576a7’, accessed from the NEXTDB expression

database by the Kohara lab, National Institute of Genetics, Mishima, Japan) and by microarrays (using a comparison between wild type and mutants lacking gonads) (Reinke and Cutter 2009). Additionaly, in Chapter 2, I determined that *C. elegans* CHL-1 had a role in ensuring a normal diakinetic karyotype. The interpretation of this result, however, could be confounded by the presence of both mitotic and meiotic cells in the *C. elegans* gonad (see 2.4 Discussion). Extra diakinetic bodies as revealed by 4',6-diamidino-2-phenylindole (DAPI) could indicate partial defects with cohesion establishment (Chan et al. 2003; Pasierbek et al. 2003), pairing (Phillips et al. 2005), synapsis (Colaiácovo et al. 2003), SPO-11-induced double-strand break formation (Dernburg et al. 1998), or the repair of broken DNA (Alpi et al. 2003).

In order to further investigate the mitotic and meiotic functions of CHL-1, I examined the *chl-1* mutant germline phenotype in finer detail. First, by determining the localization of RAD-51 (Alpi et al. 2003), I would determine if the germline double-strand breaks were present, and if so, if the repair of such breaks were compromised by a lack of CHL-1 function. A defect in the repair of double-strand breaks in the germline could in theory be genetically reversed by additionally inactivating SPO-11, whose activity is required for the generation of meiotic double-strand breaks (Dernburg et al. 1998). To complement this functional analysis, I attempted to determine the localization of the CHL-1 protein by constructing an epitope-tagged allele of *chl-1* using the newly developed CRISPR-Cas9 techniques.

3.2 Materials and methods

3.2.1 Strains used

Strains were maintained on agar seeded with *Escherichia coli* (strain OP50) as described (Brenner 1974) or in cultures frozen in liquid nitrogen between experiments. Animals with the

tm2188 allele were derived from mutants generated by the lab of Shohei Mitani of the Japan National Bioresource Project, as described in Chapter 2.

Strain AV106 (Dernburg et al. 1998) was obtained from the Caenorhbaditis Genetics Center (CGC, College of Biological Sciences, University of Minnesota), and the *spo-11(ok79)* mutation was re-balanced over the GFP-marked translocation *nT1[qIs51]* (Edgely et al. 2006; Fernandez et al. 2012) to yield KR5229 *spo-11(ok79)/nT1[qIs51] (IV); +/nT1 (V).* The *spo-11(ok79)* homozygotes were identified by a lack of GFP expression (indicating the absence of *nT1[qIs51]*). The *chl-1(tm2188)* mutation was crossed into KR5229 to yield KR5316 *chl-1(tm2188)/+ (III); spo-11(ok79)/nT1[qIs51] (IV); +/nT1 (V).* The *chl-1(tm2188); spo-11(ok79)* double homozygotes were identified by a lack of GFP expression (indicating the absence of *nT1[qIs51]*) and the uncoordinated phenotype conferred by *chl-1(tm2188)* (see Chapter 2).

Injections of CRISPR-Cas9 were done in VC2010, a fully sequenced, Bristol N2 wild type sub-culture kept at the Moerman Gene Knockout Lab at the University of British Columbia (Flibotte et al. 2010). The resulting mutation (*h2877*) was genetically balanced over the reciprocal translocation balancer *hT2[qIs48] (I; III)* to make strain KR5345. This strain, due to the GFP markers (*myo2::GFP, pes-10::GFP, ges-1::GFP*) and lethal mutations linked to the translocation (Edgely et al. 2006; Fernandez et al. 2012), segregated only GFP-positive *h2877* heterozygotes and GFP-negative *h2877* homozygotes.

3.2.2 Immunofluorescence and laser scanning confocal microscopy

Rabbit polyclonal antibodies raised against *C. elegans* RAD-51 were obtained from Novus Biologicals (Novus #29480002) and directed against the RAD-51 epitopes in dissected and fixed adult hermaphrodite gonads. Briefly, 1-day post-L4 animals were treated with 10 mM

levamisole in phosphate-buffered saline (PBS, with 10 mM PO_4^{3-}, 137 mM NaCl, 2.7 mM KCl, pH 7.4) and cut open with needles to allow the gonad arms to extrude from the body. Extruded gonads were fixed for 1 hour at room temperature with 1% formaldehyde (m/m) in PBS. After 3 washes with PBS with 1% Tween-20 (v/v), gonads were submersed in methanol at -20°C for 3 hours. After 3 subsequent washes with PTwB (PBS with 1% Tween-20 [v/v] and 0.5% bovine serum albumin [m/m]), gonads were incubated with the αRAD-51 antibodies (1 μg/mL diluted with PTwB) at 4°C overnight. After 3 additional washes with PTwB, the gonads were incubated with DyLight 488-conjugated polyclonal goat anti-rabbit antibodies (Novus NBP1-72944, at 2 μg/mL in PTwB) for 1 hour at room temperature. Unbound antibodies were washed away with 3 final rounds of PTwB, with the last round also containing 5 μg/mL of 4',6-diamidino-2-phenylindole (DAPI). The gonads were then mounted on a glass slide with Fluoroshield mounting medium (Sigma F6182) for laser scanning confocal microscopy.

Laser scanning confocal microscopy was performed on a Zeiss Axiovert 200M inverted microscope with the LSM5 Pascal laser setup (courtesy of the Moerman lab, University of British Columbia) or the Olympus FV1000 MPE laser scanning confocal microscope (courtesy of the Bioimaging Centre, University of British Columbia). Stained gonads were viewed and imaged with 60x objectives, and images were taken so that a single pixel of the image was smaller than half the optical resolution of the 60x lens (the Nyquist limit). The Δz (the spacing between each optical slice) was set at 0.5 μm or smaller to capture the chromosomal structures. The gonad was imaged fully from top to bottom, typically ranging from 10 to 20 slices (5 μm to 10 μm) in thickness depending on variability in the tissue preparation.

Microscopy images were traced onto transparency films for the counting of αRAD-51 foci. The length of the gonad was divided into 7 zones – from the distal tip to the bend of the

gonad arm, immediately before the point at which diplotene and diakinetic oocytes appear and where the nuclei pack less tightly. The number of αRAD-51 foci was then recorded for each nucleus and tallied over 2 gonad arms per genotype.

3.2.3 Construction of pGC1, a gene conversion template for the haemagglutinin epitope-tagged *chl-1* transgene

The generation of polyclonal antisera against the wild type CHL-1 was unsuccessful. The N-terminus of CHL-1 was expressed in *E. coli* driven by a lactose-inducible promoter in the plasmid pGEX-5X-3 (GE Life Sciences). The resulting insoluble, overexpressed protein, sent as acrylamide gel slices to Thermo Scientific Pierce facilities, failed to generate a reactive antiserum from the test rabbit (data not shown). Attempts were then made to incorporate a haemagglutinin epitope tag in CHL-1 at the N-terminus.

pGC1 was a 16,444-bp plasmid constructed from pCFJ151 (Addgene #19330), originally designed for the template-directed integration of transgenes using *Mos1*-mediated single-copy insertion (*Mos*SCI) developed by Frøkjaer-Jensen *et al.* (Frøkjaer-Jensen et al. 2008). Briefly, pCFJ151 was doubly digested by *Xho*I and *Afl*II (New England Biolabs) according to the manufacturer's recommendations. It was purified with a silica column (QIAquick PCR Purification Kit, Qiagen #28106) to rid the mixture of buffering salts, short DNA fragments and restriction enzymes.

In addition, two blunt-end PCR products were generated using Phusion polymerase (New England Biolabs) and two primer pairs C1+, C2- and C3, C6- (Figure 3.1a and Appendix B). The first amplicon contained the haemagglutinin epitope tag and the sequences upstream of *chl-1* - including up to 1000 base pairs upstream of *hat-1,* a gene with which *chl-1* shares transcription

control (Allen et al. 2011). The second amplicon contained the haemagglutinin epitope tag, the *chl-1* coding region, and the 3' UTR.

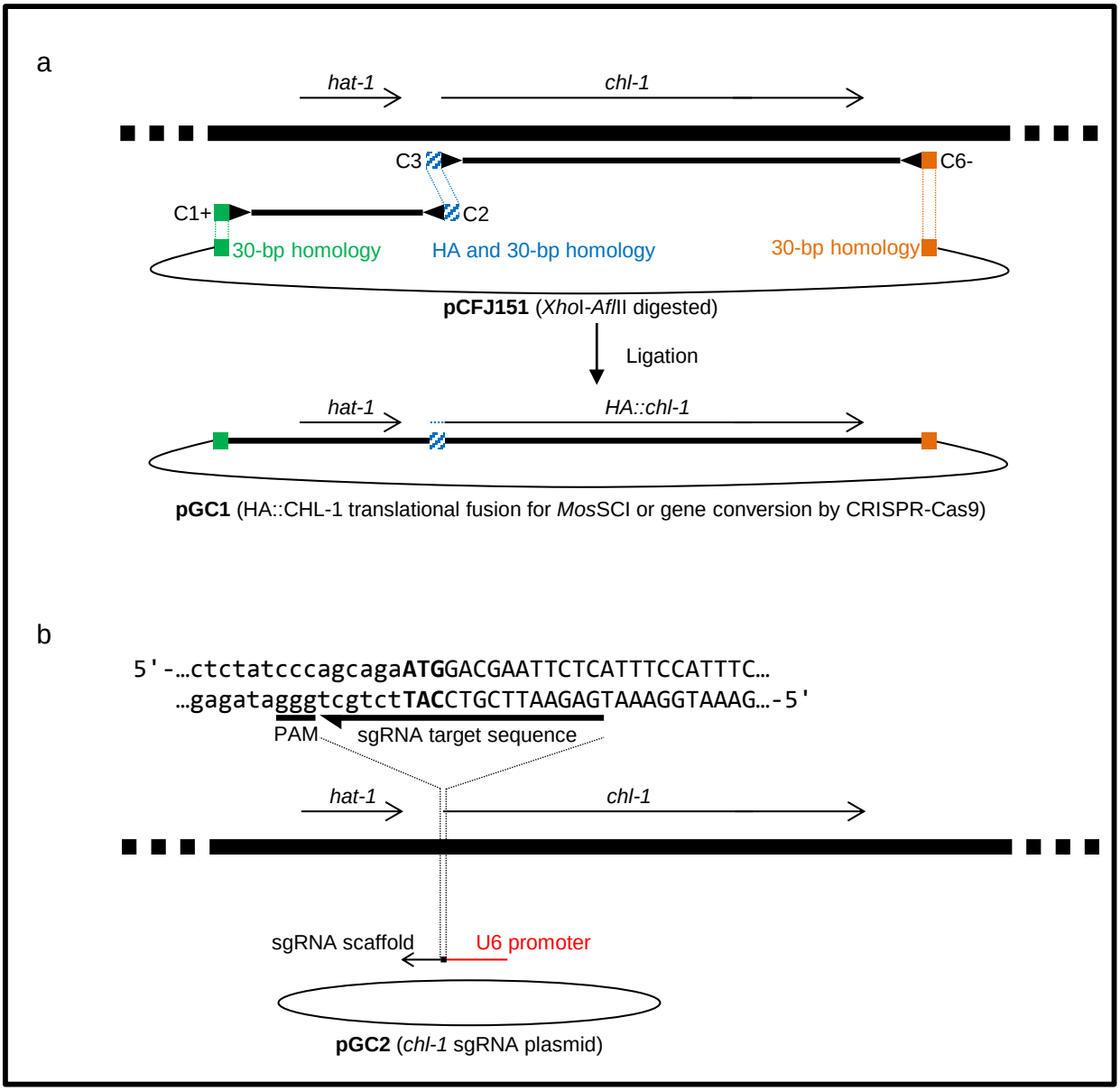

Figure 3.1: Design of gene conversion template and sgRNA for the addition of a haemagglutinin tag at the 5' end of *chl-1*.
a) The gene conversion template for the addition of haemagglutinin contains full-length coding sequences of *hat-1* and *chl-1*. This is so the conversion template might be used for MosSCI in a future experiment. b) The sgRNA target sequence in relation to the start codon (bolded) and the protospacer adjacent motif (PAM) sequence.

The purified plasmid fragment was subsequently ligated to the two blunt-end PCR products using a mixture of dNTPs (Applied Biological Materials), T5 exonuclease, Phusion polymerase and *Taq* ligase (New England Biolabs) following a single-step, isothermal protocol developed by Gibson *et al*. with an hour-long incubation at 50°C (Gibson et al. 2009). All three DNA fragments possess 30-nucleotide homologies with adjacent fragments to ensure ligation into a functional plasmid. Following the ligation reaction, the unpurified mixture was used to transform DH5α *E. coli* cells (Invitrogen) selected for resistance to 100 μg/mL of ampicillin on agar. DNA from single ampicillin-resistant colonies was prepared by alkaline lysis-silica column purification (QIAprep Spin Miniprep Kit, Qiagen), digested and Sanger-sequenced to isolate the clone containing pGC1.

At the time of the experiments, the use of relatively short, single-stranded DNA as a template for gene conversion following CRISPR-Cas9 had just been developed (Zhao et al. 2014; Arribere et al. 2014). Double-stranded DNA as a template for gene conversion (or more precisely, wholesale integration of transgenes) had also been developed by at least one group (Dickinson et al. 2013), although the mechanics of mutant selection differ from this work. The decision to use the pGC1 as a double-stranded gene conversion template allowed the possibility that of using pGC1 in single-copy genome integration via *Mos*SCI (Frøkjaer-Jensen et al. 2008).

3.2.4 Selection of the sgRNA target

The haemagglutinin epitope tag (HA) was engineered at the 5' end of *chl-1* using an sgRNA target close to the *chl-1* start codon. The target, 5'-GAGAATTCGTCCATTCTGCT-3' followed by 5'-GGG-3' protospacer adjacent motif [PAM (Mojica et al. 2009)] on the anti-sense

strand of *chl-1*, was chosen so that the repair template pGC1 and potential gene-converted *chl-1* would not be recognized by the sgRNA (Figure 3.2).

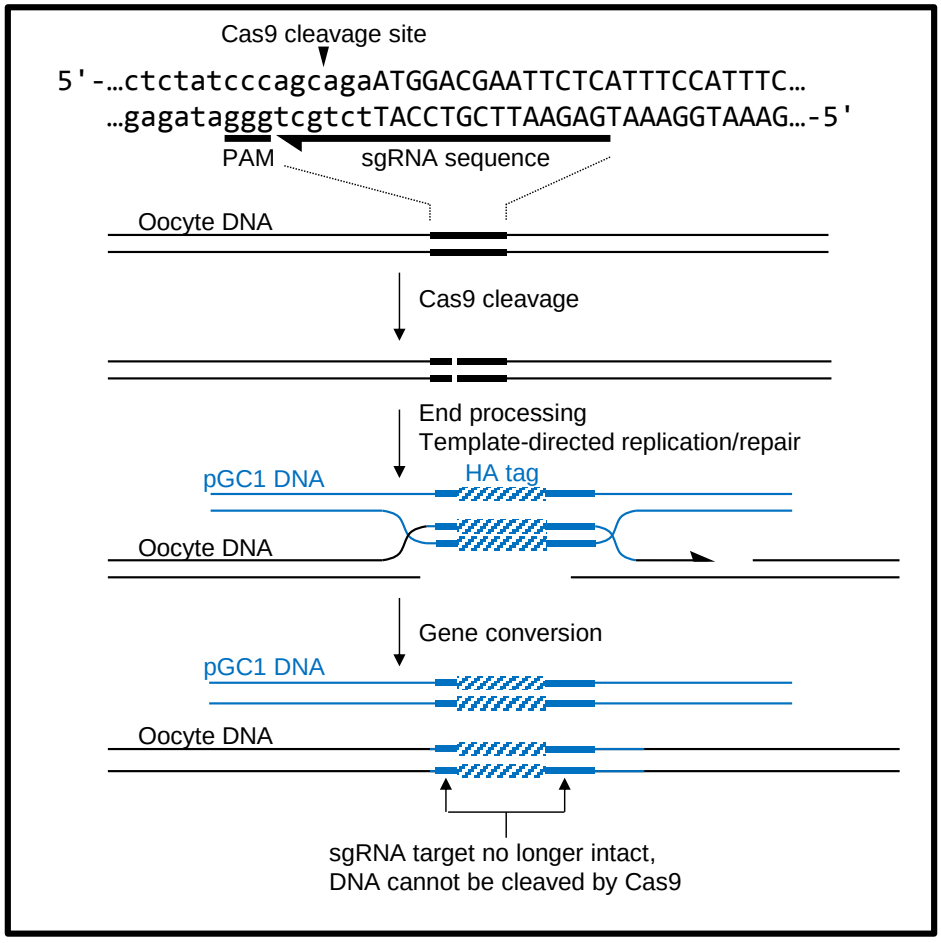

Figure 3.2: Proposed gene conversion mechanism to insert the haemagglutinin (HA) tag

3.2.5 Construction of the pGC2, a plasmid with *chl-1*-targeting sgRNA

Plasmid pGC2 encoded a synthetic sgRNA gene targeting *chl-1* based on a plasmid constructed by Friedland *et al.* (Addgene #46169) (Friedland et al. 2013). Briefly, with the *unc-119* sgRNA plasmid as a template, two fragments of the pGC2 were generated by using PCR with primer pairs chl-5'-sgRNA+ and AmpR1(-), and chl-5'-sgRNA- and AmpR1(+) (Appendix B). Primers chl-5'-sgRNA+ and chl-5'-sgRNA- contain the 20-bp *chl-1* target sequence

(gagaattcgtccattctgct and reverse complement) which replaces the *unc-119*-specific sequence on the template. The two PCR fragments were then ligated using the single-step, isothermal protocol developed by Gibson *et al.* by an incubation at 50°C with dNTPs, buffering salts, T5 exonuclease, Phusion polymerase and *Taq* ligase (New England Biolabs) (Gibson et al. 2009). Following the ligation reaction, the unpurified mixture was used to transform DH5α *E. coli* cells (Invitrogen) selected on 100 μg/mL ampicillin agar. DNA from single ampicillin-resistant colonies was prepared by alkaline lysis followed by column purification (QIAprep Spin Miniprep Kit, Qiagen), restriction-mapped and Sanger-sequenced to identify the colony containing the desired plasmid pGC2.

3.2.6 Microinjection of transgenic DNA and screening for gene conversion events

A total of 71 N2 hermaphrodites (P_0 generation) were injected with a mixture comprised of 47.5 ng/μL of the Cas9 endonuclase plasmid [constructed by Friedland *et al.*(Friedland et al. 2013), Addgene #46168], 1 ng/μL of pGC1, 45 ng/μL of pGC2, and co-injection markers pPD118.20 at 2.5 ng/μL (containing *myo-3::gfp*, Addgene #1592) and pPD118.33 at 5 ng/μL (containing *myo-2::gfp*, Addgene #1596). The successfully injected P_0 animals were then identified by the presence of GFP-positive F_1s. At the time of the injections, results from Zhao *et al.* indicated that gene conversion events could be identified in both marked F_1 animals as well as its unmarked siblings (Zhao et al. 2014); I therefore decided to screen marked F_1s (GFP-positive) as well as their unmarked siblings (GFP-negative), which totalled 125 F_1 animals.

The F_1 animals were plated individually during egg-laying, after which they were individually treated with lysis buffer (30 mM Tris pH 8,100 mM NaCl, 0.7% Tween 20 and 100 μg/ml proteinase K) at 57°C for 1 hour to extract the DNA and then at 95°C for 15 minutes to

inactivate the proteinase K. This mixture was used for PCR without further purification. Genotyping was done with PCR using 3 primers: a *chl-1*-specific primer (geno3), a primer that binds upstream of *hat-1* but not to pGC1 (geno2) and an HA-specific primer (geno2) (Table 3.1 and Appendix B). The geno1-geno3 amplicon (~3600 bps) would be present regardless of the gene conversion event as both primers bind to the wild type genomic DNA. This acted as a positive control for the PCR reaction. The geno1-geno2 amplicon (3084 bps) would only be present if the gene conversion was successful. To ensure that primer geno2 bound to HA-tagged *chl-1* and was competent for PCR, I performed an additional reaction with C1+(trunc) (Table 3.1 and Appendix B).

The F_2 progeny of successfully gene-converted F_1s would be genotyped for homozygosity of the HA epitope tag. Additionally, the F_2 animals were screened for the sterile-uncoordinated (Stu) phenotype, which is the loss-of-function phenotype of *chl-1* (See Chapter 2).

Template and primers	PCR products of		
	C1+(trunc) geno2	**geno1 geno2**	**geno1 geno3**
Wild type genomic DNA 		None observed	3591 bps (observed)
pGC1 DNA 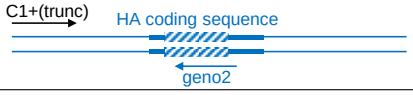	3049 bps (observed)		
Genomic DNA after gene conversion at *chl-1* (hypothetical) 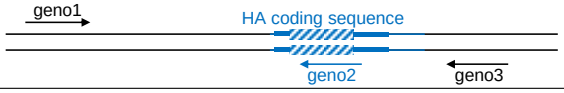		3084 bps (predicted)	3621 bps (predicted)

Table 3.1: Primers used in a PCR-based screen for HA-tagged *chl-1*

3.2.7 Detection of the breakpoints of the rearrangement

I determined that the CRISPR-Cas9 protocol used here led to a chromosome rearrangement involving *chl-1* (see 3.3 Results) rather than the intended insertion of an HA tag to the 5' end of *chl-1*. This rearrangement was designated as *h2877*. A series of primers were

designed to produce overlapping PCR amplicons in an attempt to identify the nature of *h2877* (Figure 3.3 and Appendix B). Individual *h2877* homozygotes were treated with lysis buffer (30 mM Tris pH 8,100 mM NaCl, 0.7% Tween 20 and 100 μg/ml proteinase K) at 57°C for 1 hour to extract the DNA and then at 95°C for 15 minutes to inactivate the proteinase K. This mixture was used for PCR without further purification. In total, 18 reactions were attempted, 12 of which also on wild type DNA from N2 animals (Figure 3.3). Reactions whose predicted wild-type products were less than 1000 bps were performed using 0.4 mM of each primer in a *Taq* polymerase mix (50 mM Tris at pH 8.3, 50 mM KCl, 35 μM Na_2HPO_4, 0.05% Tween-20, 2.0 mM $MgCl_2$, 0.25 mM of each dNTP, and 1 unit of *Taq* polymerase [Advanced Biological Materials]) and the program "CO_55" (94°C for 4:00; then 34 rounds of 94°C for 0:30, 55 °C for 0:30, and 72°C for 1:00; ending with 72°C for 10:00). Reactions whose predicted wild-type products were between 1000 and 1500 bps were performed using a *Taq* polymerase mix (same as above) and the program "CO_55_15" (94°C for 4:00; then 34 rounds of 94°C for 0:30, 55 °C for 0:30, and 72°C for 1:30; ending with 72°C for 10:00). Reactions whose predicted wild-type products exceeded 1500 bps were performed using a Phusion polymerase mix (1× HF buffer, 200 μM of each dNTP, 0.5 μM of each primer, and 0.4 units of Phusion polymerase) and the program "PHU6K55" (98°C for 0:30; then 36 rounds of 98°C for 0:10, 55 °C for 0:30, and 72°C for 4:00; ending with 72°C for 10:00).

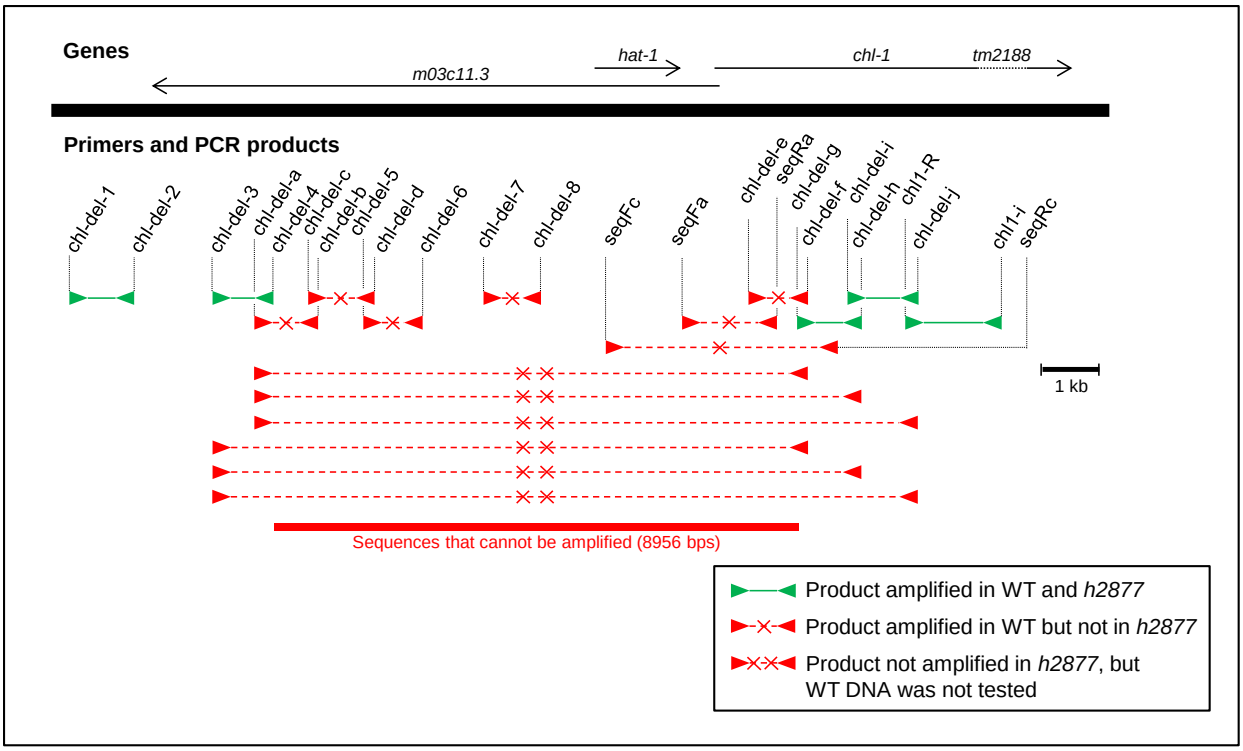

Figure 3.3: Relative genomic positions of the PCR primers in this study.
These are designed to detect the breakpoints of the rearrangement generated from the CRISPR-Cas9 protocol (see sections 3.2.3 to 3.2.6) targeted against *chl-1*

3.3 Results

3.3.1 CHL-1 function is required in the germ line for the timely repair of DNA double-strand breaks

A central part of the meiotic program of a maturing gamete is the DNA double-strand break initiated by the SPO-11 protein. Various enzymatic activities then expose a stretch of single-stranded DNA, and Rad51 and Dmc1 orthologues make these ends amenable to strand invasion and the eventual meiotic recombination [Reviewed in (Keeney et al. 2014)]. Given the importance of this process in the germline and the goal to uncover potential meiotic functions for CHL-1, I chose to examine the dynamics of DNA breakage in closer detail in *chl-1(tm2188)* mutants. The *C. elegans* RAD-51 protein, an orthologue of the *Saccharomyces cerevisiae* Rad51,

marks the sites of DNA double-strand breaks in the germ line (Alpi et al. 2003). The number of DNA breaks and the efficiency at which their repair takes place was inferred by staining the *C. elegans* gonad with anti-RAD-51 antibodies.

The gonad arm was divided into seven segments of roughly equal longitudal length. The number of RAD-51 foci per nucleus in each successive region was then determined, corresponding to the progression of oocyte nuclei maturation. In wild-type animals, the average number of foci per nucleus increases as nuclei progress from mitotic replication to early meiosis (Figure 3.4a-b) due to the action of the SPO-11 protein which generates DNA double-strand breaks necessary for meiotic crossovers (Dernburg et al. 1998). As the DNA double-strand breaks resolve into meiotic crossovers and non-crossovers, the number of foci per nucleus decreases (Figure 3.4a-b).

The *chl-1(tm2188)* mutants show a different anti-RAD-51 staining pattern. There is an increased number of RAD-51 foci throughout both the mitotic and the meiotic gonad (Figure 3.4c-d), indicating that there is a higher number of RAD-51-associated double-stranded DNA breaks per nucleus, and a larger proportion of nuclei (80% compared to 30% in wild type) did not completely resolve these breaks by the end of gonad segment examined (zone 7). As the DNA double-strand breaks could originate from SPO-11 activity or from un-repaired DNA damage in the mitotic region of the gonad, I eliminated the meiotic source of DNA double-strand breaks by crossing in the *spo-11(ok79)* mutation.

Mutations in *chl-1*and *spo-11* have opposing effects on the number of meiotic double-strand breaks in the germline. Wild-type CHL-1 is required for the timely repair of double-strand breaks (DSBs) generated by SPO-11. While knocking out *chl-1* greatly increased the number of DSBs in the germline compared to wild-type germlines (Figure 3.4a-d), additionally knocking

out *spo-11* reduces the number of DSBs in the meiotic germline of *chl-1(tm2188)* mutants (Figure 3.4c, d, g, h); however, there is still an elevated number of DSBs in the early, mitotic zones of the germline in *chl-1(tm2188)* and *chl-1(tm2188); spo-11(ok79)* mutants compared to wild-type and *spo-11(ok79)* mutants (cf. Figure 3.4c-d vs a-b; g-h vs. e-f), which may indicate mitotic, replicative problems encountered by germline nuclei in the absence of CHL-1 function.

Aside from the DSB numbers in the meiotic germline, *chl-1* and *spo-11* have independent phenotypic effects. Like *chl-1(tm2188)* single mutants and unlike *spo-11(ok79)* single mutants, *chl-1(tm2188); spo-11(ok79)* double mutants do not lay eggs. The sterility due to a lack of CHL-1 function is thus unrelated to the excess number of unrepaired, SPO-11-mediated DSBs seen in Figure 3.4c-d. Also like *chl-1(tm2188)* single mutants and unlike *spo-11(ok79)* single mutants, *chl-1(tm2188); spo-11(ok79)* double mutants are uncoordinated, indicating that the somatic defects due to a lack of CHL-1 function are not affected by SPO-11 function.

3.3.2 The CRISPR-Cas9 protocol failed to generate a gene-converted HA-tagged *chl-1*, but instead disrupted the gene

I attempted to knock-in a haemagglutinin epitope tag at the *chl-1* locus. I sought to use the newly developed CRISPR-Cas9 techniques to generate a targeted double-strand break at the 5' end of *chl-1*. This break would then be repaired in a template-dependent manner, resulting in a haemagluttinin-tagged *chl-1* [*HA::chl-1*, see Figure 3.2]. Several variations on this transgene-templated gene conversion scheme have been developed and refined much further by several other *C. elegans* labs (Dickinson et al. 2013; Arribere et al. 2014; Zhao et al. 2014).

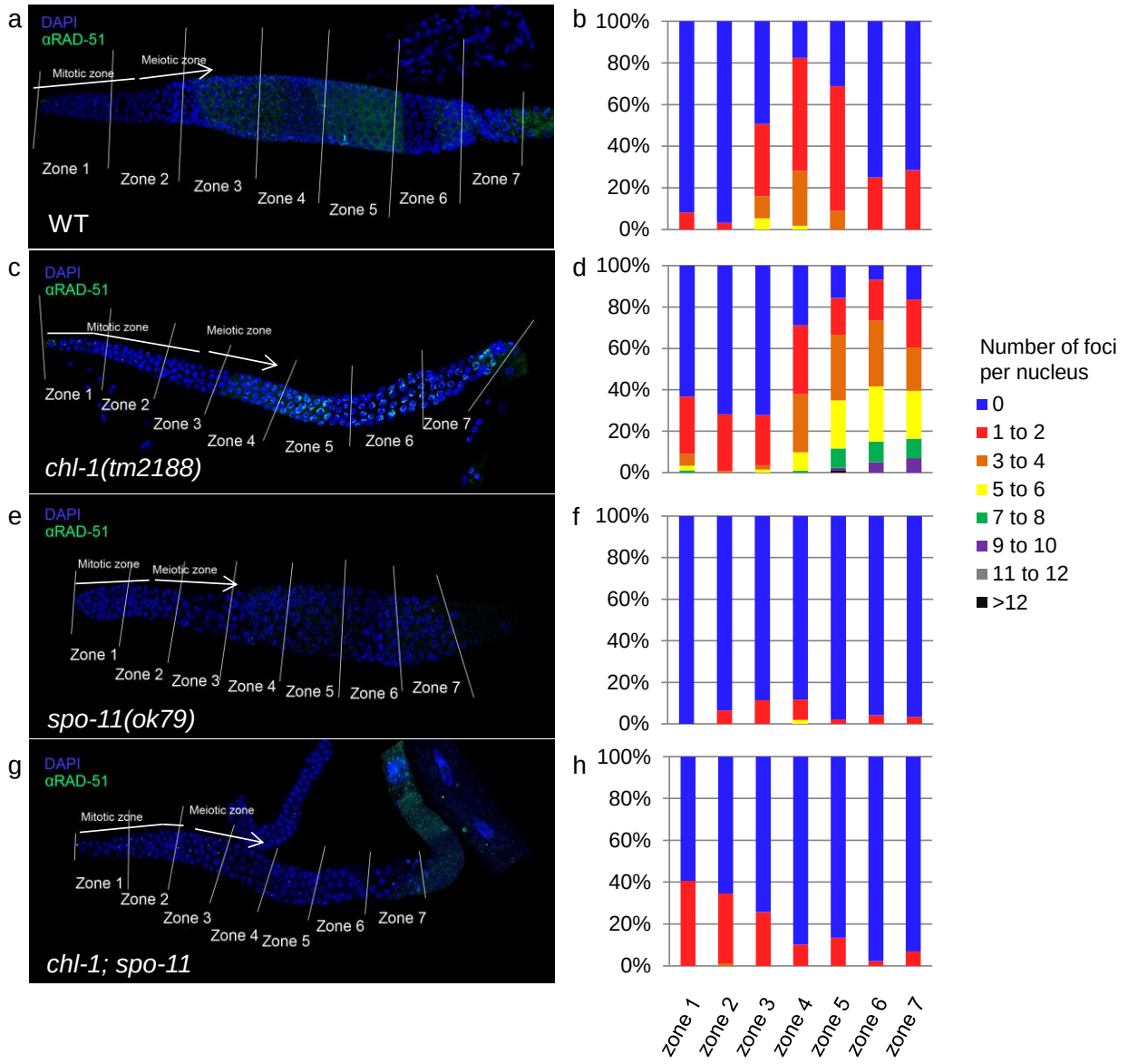

Figure 3.4: RAD-51 foci dynamics are altered in *chl-1(tm2188)* mutants.
With functional SPO-11 and CHL-1, RAD-51 foci accumulation peaks in the middle of the germline (roughly corresponding to mid-pachytene) (a and b). Without functional CHL-1, RAD-51 foci numbers are higher, and persist into zone 7, roughly corresponding to late pachytene (c and d). Without functional SPO-11, very few RAD-51 foci were observed (e and f). Without functional SPO-11 and CHL-1, there was an increase in the proportion of nuclei with one or two RAD-51 foci in zones 1-3, but the number of RAD-51 foci remains otherwise low thereafter (g and h). There is slide-to-slide variability on the apparent background staining of the anti-RAD-51 antisera outside the nuclei (*e.g.* a and g), and these do not appear to affect the formation of the nuclear foci counted here.

None of the 125 F_1 animals screened after microinjection showed any signs of HA integration. However, one of these animals gave rise to sterile-uncoordinated (Stu) progeny that phenocopied the *chl-1(tm2188)* homozygotes. Cytological analyses revealed that these Stu animals also had abnormal diakinetic karyotypes similar to *chl-1(tm2188)* homozygotes (data not shown). This indicated that a mutation, perhaps in *chl-1*, had occurred. This mutation, *h2877*, was balanced by the GFP-marked translocation balancer *hT2[qIs48]*, and the resulting strain was named KR5346, with the putative genotype *+/hT2[qIs45] (I); stu(h2877)/hT2 (III)*. This strain predictably segregated GFP-marked, superficially wild type animals and non-GFP Stu animals.

3.3.3 The *h2877* mutation failed to complement *chl-1(tm2188)*

To determine if the new *h2877* mutation disrupted the *chl-1* gene, males from KR4676 (*+/+ [I]*; *chl-1[tm2188]/eT1 [III]; +/eT1 [V]*) were mated to hermaphrodites from KR5345 (*+/hT2[qIs48] [I]; stu[h2877]/hT2 [III]; +/+ [V]*) for 2 days. Mated hermaphrodites were plated individually and checked for the presence of male F_1s, which indicating a successful cross. As the KR5345 hermaphrodite would naturally give rise to Stu progeny from a self-cross, non-GFP Stu F_1 animals were checked for the presence of the paternal *tm2188* allele by PCR (with primers chl1-F, chl1-R and chl1-I, see Figure 2.2). This revealed that the non-GFP Stu F_1 animals had all inherited a copy of *tm2188*, indicating that they were outcross animals with the genotype *+/+ (I); (h2877)/chl-1(tm2188) (III); +/+ (V)*. More importantly, this meant that *h2877* failed to complement *chl-1(tm2188).*

3.3.4 The *h2877* mutation is a chromosomal rearrangement which disrupted other coding sequences in addition to *chl-1*

As the generation of small indels was documented previously in worms subject to CRISPR-Cas9 treatments (Friedland et al. 2013), an initial attempt was made to amplify the DNA sequence of *h2877* homozygotes using primers seqFa and seqRa, which flank 5' end of the *chl-1* gene (the site of targeted DNA break by CRISPR-Cas9) (Figure 3.3 and Appendix B). When the PCR with the *h2877* template failed but the PCR with the wild-type template succeeded, another attempt was made using primers seqFc and seqRc, placed much further apart on the genome, still with the same result (Figure 3.3). This suggested that *h2877* could in fact be a much larger chromosome rearrangement.

An additional 10 reactions were carried out on both wild type-derived and *h2877* homozygote-derived genomic DNA. Reaction products from 800 to 1500 bps were observed from the wild-type template, but not from the *h2877* template. The reactions which failed with *h2877* template DNA all fell within a 9-kb range, indicating that the *h2877* lesion disrupted the DNA sequence from *m03c11.3* to *chl-1* (Figure 3.3, red with a single '×'). Thus, the two breakpoints of the *h2877* lesion appeared to be located

(a) Between the primer sequences of chl-del-4 and chl-del-c and

(b) Between the primer sequences of seqRa and chl-del-g.

To test if *h2877* were a simple deletion with these breakpoints, I attempted reactions on the *h2877*-derived genomic template using all 6 combinations of primers chl-del-3, chl-del-a, chl-del-f, chl-del-h and chl-del-j. If *h2877* were a deletion, these reactions would be expected to give PCR products. None of these 6 reactions worked (Figure 3.3, red with two ×s), so *h2877* may be a chromosomal rearrangement more complex than a simple deletion. Taken together,

these PCR assays determined that coding sequences between *m03c11.3* and *chl-1* were affected by the *h2877* lesion. These PCR assays, however, were unable to determine the nature of the *h2877* lesion or its precise breakpoints.

3.4 Discussion

In this chapter, I describe the requirement of CHL-1 function in the *C. elegans* germline for the timely resolution of SPO-11-induced double-strand breaks. Compared to wild-type animals, *chl-1(tm2188)* mutants have an increased number of SPO-11-induced double-strand breaks which appear to be persistent in the meiotic germline. The timely resolution of these DSBs may be linked to the promotion of sister-chromatid cohesion by CHL-1. Homozygotes for a temperature-sensitive mutation in *smc-3*, which encodes an SMC subunit of cohesin, also show an increased number of persistent SPO-11-induced DSBs in the meiotic germline (Baudrimont et al. 2011).

By using a *spo-11* mutation, I was able to test if the excess number of DNA double-strand breaks made by SPO-11 was responsible for the sterility phenotype seen in *chl-1(tm2188)* mutants. The inability of *chl-1(tm2188)* or *h2877* homozygotes to produce any embryos suggests the possibility that cell progression in the germ line has stopped completely. Normally, an excess number of breaks induced by either SPO-11 or ionizing radiation could trigger the DNA damage response, arresting cells in the germline (Gartner et al. 2000; Garcia-Muse and Boulton 2005). In the *chl-1(tm2188)* mutant, germ cell nuclei accumulate unresolved DNA double-strand breaks marked by RAD-51 (Figure 3.4c-d). However, with an additional mutation in *spo-11* lowering the total number of RAD-51-marked double-strand breaks (Figure 3.4g-h), *chl-1(tm2188); spo-11(ok79)* animals still failed to produce embryos. This suggests that even without the DSBs

generated by SPO-11, a lack of CHL-1 function was sufficient to arrest developing oocytes. The modestly elevated number of RAD-51 foci in the mitotic region of the *chl-1(tm2188)* germ line, therefore, could be indicative of the replicative problems encountered by the replicating nuclei in the absence of CHL-1 function.

Also in this chapter, I describe the fortuitous knock-out of *chl-1* in an attempt to generate an epitope-tagged allele using the emerging technique of CRISPR-Cas9. This knock-out allele *h2877* disrupted the 5' end of the *chl-1* gene and failed to complement the *tm2188* allele with respect to the sterility and the uncoordinated movement phenotypes. With this result, I showed that both *tm2188* and *h2877* were loss-of-function alleles of *chl-1*.

CRISPR is an emerging technique for *C. elegans* genetics – while many groups have reported success with the technique for generation of small indels, only a handful have reported success with gene conversion/transgene integration with the technique. Fewer yet have described larger or more complex rearrangement. The *h2877* allele represented a cryptic chromosomal rearrangement whose exact sequence structure could not be determined at this time. The available data suggested that there was a loss of sequence information in the coding sequence *m03c11.3* (lack of PCR product from chl-del-a and b, c and d, e and f, 5 and 6, and 7 and 8) and in *chl-1* (lack of PCR product from seqFa-seqRa, seqFc-Rc, and chl-del-e and f). For *hat-1*, the PCR assays did not determine whether or not it was disrupted, only that it was simply no longer next to *chl-1*. Additionally, combinations of chl-del-3, chl-del-a, chl-del-f, chl-del-h and chl-del-j could not amplify any sequence, so *h2877* was likely not a simple 9-kb deletion. Short of obtaining a genomic sequence, brood analysis of the unbalanced heterozygote (*h2877/+*) could help eliminate certain other possibilities such as inversions or translocations.

In Chapter 4, I will describe the generation of small deletion alleles of the *rec-1* gene using CRISPR-Cas9. Most of these deletion alleles contained repair signatures which appeared consistent with non-homologous end-joining (NHEJ) events (see Figure 4.2), with deletion breakpoints bound by small stretches of homology ranging from 1 to 5 base pairs. This suggests that NHEJ is active when Cas9 generates the DSB. Thus, to improve knock-ins by CRISPR-Cas9, it may be necessary to suppress the NHEJ machinery in order to promote the incorporation of the knock-in sequence by homologous recombination repair (Ward 2015). However, this viewpoint is being challenged by recent results from the Tijsterman group (Leiden University Medical Center) that DNA polymerase θ (POLQ-1 in *C. elegans*) may be mediating the repair process after the Cas9-induced DSB rather than NHEJ (van Schendel et al. 2015). Thus, a more thorough understanding of DSB repair is still needed to make predictable genome edits through CRISPR-Cas9 protocols.

Chapter 4: REC-1 and HIM-5 distribute meiotic crossovers and function redundantly in meiotic double-strand break formation in *Caenorhabditis elegans*

[A version of this chapter has been published in *Genes and Development* (Chung et al. 2015).]

4.1 Introduction

DNA double-strand breaks (DSBs) are one of the most deleterious lesions to our genome, yet are induced during meiosis to promote the exchange of genetic material between homologous chromosomes. Accordingly, generation of meiotic DSBs is tightly regulated by kinases and is coordinated with cell cycle progression to ensure their proper timing and repair in order to generate meiotic crossover events (Lui and Colaiácovo 2013; Baudat et al. 2013; de Massy 2013; Keeney et al. 2014). Although meiotic crossover events are distributed non-randomly along the chromosome in many taxa (Brenner 1976; Kaback et al. 1989; Oliver et al. 1992; Kliman and Hey 1993; Barnes et al. 1995; Nachman and Churchill 1996; Yu et al. 2001; Solignac et al. 2007; Ross et al. 2011; Giraut et al. 2011), the precise mechanism by which crossover distribution patterns are established remains poorly understood.

In the self-fertilizing hermaphrodite *C. elegans*, autosomes have highly recombinogenic arms flanking lowly recombinogenic centers (Barnes et al. 1995). Moreover, crossover interference across the autosomes is almost complete, resulting in a single crossover event per homologue pair in most meioses (Hodgkin et al. 1979; Zetka and Rose 1995; Meneely et al. 2002; Hillers and Villeneuve 2003; Nabeshima et al. 2004; Lim et al. 2008; Gabdank and Fire 2014). A recessive mutation in the *rec-1* gene randomizes the distribution of the meiotic recombination events while preserving crossover interference such that an increased crossover

frequency in the autosomal centers is accompanied by a decreased crossover frequency in the autosomal arms (Rose and Baillie 1979; Zetka and Rose 1995). While the total number of crossover events remains unaltered at one per homologue pair, their position differs dramatically between mutant *rec-1* and wild type. Notably, *rec-1* was the first locus described in *C. elegans* to exert such genetic control of the meiotic crossover pattern without perturbing crossover interference. Because of this altered recombination phenotype and the absence of any additional effects on development or fecundity (Rattray and Rose 1988), mapping of *rec-1* by conventional linkage analysis was not possible, and the identity of *Caenorhabditis elegans rec-1* remained unknown for more than 30 years after the description of its mutant phenotype. This is in contrast with several other *C. elegans* loci which, while exerting a similar genetic control over the meiotic crossover distribution as *rec-1*, were initially identified on the basis of severe meiotic non-disjunction phenotypes – such as *xnd-1* (Wagner et al. 2010) and *him-5* (Hodgkin et al. 1979; Meneely et al. 2002, 2012) – or on the basis of *a priori* knowledge of the gene product or function – such as *slx-1* (Saito et al. 2012, 2013).

In this study, I determined the molecular identity of *rec-1* using whole-genome sequencing data (Rose et al. 2010). With this, I was able to generate putative *rec-1* alleles using genome-editing techniques in *C. elegans*. Genetic analysis of a putative *rec-1* phospho-mutant transgene revealed a critical role for phosphorylation in patterning meiotic crossovers *in vivo*. Furthermore, genetic analysis of *rec-1* and *him-5* mutants revealed that they share limited functional redundancy with respect to double-strand break formation. Thus, my data highlight an evolutionary and functional relationship between *rec-1* and *him-5* in the generation of meiotic DSBs and their distribution on meiotic chromosomes.

4.2 Materials and methods

4.2.1 Worm strains used

Unless otherwise noted, strains were kept at 20°C on NGM agar seeded with *E. coli* strain OP50 as previously described (Brenner 1974). BC313 *rec-1(s180) (I)*was isolated as described (Rose and Baillie 1979). Additional mutations in *rec-1* were generated by directed mutagenesis using CRISPR-Cas9 protocols described previously (Friedland et al. 2013). Strains with transgenic *rec-1* alleles were generated by the Boulton lab (Crick Institute) using *Mos*I-mediated single-copy insertion (*Mos*SCI) (Frøkjær-Jensen et al. 2008) by microinjection into Unc-119 segregants from strain EG6699 (*ttTi5605 [II]; unc-119[ed3] [III]; oxEx1578).* This strain was obtained from the Caenorhabditis Genetics Center (CGC), funded by NIH Office of Research Infrastructure Programs (P40 OD010440). The two *him-5* mutant isolates used in our study *(e1490* and *ok1896)* were characterized previously (Meneely et al. 2012) and archived at the CGC. Additional strains and their genotypes are listed in Appendix A.

4.2.2 Reagents for microinjection

Plasmid originated from the Calarco lab (Friedland et al. 2013) were requested from Addgene (Addgene ID 46168 and 46169, respectively). The remaining reagents and the overall protocol were largely based on the work of Friedland *et al.* (Friedland et al. 2013) with the following modifications. The sgRNA target sequence was changed to 5'-GAACTGGATAACTGGCCGGC-3', found on the anti-sense strand in the second exon of *rec-1*. The construction of this new sgRNA plasmid was done in an analogous manner as described in 3.2.5.

Co-injection markers, *myo-2::GFP* (GFP expressed in pharyngeal muscle) and *myo-3::GFP* (body wall muscle), came from the Fire lab and used in lieu of the corresponding mCherry markers used by Friedland *et al*. The microinjection mixture concentrations were altered slightly: 45 ng/µL of the plasmid containing *cas9*, 45 ng/µL of the plasmid containing the synthetic sgRNA gene, 2.5 ng/µL of the plasmid containing *Pmyo-2::GFP*, and 5 ng/µL of the plasmid containing *Pmyo-2::GFP*. This was microinjected into one or both gonad arms of young adult hermaphrodite animals (Kadandale et al. 2009). It was hoped that a palindromic oligo that would aid in genotyping would integrate at the site of the Cas9 incision (but it never did), and this oligo was added to the micro-injection mix at 5 ng/µL. This oligo was not detected by genotyping experiments and appeared to have been inconsequential to the outcome of the experiments.

Targeting transgenes from the Boulton lab (Crick Institute, London) containing wild type *rec-1*, putative phospho-mutant *rec-1(8S/T>A)*, and putative phospho-mimetic *rec-1 (8S/T>E)* were constructed by synthesizing DNA fragments (GeneArt) and cloning them to pCFJ151 using standard techniques (Frøkjær-Jensen et al. 2008). All cloning PCR amplifications were done with Q5 high-fidelity DNA polymerase (New England Biolabs). Integrated *rec-1* transgenic lines were made as described previously by injection into Unc-119 segregants from EG6699 - *ttTi5605 (II); unc-119(ed3) (III); oxEx1578* (Frøkjær-Jensen et al. 2008).

Integrated *rec-1* transgenic lines were made as described previously by injection into Unc-119 segregants from EG6699 - *ttTi5605 (II); unc-119(ed3) (III); oxEx1578* (Frøkjær-Jensen et al. 2008). The integrated wild type *rec-1(+),* phosphor-mutant *rec-1(8S/T>A)* and phosphor-

mimetic *rec-1(8S/T>E)* were designated *dwSi4[rec-1(+) Cbr-unc-119(+)]*, *dwSi6[rec-1(8S/T>A) Cbr-unc-119(+)]* and *dwSi5[rec-1(8S/T>E) Cbr-unc-119(+)]* respectively.

4.2.3 Finding a suitable target for Cas9 cleavage

The goal of our targeted mutagenesis was to generate a null allele of *y18h1a.7* that would phenocopy the existing *s180* allele of *rec-1*. Several sites at the 5' end of *y18h1a.7* could potentially lead to the deletion of the start codon; however, this was not ideal as there was a second methionine residue not too far downstream, which could be used as an alternative translation start site, generating a nearly wild-type protein. Thus a Cas9 target site in the following exon (exon 2) was chosen. A C→T nonsense mutation within the second exon of *y18h1a.7* was a candidate for the *s180* mutation (Rose et al. 2010), so an out-of-frame deletion in this exon would likely phenocopy *rec-1(s180)*. Thus, a Cas9 target site was chosen, overlapping a *Nae*I restriction site which could be used for genotyping this locus (Figure 4.3). This Cas9 target site was cloned into the plasmid containing the synthetic sgRNA gene, replacing the original target sequence derived from *unc-119*.

4.2.4 Screening for *y18h1a.7* mutants

Mutations in *y18h1a.7*, a candidate for *rec-1*, were not expected to have a morphological or developmental phenotype. All mutant screening was done by Sanger sequencing at the *y18h1a.7* locus.

GFP-expressing hermaphrodite F_1 animals arising from the injected P_0 were individually plated, allowed to lay eggs for one day, then treated with lysis buffer (30 mM Tris pH 8,100 mM NaCl, 0.7% Tween 20 and 100 μg/ml proteinase K) at 57°C for 1 hour to extract the DNA and then at 95°C for 15 minutes to inactivate the proteinase K. The 5' end of the *y18h1a.7* locus was then amplified by PCR using primers "y18 CRISPR seq Fi" (CGCCATGTGCCTTTAGTACC) and "y18 CRISPR seq Ri" (GCAGTTTCTGGTGATTTTCG) with the program "CO_55" (94°C for 4:00; then 34 rounds of 94°C for 0:30, 55 °C for 0:30, and 72°C for 1:00; ending with 72°C for 10:00). The expected wild type band size was 465 bps. Sanger sequencing was then performed with one of the two primers used for PCR. The F_1 animals with obvious double peaks in their Sanger chromatograms were likely heterozygous for a mutation in *y18h1a.7*. Their progeny were kept and the mutation was made homozygous over an additional 1 to 2 generations. The protocol is summarized in Figure 4.1.

4.2.5 Determination of recombination frequency

The *rec-1(s180)* homozygous animals were known to affect the distribution of crossover events across the chromosome, but the overall frequency of meiotic crossovers across individual chromosomes remained roughly 0.5 (Zetka and Rose 1995). This meant that recombination frequency increases at certain intervals were compensated by decreases in other intervals. Two well characterized genetic intervals were chosen for this work: *dpy-5 – unc-13*, where the recombination frequency increased in *rec-1(s180)* homozygotes compared to wild type

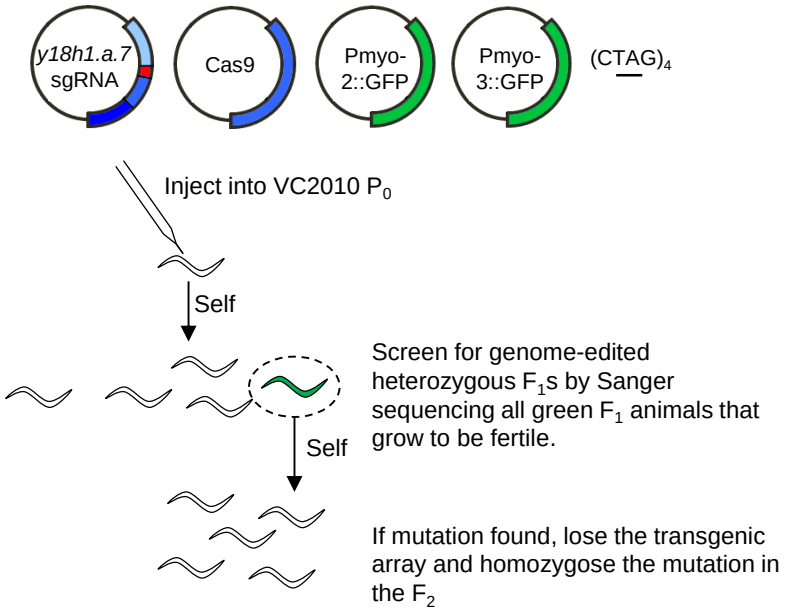

Figure 4.1: Protocol for the directed mutagenesis of *y18h1a.7* using CRISPR-Cas9.

animals, and *unc-101 – unc-54*, where the recombination frequency decreased in *rec-1(s180)* homozygotes compared to wild type animals (Zetka and Rose 1995).

Hermaphrodite animals, with or without *rec-1* mutations and homozygous for *dpy-5(e61)* and *unc-13(e51)*, were mated with homozygous *rec-1(+)* or *rec-1(-)* males (the '-' allele denotes either *s180*, *h2875* or *h2872*). The non-Dpy, non-Unc F_1 hermaphrodites, carrying *dpy-5(e61) unc-13(e51)* in *cis*, were allowed to self. All of their progeny in the F_2 were scored based on the phenotypes: wild type, Dpy, Unc or DpyUnc. I then calculated the recombination frequency in this interval using the formula $1 - \sqrt{1 - 2R}$, where $R = \frac{[Number\ of\ Dpys + number\ of\ Uncs]}{[Total\ number\ of\ progeny]}$ (Brenner 1974; Zetka and Rose 1995). This recombination frequency calculation takes into account recombination events in both the egg and the sperm from the hermaphrodite.

Initially, to avoid ascertainment bias (*i.e.* the experimenter looking specifically for Dpy or Uncs on a plate arising from an F_1 *h2875* homozygote), I scored all the F_2 animals blindly, with the *rec-1* genotype kept a secret and only revealed to me by another member of the lab after all the F_2 animals were counted. The single-blind scoring was also repeated by another member (A. S. Tam) in the lab for confirmation.

For the *unc-101 – unc-54* interval, hermaphrodite animals bearing heterozygous mutations *unc-101(m1)* and *unc-54(e190)* in *cis* were allowed to self, with or without *rec-1(-),* and all their progeny were scored based on the movement phenotypes: wild type, Unc-101 and Unc-54. Because the movement phenotypes of *unc-54(e190)* single mutants and *unc-101(m1) unc-54(e190)* double mutants were identical, the recombination frequency was calculated using the formula$1 - \sqrt{1 - 2R}$, where the modified R is inferred to be $\frac{2[number\ of\ Unc-101s]}{[Total\ number\ of\ progeny]}$ (Brenner 1974; Zetka and Rose 1995). This recombination frequency takes into account recombination events in both the egg and the sperm from the hermaphrodite.

The *rec-1(h2875)* was generated in an N2 (Bristol) genetic background. This original strain was outcrossed six times to strain CB4856, a Hawaiian *C. elegans* isolate that contains a set of well-characterized single-nucleotide differences from N2 (Wicks et al. 2001). Separately, the original *rec-1(h2875)*-bearing strain was backcrossed six times to N2. The N2-backcrossed strain bearing *h2875* was designated KR5305; the CB4856-outcrossed strain was KR5306.

Hermaphrodite animals from KR5306 (Hawaiian) were mated with males from KR5305 (Bristol). The mated hermaphrodites were transferred to individual plates, where the appearance of F_1 males indicated a successful cross. Outcross hermaphrodite F_1 progeny animals were

identified by being younger than the oldest outcross male F_1 progeny. These outcross hermaphrodite F_1 animals were picked out as L4s (to ensure they did not mate with their siblings) and backcrossed to an N2 male. As a control, analogous crosses were performed, but starting with N2 and CB4856 instead (*i.e.* no mutation in *rec-1*). The resulting F_2 male animals were collected for genotyping across five polymorphic sites. Each of these F_2 animals each represented a single product of an F_1 oocyte meiosis.

The collected F_2 males were treated with lysis buffer (30 mM Tris pH 8,100 mM NaCl, 0.7% Tween 20 and 100 μg/ml proteinase K) at 57°C for 1 hour to extract the genomic DNA and then at 95°C for 15 minutes to inactivate the proteinase K. The genomic DNA was divided into 5 aliquots for 5 PCR reactions using the primer pairs (listed in Appendix B) with the program "CO_55" (94°C for 4:00; then 34 rounds of 94°C for 0:30, 55 °C for 0:30, and 72°C for 1:00; ending with 72°C for 10:00). The PCR products were digested, without purification, with *Aat*II, *Spe*I, *Acc*I, *Dra*I and *Hind*III (New England Biolabs) according to the manufacturer's specifications. The five sites were chosen based on the work by Mets and Meyer (2009) with modifications to optimize the PCR and restriction reactions (Mets and Meyer 2009). From the five genotypes across the chromosome, it was possible to deduce where a recombination event took place in the F_1 and if there were multiple crossover events in the hermaphrodite oocyte.

4.2.6 Analysis of tandem repeats in the *rec-1* (DNA) and REC-1 (amino acid) sequence

The tandem repeat structure in the third exon of *rec-1* was initially detected by visual inspection. The repeats boundaries were determined manually by maximizing the number of

repeats and their sequence similarities. The corresponding repeat in the amino acid sequence was checked using the program RADAR (Heger and Holm 2000).

4.2.7 Identification and analysis of *rec-1* and *him-5* orthologues in several *Caenorhabditis* species

Based on previously published genomes, their respective gene annotations and the RNA sequencing data deposited at WormBase (WS243) and ModENCODE (Celniker et al. 2009), I identified the synteny block containing *rec-1* in six other *Caenorhabditis* species. Using the putative open reading frames around *rec-1* and the relative positions and orientations of their orthologues in the six *Caenorhabditis* species, I identified a putative open-reading frame that is positionally equivalent to *rec-1*.

Subsequent profile-based similarity searches performed by the Ponting lab (University of Oxford) employed HMMer (Finn et al. 2011) against the UniRef50 database (Suzek et al. 2007) using an alignment of the N-terminal region conserved in the *Caenorhabditis* proteins (including *C. briggsae*, *C. sinica [sp. 5]*, *C. brenneri*, *C. remanei*, *C. tropicalis*, and *C. japonica*) encoded by genes syntenic with *C. elegans rec-1*. These searches identified the *C. elegans* HIM-5 protein sequence as being statistically significantly similar to these proteins ($E = 6 \times 10^{-3}$) (Chung et al. 2015).

4.2.8 Immunofluorescence and microscopy

Fixation and immunostaining of gonads were performed as described (Chan et al. 2003) by the Yanowitz lab (Magee-Womens' Institute, Pittsburgh), and the quantification of the RAD-

51 foci was done in the Rose lab. The following antibodies were used (at the specified concentrations): rabbit anti-RAD-51 (1:1000) (Rinaldo et al. 2002), guinea pig anti-HIM-8 (1:500) (Phillips et al. 2005), and anti-SYP-1 (1:2000) (Colaiácovo et al. 2003). Corresponding secondary antibodies conjugated to Alexa-488, Alexa-568 and Alexa-633 were obtained from Invitrogen (Carlsbad, CA) and used at 1:1000 to 1:2000 dilution. Immunostained tissues were then mounted in Prolong Gold with DAPI (Invitrogen) and imaged on Nikon A1r confocal microscope (Nikon Instruments, Melville, NY) in 0.2-μm increments on the *z*-axis. Analysis of stained nuclei was carried out as described (Colaiácovo et al. 2003).

4.3 Results

4.3.1 Targeted knockout of *y18h1a.7,* a candidate coding sequence for *rec-1*, by CRISPR-Cas9

Despite the difficulties of scoring a second generation crossover phenotype, genetic mapping positioned the *rec-1* gene to an interval on chromosome I (N.J. O'Neil and A.M. Rose unpublished data). The genomic sequence of a strain carrying the *rec-1(s180)* mutation contained 441 single-nucleotide differences when compared to the wild-type progenitor (Rose et al. 2010). Using the map position of the *rec-1(s180)* mutation and the DNA sequence information, a nonsense mutation affecting the coding sequence *y18h1a.7* was identified (J.S.C Chu and A.M. Rose, unpublished data). RNAi knockdown of *y18h1a.7* resulted in an altered distribution of crossover events that partly recapitulated the Rec-1 phenotype (J. Luce, M. R. Jones, A.M. Rose, unpublished data).

In order to confirm *y18h1a.7* is the coding region whose mutation confers the Rec-1 phenotype, I targeted the transgenic Cas9 enzyme (Friedland et al. 2013) to cut the second exon of the gene, the same exon predicted to be disrupted by the nonsense mutation in *rec-1(s180).* In total, 79 animals were injected. About 25% (21/79) of all injected animals generated F_1s with GFP expression. This is in line with my injection success frequency in other experiments not involving CRISPR-Cas9 reagents. A total of 60 GFP-positive F_1s were identified, of which roughly 33% (20/60) were sick or slow-growing and were not subject to further screening. Of the 40 remaining animals, 10% (4/40) showed a mutation in *rec-1*. Figure 4.2a summarizes these injection results.

Several unusual inheritance patterns were observed after injection of CRISPR-Cas9 reagents. Sanger sequencing of F_1 animal #51.12 (see Figure 4.2a) revealed that it was a mosaic, carrying three different alleles – the wild-type allele, a 1-bp deletion and an 8-bp deletion. Amazingly, all three alleles were transmitted to the F_2 and F_3. Therefore, three distinct populations of germ cells likely existed in the F_1 animal #51.12 to give rise to F_2s with different diploid combinations of these three alleles.

Animal F_1 #51.8 appeared to carry a 4-bp deletion determined by Sanger sequencing; however, none of its offspring tested positive for this deletion (see Figure 4.2a). Instead, one of its offspring (F_2 #51.8.7) carried homozygous 64-bp deletion; in addition, the GFP transmission persisted in subsequent generations. A reasonable explanation is that the GFP transgene integration occurred in the F_1 #51.8 animal off-target (as Sanger sequencing of *y18h1a.7* did not reveal a GFP insertion), and homozygosed by F_2 generation in animal #51.8.7, so it could not be lost in the F_2 and onward. Additionally, the action of Cas9 appeared to have persisted in F_1 #51.8 such that it gave rise to both sperm and egg with the 64-bp deletion.

The 4-bp deletion detected in F_1 #51.8 was identical in sequence to the 4-bp deletion found in F_1 #78.6 (see Figure 4.2a and b). Also, the 64-bp deletion detected in F_2 #51.8.7 was identical in sequence to the 64-bp deletion found in F_1 #51.15 (see Figure 4.2a and b). Additionally, a closer examination of the deleted sequences revealed that the deletion breakpoints could not be unambiguously assigned due to small stretches of homology (from 1 bp to 5 bps) at the breakpoints (Figure 4.2b), which was consistent with but not exclusive to the repair outcomes by canonical non-homologous end-joining (Pannunzio et al. 2014). Taken together, these results indicate that the DSB made by Cas9 at this site was being repaired in a predictable manner to generate specific sequence deletions.

4.3.2 The molecular identity of *rec-1* is coding sequence *y18h1a.7* on chromosome I

The four new alleles of *y18h1a.7* were all frame-shift alleles (see Figure 4.2b and Figure 4.3). The largest deletion, *h2875,* conferred a recessive increase of recombination frequency in the *dpy-5 – unc-13* genetic interval, as had been described for *s180* [Figure 4.4a-e and Ref. (Zetka and Rose 1995)]. In addition, *h2875* failed to complement *s180* with respect to the recombination frequency in both the *dpy-5 – unc-13* and *unc-101 – unc-54* intervals (Figure 4.4f and Figure 4.5). The smaller deletion, *h2872*, also failed to complement *s180* with respect to the frequency of recombination in the *dpy-5 – unc-13* interval (Figure 4.4g). Furthermore, a single wild-type copy of *y18h1a.7* (*dwSi4[rec-1(+)]*) inserted into Chromosome II via *Mos1*-mediated single-copy insertion [*Mos*SCI (Frøkjær-Jensen et al. 2008)] restored the wild-type frequency of recombination events in the *dpy-5 – unc-13* interval (Figure 4.4h).

a

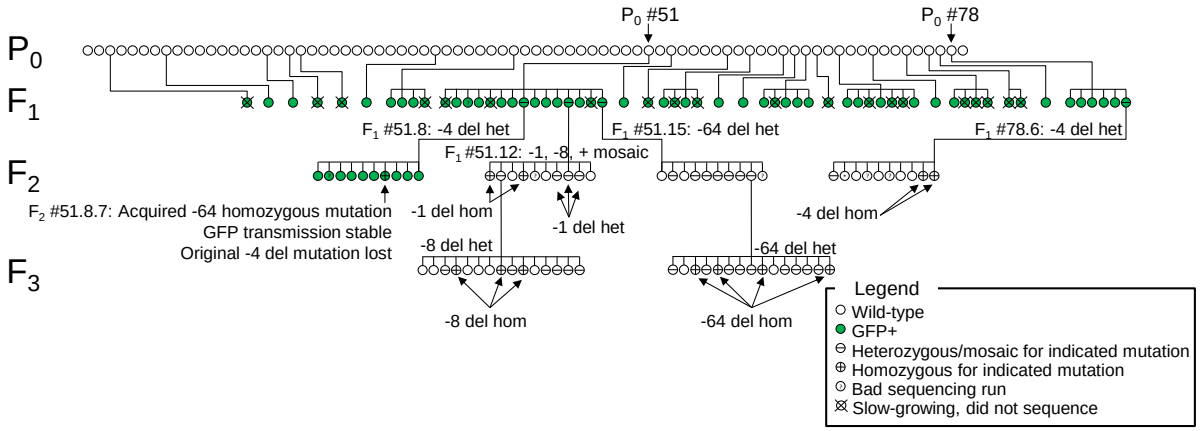

b

Allele and extent of homology	Alternative interpretations of the deletion breakpoints
Wild-type	5'-CCGATTTATCGCCAGCCGGCCAGTTATC…GTGGAGAAATTG-3'
h2872 (Δ1bp from F_1 #51.12) 1-bp homology	5'-CCGATTTATCGCCAGCC-**G**CCAGTTATC…GTGGAGAAATTG-3' 5'-CCGATTTATCGCCAGCC**G**-CCAGTTATC…GTGGAGAAATTG-3'
h2873 (Δ4bp from F_1 #78.6) 3-bp homology	5'-CCGATTTATCGCCA----**GCC**AGTTATC…GTGGAGAAATTG-3' 5'-CCGATTTATCGCCA**G**----**CC**AGTTATC…GTGGAGAAATTG-3' 5'-CCGATTTATCGCCA**GC**----**C**AGTTATC…GTGGAGAAATTG-3' 5'-CCGATTTATCGCCA**GCC**----AGTTATC…GTGGAGAAATTG-3'
h2874 (Δ8bp from F_1 #51.12) 5-bp homology	5'-CCGATTTATC--------**GCCAG**TTATC…GTGGAGAAATTG-3' 5'-CCGATTTATC**G**--------**CCAG**TTATC…GTGGAGAAATTG-3' 5'-CCGATTTATC**GC**--------**CAG**TTATC…GTGGAGAAATTG-3' 5'-CCGATTTATC**GCC**--------**AG**TTATC…GTGGAGAAATTG-3' 5'-CCGATTTATC**GCCA**--------**G**TTATC…GTGGAGAAATTG-3' 5'-CCGATTTATC**GCCAG**--------TTATC…GTGGAGAAATTG-3'
h2875 (Δ64bp from F_1 #51.15) 2-bp homology	5'-CC----------…---**GA**GAAATTG-3' 5'-CC**G**----------…----**A**GAAATTG-3' 5'-CC**GA**----------…-----GAAATTG-3'

Figure 4.2: Results of the targeted mutagenesis of the *y18h1a.7* locus.
a) Summary of all injected animals and progeny tested for mutation in *y18h1a.7*. Several unusual inheritance patterns were observed in the two generations after injection. See text for details. b) The deletion breakpoints could not be unambiguously assigned due to small stretches of homology (from 1 bp to 5 bps) at either end of the deletion.

Similar to observations from *rec-1(s180)* homozygotes, which appear to maintain strict crossover interference (Zetka and Rose 1995), we found no evidence of double crossovers in the oocytes of *rec-1(h2875)* homozygotes (Figure 4.6). Like *rec-1(s180)* homozygotes (Rattray and

Rose 1988), *rec-1(h2875)* homozygotes also had a mild increase in the number of spontaneous male progeny (0.35%, *N* = 3118) compared to wild type (0.05%, *N* = 2574). This suggested that REC-1 may be involved in proper disjunction of the X chromosome but not of the autosomes, since the overall embryonic hatching frequency was unchanged from wild type (*h2875* homozygotes: 98.7%, *N* = 3118 compared with wild-type: 98.4%, *N* = 2574). Collectively, these results establish that the altered recombination phenotype is caused by disruption of the gene encoded by *y18h1a.7*.

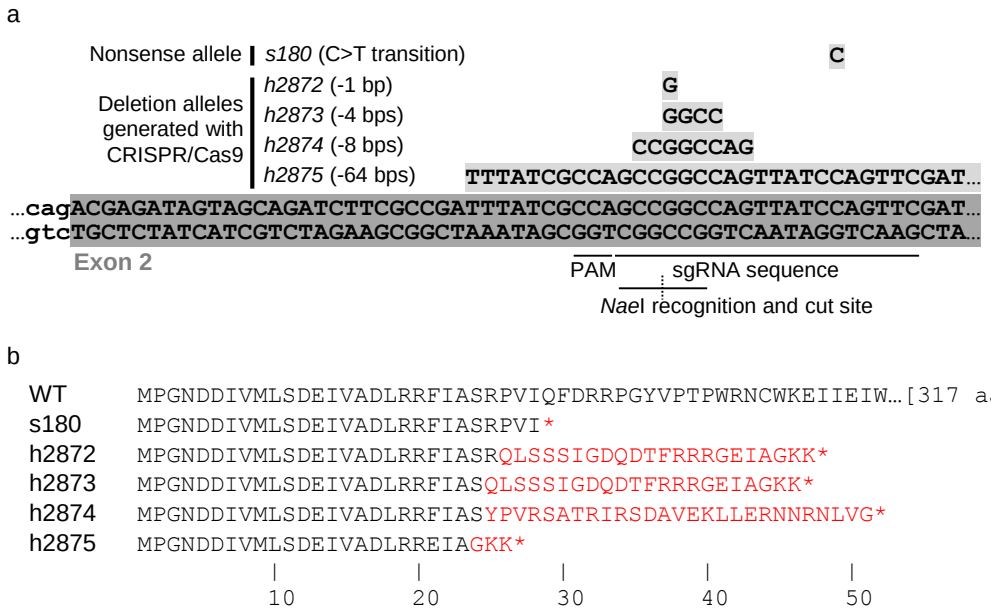

Figure 4.3: The mutant alleles of *rec-1* and their predicted translation products.
a) The *s180* allele was identified by a whole-genome sequencing experiment described previously (Rose et al. 2010). Four alleles of *rec-1* were generated by CRISPR-Cas9 (Friedland et al. 2013) using the same target guide RNA sequence and the protospacer adjacent motif (PAM). b) The mutant alleles of *rec-1* encode truncated versions of REC-1. Amino acid differences with the wild-type (WT) translation are colored in red.

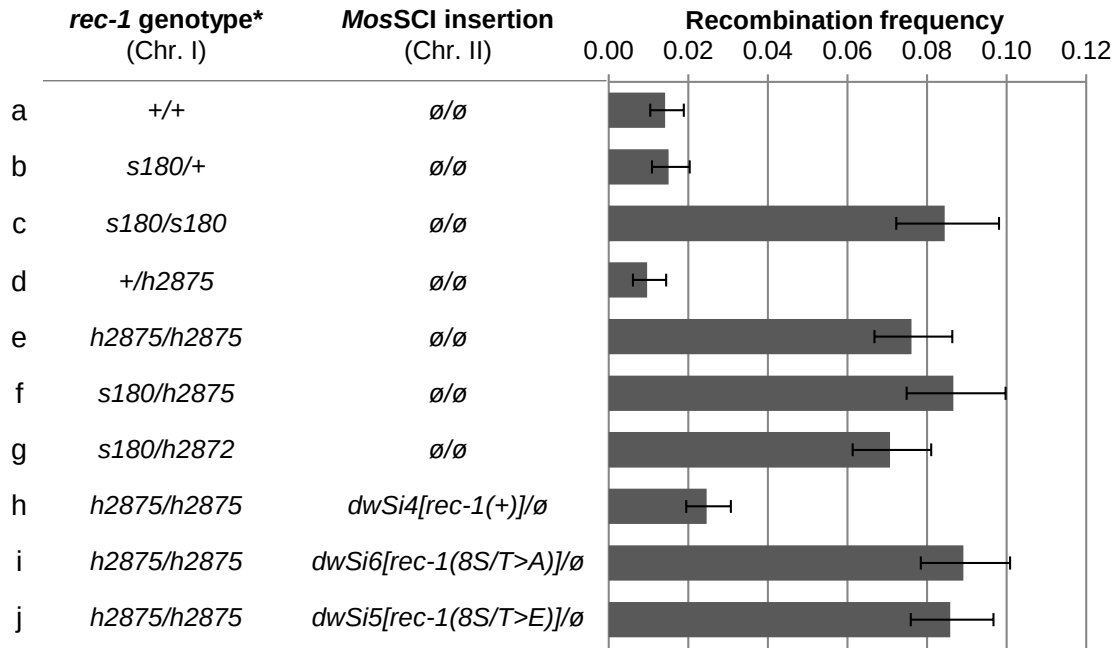

Figure 4.4: Mutations in *rec-1* cause an increased recombination frequency in the *dpy-5 – unc-13* genetic interval.
a) to c) The *s180* allele of *rec-1* confers a recessive increase of recombination frequency in this interval. d) and e) The *h2875* allele of *y18h1a.7* also confers a recessive increase of recombination frequency in this interval. f) and g) *h2875* and *h2872* alleles of *y18h1a.7* fail to complement *rec-1(s180)*. h) The re-introduction of wild type *rec-1* by *Mos*SCI reverses this increase in recombination frequency. i) and j) The insertion of *rec-1* mutated at putative phosphorylation sites fail to rescue the altered recombination phenotype. See the text for a description on the alleles. ø indicates the absence of a *Mos1* mediated transgene insertion. *Where applicable, the first allele indicate the homologue bearing the *dpy-5* and *unc-13* mutations. Error bars indicate the 95% Copper-Pearson confidence interval. The expression of the transgenes from h) to j) were inferred from a GFP-tagged construct (Chung et al. 2015).

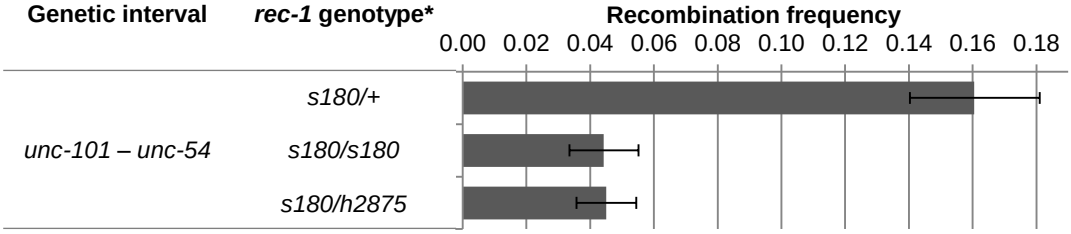

Figure 4.5: Mutations in *rec-1* alter recombination frequencies in the *unc-101 – unc-54* interval.
The targeted deletion of *y18h1a.7/rec-1 (h2875)* fails to complement the decreased recombination frequency in the *unc-101 – unc-54* genetic interval. *The first allele indicates the homologue bearing the *unc-101* and *unc-54* mutations. Error bars indicate 95% CI.

a

Gamete type	Genotype at					Numbers observed in	
	Site A*	Site B	Site C	Site D	Site E	*rec-1(+)*	*rec-1(h2875)*
i	*B*	*B*	*B*	*B*	*B*	38	27
ii	*H*	*H*	*H*	*H*	*H*	29	41
iii	*B*	*H*	*H*	*H*	*H*	8	5
iv	*H*	*B*	*B*	*B*	*B*	10	2
v	*B*	*B*	*H*	*H*	*H*	1	6
vi	*H*	*H*	*B*	*B*	*B*	2	5
vii	*B*	*B*	*B*	*H*	*H*	2	4
viii	*H*	*H*	*H*	*B*	*B*	1	7
ix	*B*	*B*	*B*	*B*	*H*	4	4
x	*H*	*H*	*H*	*H*	*B*	3	5
with >1 crossover	(not observed)					0	0
					Total	98	106

b

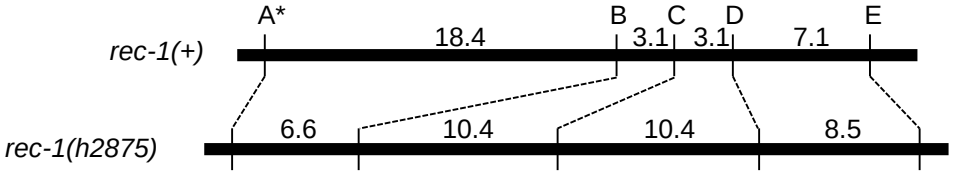

Figure 4.6: Meiotic crossover events are redistributed in oocytes from *rec-1(h2875)* mutants.
The redistribution of crossover events with no double-crossover has previously been observed in *rec-1(s180)* homozygotes using two-point mapping in hermaphrodites (Zetka and Rose 1995). a) Oocyte genotypes derived from Bristol/Hawaiian hybrid animals in *rec-1(+)* and *rec-1(h2875)* genetic backgrounds. Strict crossover interference is observed in both genetic backgrounds in the interval defined by marker A* and E. *B* = Bristol allele, *H* = Hawaiian allele. b) The *h2875* mutation distorts the oocyte genetic map, shown here with distances represented in map units (100 × [recombination frequency]). While the overall frequencies of recombination between markers A* and E and those between markers D and E are not significantly different between the two genetic backgrounds (χ^2-test, $p = 0.525$ and 0.721 respectively), the individual intervals A* to B, B to C and C to D have significantly different recombination frequencies (χ^2-test, $p = 0.0105$, 0.0389 and 0.0389 respectively).

4.3.3 Phosphorylatable residues in REC-1 are required for proper function

The predicted amino acid sequence of REC-1 contains four copies of a sequence each containing two consensus cyclin-dependent kinase (CDK) phosphorylation motifs S/T-P (Figure 4.7a). The phosphorylation sites were mapped by peptide array phosphorylation analyses by the Boulton lab (Crick Institute, London). Phosphorylation of these peptides by whole worm extracts could be inhibited by roscovitine, a CDK inhibitor. Further, *in vitro* phosphorylation by recombinant CDK4 could be detected on full-length recombinant REC-1. Altogether, these results suggest that REC-1 is target for phosphorylation by a kinase in the CDK family (Chung et al. 2015).

To test whether the pattern of meiotic recombination events in *C. elegans* is affected by mutating the S/T-P motifs in REC-1, I used mutated transgenic alleles of *rec-1* integrated into the *ttTi5605* site on chromosome II by the Boulton lab. One construct, *dwSi6[rec-1(8S/T>A)]*, replaced the 8 serine/threonine codons with alanine codons (Figure 4.7b), and encoded a protein product which could not be phosphorylated by CDK4/cyclin D3 *in vitro* (Chung et al. 2015). A second construct, *dwSi5 [rec-1(8S/T>E)]*, replaced the 8 serine/threonine codons with glutamic acid codons (Figure 4.7b), and encoded a form of REC-1 mimicking constitutive phosphorylation at these eight S/T-P motifs. In contrast to the rescuing wild-type transgene, *dwSi4[rec-1(+)]*, neither *dwSi6[rec-1(8S/T>A)]* nor *dwSi5 [rec-1(8S/T>E)]* alleles were able to rescue the altered recombination phenotype of *rec-1(h2875)* (Figure 4.4h-j). Integrated, C-terminal GFP-tagged versions of *rec-1(+), rec-1(S/T>A)* and *rec-1(S/T>E)* could be detected by anti-GFP antisera at comparable levels regardless of the S/T amino acid changes (Chung et al. 2015), which suggest that the expression of integrated mutant *rec-1(S/T>A)* and *rec-1(S/T>E)* is

unaffected by these amino acid changes. These results establish that the eight S/T-P motifs within REC-1 are important for establishing the normal pattern of meiotic recombination events in *C. elegans*. Since the transgene containing the phospho-mimetic changes within the eight S/T-P motifs was also unable to rescue the Rec-1 phenotype, it is possible that de-phosphorylation of these sites is also important for REC-1 function *in vivo*.

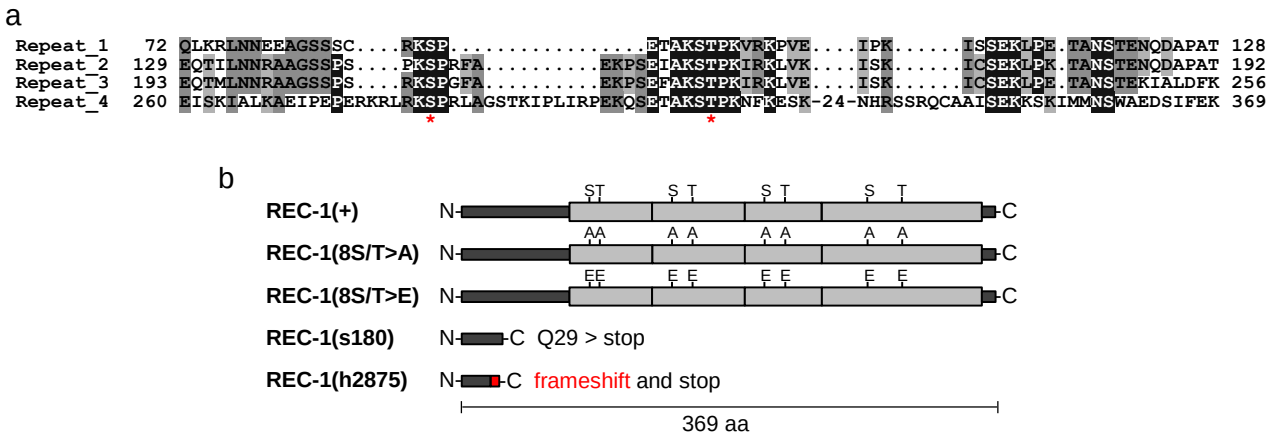

Figure 4.7: REC-1 internal repeats contain consensus CDK phosphorylation sequences. a) Alignment of the four repeats (Repeat_1 to _4) of REC-1 and the position of putative CDK phosphorylation sites (red asterisk). Identical residues are highlighted in black and regions of similarity are highlighted in grey. b) Schematic representation of wild type [REC-1(+)], potentially phospho-mutant [REC-1(8S/T>A)], potentially phospho-mimetic [REC-1(8S/T>E)] and truncated [REC-1(s180), REC-1(h2875)] versions of proteins showing relative sites of the eight-residue substitutions or the deleted regions.

4.3.4 The *rec-1* gene and the *him-5* gene are paralogues

Phylogenetic analysis revealed that *rec-1* resides in a synteny block of genes on Chromosome I that is conserved in order and orientation and is shared among at least six other *Caenorhabditis* species – *C. briggsae, C. remanei, C. brenneri, C. sinica (sp. 5), C. tropicalis* and *C. japonica* (Figure 4.8a). Within the synteny blocks is a coding region of a similar size and

in the same orientation and position as that of the *rec-1* gene in *C. elegans* (open reading frames in black, Figure 4.8a). Notably, the translation product of the *C. remanei* open reading frame contains a short stretch of sequence similarity to *C. elegans* REC-1 at the N terminus (Figure 4.8b). Although the overall sequence match to *C. elegans* REC-1 is not strong, the translation products of the open reading frames (ORFs) in this position in the six other species have notable sequence similarity to each other (Figure 4.8c) and all contain an R-F-x-x-L-P/S motif (Figure 4.8c-d). Surprisingly, the ORFs in this position in the other species encode proteins that all share sequence similarity with HIM-5, whose coding sequence is located on *C. elegans* Chromosome V, outside the *rec-1* synteny block. HIM-5 contains the R-F-x-x-L-P/S motif that *C. elegans* REC-1 is lacking (Figure 4.8c-d). Thus, in other *Caenorhabditis* species, the positionally equivalent gene to *C. elegans rec-1* shares more sequence similarity with *C. elegans him-5* than with *C. elegans rec-1*. Altogether,

(1) The similarity between *C. elegans* REC-1 and the *C. remanei* ORF translation product,

(2) The positional equivalence of *C. elegans rec-1* to the ORFs in six other *Caenorhabditis* species which are related to *him-5*, and

(3) The phenotypic similarity between *rec-1* and *him-5* mutants with respect to the distribution of crossover events (Meneely et al. 2012)

strongly suggest that REC-1 is a distantly related paralogue of HIM-5.

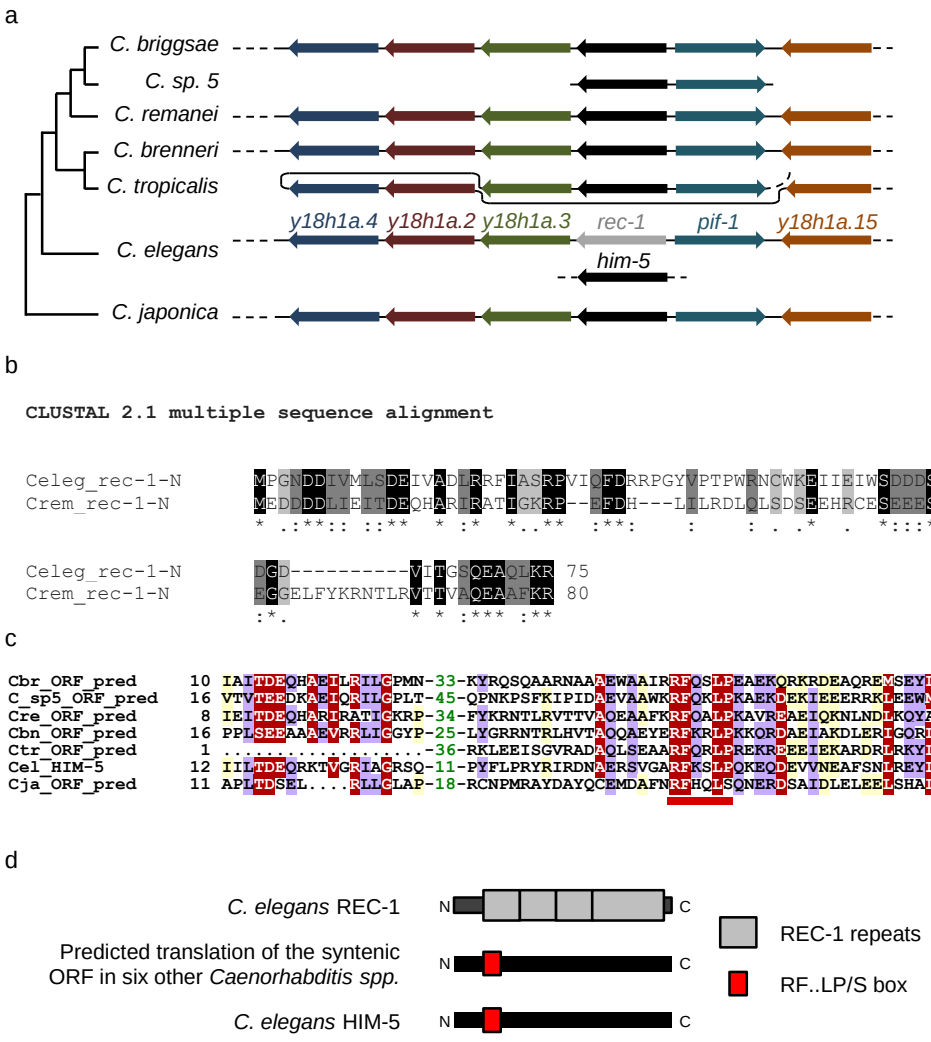

Figure 4.8: Phylogenetic analysis of *rec-1* and the surrounding synteny block reveals the identity of *rec-1* homologues.

a) The synteny block that contains *rec-1* appears to be conserved in six other *Caenorhabditis* species. Gene order and relative orientation are shown, but not to scale. The putative open reading frame between *y18h1a.3* and *pif-1* orthologues has a higher degree of sequence similarity to *C. elegans him-5* (indicated in black) than to *rec-1* (indicated in grey). The species are grouped on a phylogenetic tree suggested by Félix, Braendle and Cutter (Félix et al. 2014). Open reading frames with sequence similarity are depicted with the same colour. b) Alignment of *C. elegans* REC-1 and the putative *C. remanei* orthologue reveals sequence similarity at the N termini of these predicted translations. c) Multiple alignment of the N-terminal regions of open reading frames shown in grey in a): the *C. elegans* HIM-5 sequence (Cel_HIM-5) and orthologues in *C. briggsae* (Cbr_ORF_pred), *C. sp. 5* (C_sp5_ORF_pred), *C. remanei* (Cre_ORF_pred), *C. brenneri* (Cbn_ORF_pred), *C. tropicalis*(Ctr_ORF_pred), and *C. japonica* (Cja_ORF_pred). The motif R-F-x-x-L-P/S is underlined in red. The alignment was

presented with the program Belvu (Sonnhammer and Hollich 2005) using a colouring scheme indicating the average BLOSUM62 scores (which are correlated with amino acid conservation) of each alignment column: red (>2), violet (between 2 and 1) and light yellow (between 1 and 0.3). Numbers shown in green represent amino acids that have been removed from the alignment. d) The relative positions of motifs (the REC-1 repeat motifs and the RF..LP/S box) within the translation products of *rec-1* homologues.

4.3.5 *rec-1* and *him-5* are both required for normal double-strand break formation in the meiotic germline

Loss of function of *him-5* results in strong crossover suppression on the X-chromosome and an altered distribution of crossovers on both the X-chromosome and the autosomes (Meneely et al. 2012). The redistribution of meiotic crossover events on the autosomes is similar to that observed for *rec-1* loss of function. The crossover distribution phenotypes, together with their putative evolutionary link, prompted me to examine their genetic relationship. *him-5* loss-of-function reduces hatching efficiency to 60-70% (Meneely et al. 2012) whereas *rec-1* loss-of-function has no impact on hatching [see 4.3.2 and (Rattray and Rose 1988)]. The Yanowitz lab observed that, in contrast to the single mutants, the *rec-1; him-5* double mutant exhibited even lower hatching frequency at 20-50% (Chung et al. 2015). In addition, these double mutants exhibited a markedly higher frequencies of univalent formation at diakinesis rescuable by γ ray irradiation, indicating that *rec-1; him-5* double mutants may be defective for strand exchange at meiosis I (Chung et al. 2015). These phenotypes suggested that *rec-1; him-5* double mutants had meiotic double-strand break and crossover defects.

A reasonable possibility for a crossover defect was that meiotic chromosomes in *rec-1; him-5* double mutants failed to generate enough double-strand breaks to ensure every homologue

pair could undergo meiotic recombination (see the concept of 'DSB assurance', 1.3.1). To test this hypothesis, the Yanowitz lab immunostained the meiotic germline for RAD-51 localization. In addition, immunostaining for HIM-8, a homologue-recognizing protein required for the pairing of the X chromosomes, and SYP-1, a synaptonemal complex protein, was done to see if there were defects in chromosome pairing and synaptonemal complex formation. While chromosome pairing and synaptonemal complex formation appeared normal in single and double mutants (Chung et al. 2015), I observed a changed dynamic for the RAD-51 localization in the meiotic germline.

RAD-51 is the major protein in *C. elegans* marking DNA double-strand breaks which then become competent for initiating strand invasion and meiotic recombination (Rinaldo et al. 2002; Alpi et al. 2003). As already describe in Figure 3.4 and elsewhere, normally, the number of RAD-51 foci increases and peaks in early to mid-pachytene (Alpi et al. 2003) as more DSBs are formed by SPO-11 action (Dernburg et al. 1998) and processed into potential recombination substrates; this number then decreases as most DSBs are sealed up by the end of pachytene into crossover or non-crossover events. Briefly, the meiotic germline was divided into 7 regions (transition zone, and zones 1-6 spanning early to late pachytene) according to the position of the oocyte nuclei relative to the gonad, in a manner similar to Figure 3.4. Every oocyte nucleus from the transition zone until late pachytene was accounted for, and the number of RAD-51 foci was counted for gonads derived from wild-type animals, *rec-1* single mutants, *him-5* single mutants, and *rec-1; him-5* double mutants.

I observed differences in both the number and temporal localization of RAD-51 in single mutants and in *rec-1; him-5* double mutants. In wild type, I counted an overall average of just

under 3 RAD-51 foci per oocyte nucleus, with the most abundant signal in the mid-pachytene stage of meiosis, which corresponds to zone 3 in Figure 4.9a-b where some nuclei with 6 - 7 RAD-51 foci can be seen. In *rec-1* and *him-5* single mutants, there were fewer RAD-51 foci overall (an average of 1 per nuclei in the total count), and in *him-5* mutants a notable shift in the presence of foci at the later stages of prophase can be seen (also observed by Meneely et al. 2012) (Figure 4.9b). Both the number and the temporal localization of RAD-51 were affected in *rec-1 him-5* double mutants; an overall average of 0.5 foci per nucleus was detected and the majority of these were in the later stages, zones 4, 5 and 6 (Figure 4.9b). Taken together, these results indicate that REC-1 and HIM-5 function are both required for the normal number of RAD-51 foci in the meiotic germline.

To confirm these result genetically, I introduced the *rad-54(ok615)* mutation to the single and the double mutants. The *rad-54(ok615)* mutants accumulate single-stranded RAD-51 filaments which cannot be further processed into exchange intermediates (Mets and Meyer 2009). The *rad-54(ok615)* mutation severely impacts fertility, and homozygotes produce very few eggs (an average of 32, Figure 4.9c) due to large numbers of unprocessed DSBs leading to apoptosis of the germline nuclei (Stergiou et al. 2011). All the eggs that are laid by *rad-54(ok615)* homozygotes fail to hatch (Figure 4.9c). In this *rad-54(ok615)* mutant background, additionally mutating *rec-1*, *him-5* or both *rec-1* and *him-5* increased the number of eggs laid and the number of hatched progeny (Figure 4.9c), likely due to the fewer number of DSBs being formed (thus decreasing the requirement for RAD-54 function). The partial rescue of the *rad-54* mutant phenotype by *rec-1; him-5* is analogous to that seen with mutants defective for meiotic DSB

formation, including *spo-11* (Stergiou et al. 2011), which reinforces a role for *rec-1* and *him-5* at this stage of meiosis I.

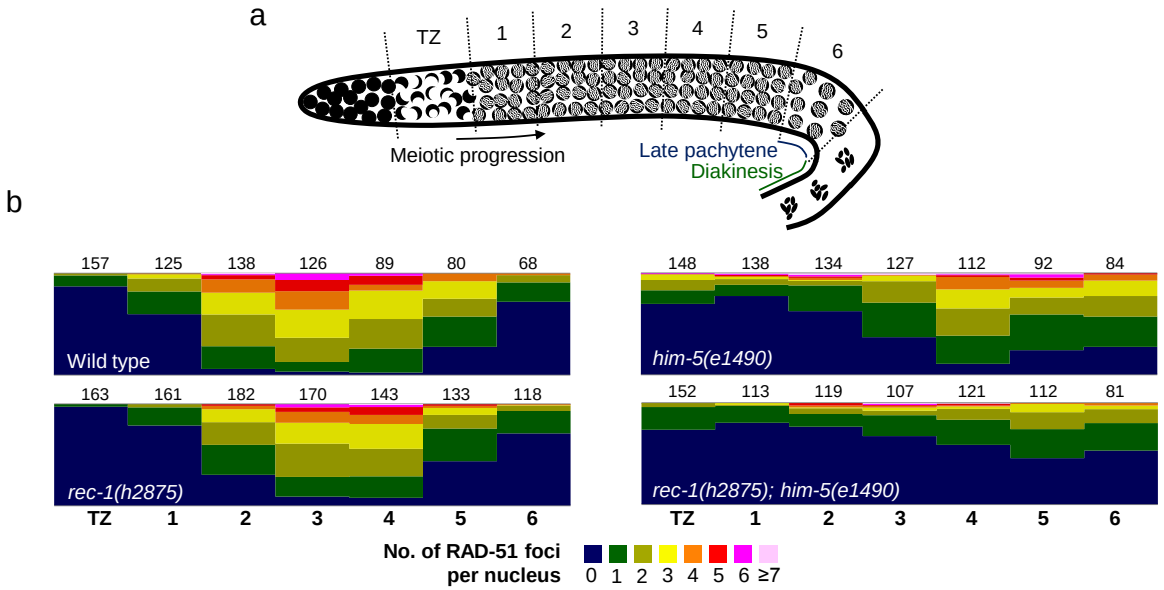

c

Genotype			*N*	Progeny count (average brood size)	Unhatched eggs (% of total progeny)	Hatched (% of total progeny)	
rec-1	*him-5*	*rad-54*				Developmentally arrested	Adult
+/+	+/+	*ok615/ok615*	**10**	**326** (32.6)	**326** (100%)	**0** (0%)	**0** (0%)
h2875/h2875	+/+	*ok615/ok615*	**7**	**1033** (147.6)	**1031** (99.8%)	**2** (0.2%)	**0** (0%)
+/+	*ok1896/ok1896*	*ok615/ok615*	**10**	**852** (85.2)	**846** (99.3%)	**5** (0.6%)	**1** (0.1%)
h2875/h2875	*ok1896/ok1896*	*ok615/ok615*	**6**	**813** (135.5)	**796** (97.9%)	**11** (1.4%)	**6** (0.7%)

Figure 4.9: Mutations in *rec-1* and *him-5* affect the dynamics of RAD-51 foci formation in the meiotic germline.
a) Schematic of *C. elegans* germline showing regions in which RAD-51 foci were quantified in individual nuclei. b) Quantification of percentage of nuclei (*y*-axis) in each region shown in a) (*x*-axis) with number of RAD-51 foci (revealed as a heat map showing range of foci from 0 to ≥7). Numbers above each stacked bar indicate the numbers of nuclei examined per region from TZ through zone 6. Two gonad arms were analyzed for each genotype. c) Mutations in *rec-1*, *him-5* or both rescue the maternal-effect embryonic lethal phenotype of *rad-54(ok615)* in two ways: by increasing the number of eggs laid ('Progeny count') and by increasing the proportion of eggs that hatch into either developmentally arrested larvae ('Developmentally arrested') or larvae that eventually grow into adult animals ('Adult'). Both effects are consistent with the decreased number of DSBs in the *rec-1*, *him-5* or double mutant genetic background.

4.4 Discussion

In all species examined the number of meiotic crossovers per unit DNA differs along the chromosome. This is seen dramatically in *C. elegans* due to near complete crossover interference along the autosomes resulting in a single crossover per homologue pair and producing a recombination map with apparent gene clusters in the central region (Brenner 1974; Barnes et al. 1995). The apparent clustering of crossovers is eliminated by mutation in the *rec-1* gene (Rose and Baillie 1979; Zetka and Rose 1995) but the identity of the mutation responsible for this phenotype remained a mystery for over 30 years. In this chapter, I report the molecular identification of the *rec-1* gene, which was the first genetic locus described that compromises the normal distribution of meiotic crossovers along the chromosome in any organism. I present evidence that the REC-1 protein contains a repeated motif, which is a CDK substrate *in vitro* [shown by the Boulton lab (Chung et al. 2015)], and its phosphorylation and subsequent de-phosphorylation appears to be required for establishing the normal distribution of meiotic crossover *in vivo* (Figure 4.4h-j). Phylogenetic analysis also revealed that REC-1 is evolutionarily related to HIM-5, albeit distantly. Functionally, REC-1 and HIM-5 cooperate to promote efficient meiotic double-strand break formation.

In species where genomic and RNA sequences are available, only those species within the *elegans-japonica* clade have a gene in the same relative orientation as *C. elegans rec-1* and situated between *pif-1* and *y18h1a.3* orthologues. Intriguingly, with the exception of *rec-1*, these positionally equivalent genes encode proteins that all share sequence similarity centered on an R-F-x-x-L-P/S box situated near the N-terminus. Using the sequence similarity shared by these R-

F-x-x-L-P/S-box genes to search the *C. elegans* genome, the Ponting laboratory identified *him-5* as the most significant hit. One reasonable possibility is that after the divergence of *C. elegans* from other *Caenorhabditis spp.*, the ancestral *rec-1/him-5* gene duplicated and became the present-day *rec-1* and *him-5*. In other species in the *elegans-japonica* clade, there remains only a single R-F-x-x-L-P/S-box gene within this synteny block.

The sequence conservation between *rec-1*, *him-5* and their orthologues is poor. Examples of poor sequence conservation can also be found in genes encoding Spo11 accessory factors in closely related yeasts (Keeney 2008; Richard et al. 2005). It has been proposed that the divergence of meiotic genes inhibits the reproductive success of inter-specific hybrids (Swanson and Vacquier 2002). Thus, the divergence of REC-1/HIM-5 orthologues may be a reflection of this principle.

Divergent as *rec-1/him-5* orthologues may be, the preference for recombination in chromosomal arms is, intriguingly, preserved through evolutionary time. Emerging genetic and genomic analyses in other *Caenorhabditis* species indicate recombination events, as in *C. elegans*, preferentially take place on the chromosome arms (Ross et al. 2011 and M. Rockman pers. comm.). Clearly the selective pressure for this preference exists among *Caenorhabditis* species, but given the poor sequence conservation of *rec-1/him-5* orthologues, additional components responsible for this preference may be different among different *Caenrhabditis* species.

The observation of a genetic interaction between *rec-1* and *him-5* clarified the relationship between these two genes, which were known to have similar mutant phenotypes in

terms of their impact on crossover distribution. The significant reduction in the number of meiotic RAD-51 foci in the *rec-1; him-5* double mutant shown here also implicates *rec-1* and *him-5* in meiotic DSB formation. Although there are significant differences between the process of meiosis in yeast and worms and between their respective meiotic mutant phenotypes, I speculate that REC-1 and HIM-5 may function as SPO-11 accessory proteins analogous to those described in *Saccharomyces cerevisiae* (reviewed in Keeney 2001, 2008; de Massy 2013). In *S. cerevaisae,* meiotic DSB formation is dependent on the phosphorylation of Mer2 by CDK and DDK (Henderson et al. 2006; Wan et al. 2008; Murakami and Keeney 2014). Data from this chapter suggest that phosphorylatable residues in REC-1 are required for REC-1 function (Figure 4.4i-j). Thus, a functional parallel can be drawn between the two CDK-dependent mechanisms that determine the position of meiotic crossover events.

In summary, loss of REC-1 function eliminates the wild-type preference for where a crossover will occur in *C. elegans* without severe accompanying phenotypic consequences. The molecular identification of the gene product responsible for this phenotype has not only provided information about how the crossover pattern is determined in this species, but has placed *rec-1* amongst a category of genes with divergent sequence that is required for crossover placement in *Caenorhabditis* species.

Chapter 5: Conclusions and discussion

In this thesis, I have characterized the functions of *chl-1* and *rec-1* in *Caenorhabditis elegans*. To summarize, my data in Chapter 2 support a role for CHL-1 in the maintenance of guanine-rich DNA sequences in the absence of DOG-1 function. My results in Chapter 3 reveal that CHL-1 is required for the timely repair or resolution of SPO-11-induced DSBs in the meiotic germline. Lastly, in Chapters 3 and 4, I describe the generation of novel mutant alleles for *chl-1* and *rec-1* using the emerging CRISPR-Cas9 technologies adapted to the *C. elegans* system. Here, I highlight the important findings presented in this thesis and discuss their implications for guanine-tract repair and meiotic recombination in *C. elegans*.

5.1 Genetic and biochemical data support CHL-1 as a backup mechanism for coping with guanine-rich structures.

In this work, I present genetic evidence that in the presence of functional DOG-1, CHL-1 has an undetectable role in maintaining the integrity of guanine-rich sequences (Figure 2.6); however, in the absence of DOG-1 function, CHL-1 is responsible for the repair or the resolution of a subset of guanine secondary structures (Figure 2.6). Given its predicted helicase activity, CHL-1 may be directly involved in the resolution of a subset of guanine structures, but only as a backup mechanism when DOG-1 is not functional. Biochemical analyses of the DDX11 from humans suggest that it has a much lower efficiency at unwinding guanine quadruplex structures than the FANCJ *in vitro* (Bharti et al. 2013). So it is conceivable that *in vivo,* the *C. elegans* CHL-1 may have a negligible effect on guanine structures under normal circumstances, because DOG-1 can act upon these structures much more efficiently; only when DOG-1 function is absent that these structures might persist long enough for CHL-1 to exert an effect.

5.2 The utility of CRISPR-Cas9 and other genome editing techniques is dependent on our understanding of DNA repair

The chromosome rearrangement near *chl-1* generated from the CRISPR-Cas9 protocol demonstrates that the generation of targeted mutants or epitope insertions through CRISPR-Cas9 can lead to unexpected mutations *C. elegans*. Several suggestions have been put forth to improve the frequency of successful targeted mutagenesis in *C. elegans*, including sgRNA target design changes (Farboud and Meyer 2015) or the knockdown of repair genes (Ward 2015). The full toolkit for CRISPR-Cas9 in *C. elegans* depends on the current understanding of DNA repair after the Cas9 cleavage.

A commonly cited mechanism for the generation of small indels after Cas9 DNA cleavage is via non-homologous end-joining (NHEJ) (Friedland et al. 2013; Ward 2015). The *rec-1* deletion alleles, with small homologies at the deletion breakpoints (Figure 4.2b), may support this view, as NHEJ repair can leave short stretches of homology (Pannunzio et al. 2014). However, a recent report challenges the view that these small indels were generated via NHEJ. Genetic evidence indicates that the mutagenic repair after Cas9 cleavage is mediated in large part by POLQ-1/Pol θ instead, and the Pol θ-mediated end-joining (TMEJ) is also able to generate the microhomologies similar to the ones seen in the *rec-1* deletion alleles (van Schendel et al. 2015). POLQ-1/Pol θ is the same polymerase involved in the mutagenic repair of G-rich DNA in *dog-1* mutants (Koole et al. 2014). Thus we are only beginning to understand to what extent repair pathways could be modulated to generate the expected type of targeted alleles.

5.3 Possible roles for REC-1 in meiotic recombination

My results are consistent with REC-1 functioning to direct extra DSBs toward the autosomal arms (biased DSB model, Figure 1.4), since *rec-1* mutants appear to have fewer DSBs in total than wild-type animals, and that *rec-1* mutants have altered distribution of crossover events. While the location of the DSBs could not be determined for this thesis, the number of DSBs was reduced, at least in the repair-deficient *rad-54* background (Chung et al. 2015). Additionally, REC-1 and HIM-5 function redundantly in the formation of DSBs such that when both functions are absent, the number of DSBs decreased dramatically. The location of the DSBs in *rec-1* or *him-5* single mutants are not known, but can be determined by a chromatin immunoprecitation experiment comparing the binding sites of RAD-51 in wild-type and in the *rec-1* or *him-5* mutant. This would clarify the role of REC-1 and HIM-5 in the 'biased DSB' model of REC-1 and HIM-5 function.

The biased CO-vs-NCO resolution model cannot be fully ruled out, although this model cannot easily explain why *rec-1* or *him-5* mutants have fewer DSBs. To test for biased CO/NCO, it is possible to measure crossover (CO) frequencies and gene conversion (NCO) frequencies across the length of an autosome. However, complications may arise, since a change in the DSB pattern across the chromosome may also change the CO/NCO ratios across the chromosome.

It remains possible that REC-1 may instead have an indirect role in shaping the meiotic pattern. One possibility I have not examined is that REC-1 functions in chromatin compaction or relaxation, thus indirectly making the autosomal arms more accessible to the DSB machinery (or the autosomal centres less accessible). An informative experiment would be to examine the chromatin states of *rec-1* mutant animals to see if any abnormal chromatin marks are being

deposited, or if LEM-2 binding sites along the autosomes have been changed [see 1.3.5 and (Kaur and Rockman 2014)].

5.4 The evolution of the *rec-1* gene

My analysis indicates that *rec-1/him-5* orthologues can be found in species within the *elegans-japonica* clade. In particular, these orthologues show sequence conservation at the RF..LP/S-box (Figure 4.8b-c). At present, it is not known what function is conferred by this six-amino-acid sequence – it is conceivable that targeted amino-acid change using current genome editing techniques could confirm that these residues are in fact essential for the function of HIM-5 and the REC-1/HIM-5 orthologues.

An obvious *rec-1/him-5* orthologue identifiable by sequence cannot be found outside the *elegans-japonica* clade – such as in the genomes of *Caenorhabditis angaria* or *Pristionchus pacificus*, where the six-gene synteny block (Figure 4.8a) is not conserved (data not shown). Sequence divergence does not appear to be unusual for genes involved in meiosis. Comparative genomics have revealed that genes with functions in meiosis often have poor sequence conservation when compared to genes in DNA repair or replication (Richard et al. 2005). Indeed, many factors required for DSB formation in *S. cerevisiae* have no orthologues identifiable by sequence in mammals, in *C. elegans*, or in some cases, in closely related yeast species (Keeney 2008). It has been proposed that the divergence of meiotic genes reduces the reproductive success of inter-specific hybrids (Swanson and Vacquier 2002). Thus, a lack of REC-1/HIM-5 orthologue outside the *elegans-japonica* clade identifiable by sequence may be a reflection of this principle.

It is not known if mutations in *rec-1/him-5* orthologues confer a similar recombination-altering phenotype as mutations in *C. elegans rec-1* or *him-5,* if they confer a clear non-disjunction phenotype seen in *C. elegans him-5* mutants, or other phenotypes. As the recombination pattern in *C. briggsae* is analogous to the one found in *C. elegans* (recombinogenic autosome arms and recombinationally suppressed autosome centres) (Ross et al. 2011), it is conceivable that the *C. briggsae rec-1/him-5* orthologue may be responsible for establishing this pattern too. Currently CRISPR-Cas9 systems are being adapted to *C. briggsae* (Bhawati Gupta, McMaster University, pers. comm.), which offers the exciting possibility of knocking out the *C. briggsae rec-1/him-5* orthologue.

5.5 Concluding remarks

In this thesis, I present my scientific journal - beginning with the characterization of a gene required for somatic cell division and guanine-tract stability, continuing with the essential role of this gene in the mitotic and the meiotic germline, and ending with the molecular identification of another gene required for the establishment of the meiotic crossover pattern. *C. elegans* provided a unique system to examine *chl-1* and *rec-1* function, which have in common roles in meiosis. The information gained from the phenotypic analysis of *chl-1* and *rec-1* mutants contributes to the increasingly detailed models of DNA repair and meiotic recombination in *C. elegans*.

Bibliography

Acquaviva L, Székvölgyi L, Dichtl B, Dichtl BS, de La Roche Saint André C, Nicolas A, Géli V. 2013. The COMPASS subunit Spp1 links histone methylation to initiation of meiotic recombination. *Science* **339**: 215–218.

Adamo A, Montemauri P, Silva N, Ward JD, Boulton SJ, La Volpe A. 2008. BRC-1 acts in the inter-sister pathway of meiotic double-strand break repair. *EMBO Rep* **9**: 287–292.

Agostinho A, Meier B, Sonneville R, Jagut M, Woglar A, Blow J, Jantsch V, Gartner A. 2013. Combinatorial regulation of meiotic holliday junction resolution in *C. elegans* by HIM-6 (BLM) helicase, SLX-4, and the SLX-1, MUS-81 and XPF-1 nucleases. *PLoS Genet* **9**: e1003591.

Ahmed S, Hodgkin J. 2000. MRT-2 checkpoint protein is required for germline immortality and telomere replication in *C. elegans*. *Nature* **403**: 159–164.

Allen MA, Hillier LW, Waterston RH, Blumenthal T. 2011. A global analysis of *C. elegans* trans-splicing. *Genome Res* **21**: 255–264.

Alpi A, Pasierbek P, Gartner A, Loidl J. 2003. Genetic and cytological characterization of the recombination protein RAD-51 in *Caenorhabditis elegans*. *Chromosoma* **112**: 6–16.

Arribere JA, Bell RT, Fu BXH, Artiles KL, Hartman PS, Fire AZ. 2014. Efficient marker-free recovery of custom genetic modifications with CRISPR/Cas9 in *Caenorhabditis elegans*. *Genetics* **198**: 837–846.

Bailey C, Fryer AE, Greenslade M. 2015. Warsaw Breakage Syndrome – A further report, emphasising cutaneous findings. *Eur J Med Genet* **58**: 235–237.

Barber LJ, Youds JL, Ward JD, McIlwraith MJ, O'Neil NJ, Petalcorin MIR, Martin JS, Collis SJ, Cantor SB, Auclair M, et al. 2008. RTEL1 maintains genomic stability by suppressing homologous recombination. *Cell* **135**: 261–271.

Barnes TM, Kohara Y, Coulson A, Hekimi S. 1995. Meiotic recombination, noncoding DNA and genomic organization in *Caenorhabditis elegans*. *Genetics* **141**: 159–179.

Baudat F, Imai Y, de Massy B. 2013. Meiotic recombination in mammals: localization and regulation. *Nat Rev Genet* **14**: 794–806.

Baudrimont A, Penkner A, Woglar A, Mamnun YM, Hulek M, Struck C, Schnabel R, Loidl J, Jantsch V. 2011. A new thermosensitive *smc-3* allele reveals involvement of cohesin in homologous recombination in *C. elegans*. *PLoS ONE* **6**: e24799.

Bhalla N, Wynne DJ, Jantsch V, Dernburg AF. 2008. ZHP-3 acts at crossovers to couple meiotic recombination with synaptonemal complex disassembly and bivalent formation in *C. elegans*. *PLoS Genet* **4**: e1000235.

Bharti SK, Khan I, Banerjee T, Sommers JA, Wu Y, Brosh RM. 2014. Molecular functions and cellular roles of the ChlR1 (DDX11) helicase defective in the rare cohesinopathy Warsaw breakage syndrome. *Cell Mol Life Sci CMLS* **71**: 2625–2639.

Bharti SK, Sommers JA, George F, Kuper J, Hamon F, Shin-ya K, Teulade-Fichou M-P, Kisker C, Brosh RM. 2013. Specialization among iron-sulfur cluster helicases to resolve G-quadruplex DNA structures that threaten genomic stability. *J Biol Chem* **288**: 28217–28229.

Birney E, Clamp M, Durbin R. 2004. GeneWise and Genomewise. *Genome Res* **14**: 988–995.

Borde V, Robine N, Lin W, Bonfils S, Géli V, Nicolas A. 2009. Histone H3 lysine 4 trimethylation marks meiotic recombination initiation sites. *EMBO J* **28**: 99–111.

Brenner S. 1974. The genetics of *Caenorhabditis elegans*. *Genetics* **77**: 71–94.

Brick K, Smagulova F, Khil P, Camerini-Otero RD, Petukhova GV. 2012. Genetic recombination is directed away from functional genomic elements in mice. *Nature* **485**: 642–645.

Cantor SB, Bell DW, Ganesan S, Kass EM, Drapkin R, Grossman S, Wahrer DC, Sgroi DC, Lane WS, Haber DA, et al. 2001. BACH1, a novel helicase-like protein, interacts directly with BRCA1 and contributes to its DNA repair function. *Cell* **105**: 149–160.

Cao L, Alani E, Kleckner N. 1990. A pathway for generation and processing of double-strand breaks during meiotic recombination in *S. cerevisiae*. *Cell* **61**: 1089–1101.

Capo-Chichi J-M, Bharti SK, Sommers JA, Yammine T, Chouery E, Patry L, Rouleau GA, Samuels ME, Hamdan FF, Michaud JL, et al. 2013. Identification and biochemical characterization of a novel mutation in *DDX11* causing Warsaw breakage syndrome. *Hum Mutat* **34**: 103–107.

Castillo Bosch P, Segura-Bayona S, Koole W, van Heteren JT, Dewar JM, Tijsterman M, Knipscheer P. 2014. FANCJ promotes DNA synthesis through G-quadruplex structures. *EMBO J* **33**: 2521–2533.

Celniker SE, Dillon LAL, Gerstein MB, Gunsalus KC, Henikoff S, Karpen GH, Kellis M, Lai EC, Lieb JD, MacAlpine DM, et al. 2009. Unlocking the secrets of the genome. *Nature* **459**: 927–930.

Chan RC, Chan A, Jeon M, Wu TF, Pasqualone D, Rougvie AE, Meyer BJ. 2003. Chromosome cohesion is regulated by a clock gene paralogue TIM-1. *Nature* **423**: 1002–1009.

Chenna R, Sugawara H, Koike T, Lopez R, Gibson TJ, Higgins DG, Thompson JD. 2003. Multiple sequence alignment with the Clustal series of programs. *Nucleic Acids Res* **31**: 3497–3500.

Cheung I, Schertzer M, Rose A, Lansdorp PM. 2002. Disruption of *dog-1* in *Caenorhabditis elegans* triggers deletions upstream of guanine-rich DNA. *Nat Genet* **31**: 405–409.

Chin GM, Villeneuve AM. 2001. *C. elegans mre-11* is required for meiotic recombination and DNA repair but is dispensable for the meiotic G(2) DNA damage checkpoint. *Genes Dev* **15**: 522–534.

Chung G, O'Neil NJ, Rose AM. 2011. CHL-1 provides an essential function affecting cell proliferation and chromosome stability in Caenorhabditis elegans. *DNA Repair* **10**: 1174–1182.

Chung G, Rose AM, Petalcorin MIR, Martin JS, Kessler Z, Sanchez-Pulido L, Ponting CP, Yanowitz JL, Boulton SJ. 2015. REC-1 and HIM-5 distribute meiotic crossovers and function redundantly in meiotic double-strand break formation in Caenorhabditis elegans. *Genes Dev* **29**: 1969–1979.

Cleaver JE, Lam ET, Revet I. 2009. Disorders of nucleotide excision repair: the genetic and molecular basis of heterogeneity. *Nat Rev Genet* **10**: 756–768.

Clejan I, Boerckel J, Ahmed S. 2006. Developmental modulation of nonhomologous end joining in *Caenorhabditis elegans*. *Genetics* **173**: 1301–1317.

Clucas C, Cabello J, Büssing I, Schnabel R, Johnstone IL. 2002. Oncogenic potential of a *C.elegans cdc25* gene is demonstrated by a gain-of-function allele. *EMBO J* **21**: 665–674.

Colaiácovo MP, MacQueen AJ, Martinez-Perez E, McDonald K, Adamo A, La Volpe A, Villeneuve AM. 2003. Synaptonemal complex assembly in *C. elegans* is dispensable for loading strand-exchange proteins but critical for proper completion of recombination. *Dev Cell* **5**: 463–474.

Cole F, Keeney S, Jasin M. 2010. Comprehensive, Fine-scale dissection of homologous recombination outcomes at a hot spot in mouse meiosis. *Mol Cell* **39**: 700–710.

Couteau F, Nabeshima K, Villeneuve A, Zetka M. 2004. A component of *C. elegans* meiotic chromosome axes at the interface of homolog alignment, synapsis, nuclear rorganization, and recombination. *Curr Biol* **14**: 585–592.

Creighton HB, McClintock B. 1931. A correlation of cytological and genetical crossing-over in *Zea mays*. *Proc Natl Acad Sci U S A* **17**: 492–497.

Deans AJ, West SC. 2011. DNA interstrand crosslink repair and cancer. *Nat Rev Cancer* **11**: 467–480.

De Boer E, Jasin M, Keeney S. 2015. Local and sex-specific biases in crossover vs. noncrossover outcomes at meiotic recombination hot spots in mice. *Genes Dev* **29**: 1721–1733.

De Massy B. 2013. Initiation of meiotic recombination: how and where? Conservation and specificities among eukaryotes. *Annu Rev Genet* **47**: 563–599.

Dernburg AF, McDonald K, Moulder G, Barstead R, Dresser M, Villeneuve AM. 1998. Meiotic recombination in *C. elegans* initiates by a conserved mechanism and is dispensable for homologous chromosome synapsis. *Cell* **94**: 387–398.

Dickinson DJ, Ward JD, Reiner DJ, Goldstein B. 2013. Engineering the *Caenorhabditis elegans* genome using Cas9-triggered homologous recombination. *Nat Methods* **10**: 1028–1034.

Ding H, Schertzer M, Wu X, Gertsenstein M, Selig S, Kammori M, Pourvali R, Poon S, Vulto I, Chavez E, et al. 2004. Regulation of murine telomere length by *Rtel*: an essential gene encoding a helicase-like protein. *Cell* **117**: 873–886.

Edgely M, Baillie DL, Riddle DL, Rose AM. 2006. Genetic balancers. *WormBook*. http://www.wormbook.org/chapters/www_geneticbalancers/geneticbalancers.html (Accessed April 30, 2010).

Fairman-Williams ME, Guenther U-P, Jankowsky E. 2010. SF1 and SF2 helicases: family matters. *Curr Opin Struct Biol* **20**: 313–324.

Farboud B, Meyer BJ. 2015. Dramatic enhancement of genome editing by CRISPR/Cas9 through improved guide RNA design. *Genetics* genetics.115.175166.

Farina A, Shin J-H, Kim D-H, Bermudez VP, Kelman Z, Seo Y-S, Hurwitz J. 2008. Studies with the human cohesin establishment factor, ChlR1. Association of ChlR1 with Ctf18-RFC and Fen1. *J Biol Chem* **283**: 20925–20936.

Félix M-A, Braendle C, Cutter AD. 2014. A streamlined system for species diagnosis in *Caenorhabditis (Nematoda: Rhabditidae)* with name designations for 15 distinct biological species. *PloS One* **9**: e94723.

Felsenstein J. 1985. Confidence limits on phylogenies: an approach using the bootstrap. *Evolution* **39**: 783–791.

Fernandez AG, Bargmann BOR, Mis EK, Edgley ML, Birnbaum KD, Piano F. 2012. High-throughput fluorescence-based isolation of live *C. elegans* larvae. *Nat Protoc* **7**: 1502–1510.

Finn RD, Clements J, Eddy SR. 2011. HMMER web server: interactive sequence similarity searching. *Nucleic Acids Res* **39**: W29–37.

Flibotte S, Edgley ML, Chaudhry I, Taylor J, Neil SE, Rogula A, Zapf R, Hirst M, Butterfield Y, Jones SJ, et al. 2010. Whole-genome profiling of mutagenesis in *Caenorhabditis elegans*. *Genetics* **185**: 431–441.

Fowler KR, Sasaki M, Milman N, Keeney S, Smith GR. 2014. Evolutionarily diverse determinants of meiotic DNA break and recombination landscapes across the genome. *Genome Res* **24**: 1650–1664.

Friedland AE, Tzur YB, Esvelt KM, Colaiácovo MP, Church GM, Calarco JA. 2013. Heritable genome editing in *C. elegans* via a CRISPR-Cas9 system. *Nat Methods* **10**: 741–743.

Frøkjaer-Jensen C, Davis MW, Hopkins CE, Newman BJ, Thummel JM, Olesen S-P, Grunnet M, Jorgensen EM. 2008. Single-copy insertion of transgenes in *Caenorhabditis elegans*. *Nat Genet* **40**: 1375–1383.

Frøkjær-Jensen C, Wayne Davis M, Hopkins CE, Newman BJ, Thummel JM, Olesen S-P, Grunnet M, Jorgensen EM. 2008. Single-copy insertion of transgenes in *Caenorhabditis elegans*. *Nat Genet* **40**: 1375–1383.

Gabdank I, Fire AZ. 2014. Gamete-type dependent crossover interference levels in a defined region of *Caenorhabditis elegans* chromosome V. *G3 Bethesda Md* **4**: 117–120.

Gao J, Kim H-M, Elia AE, Elledge SJ, Colaiácovo MP. 2015. NatB domain-containing CRA-1 antagonizes hydrolase ACER-1 linking acetyl-CoA metabolism to the initiation of recombination during *C. elegans* meiosis. *PLoS Genet* **11**: e1005029.

Garcia-Muse T, Boulton SJ. 2005. Distinct modes of ATR activation after replication stress and DNA double-strand breaks in *Caenorhabditis elegans*. *EMBO J* **24**: 4345–4355.

Gartner A, Milstein S, Ahmed S, Hodgkin J, Hengartner MO. 2000. A conserved checkpoint pathway mediates DNA damage--induced apoptosis and cell cycle arrest in *C. elegans*. *Mol Cell* **5**: 435–443.

Gengyo-Ando K, Mitani S. 2000. Characterization of mutations induced by ethyl methanesulfonate, UV, and trimethylpsoralen in the nematode *Caenorhabditis elegans*. *Biochem Biophys Res Commun* **269**: 64–69.

Gerring SL, Spencer F, Hieter P. 1990. The CHL 1 (CTF 1) gene product of *Saccharomyces cerevisiae* is important for chromosome transmission and normal cell cycle progression in G2/M. *EMBO J* **9**: 4347–4358.

Gibson DG, Young L, Chuang R-Y, Venter JC, Hutchison CA, Smith HO. 2009. Enzymatic assembly of DNA molecules up to several hundred kilobases. *Nat Methods* **6**: 343–345.

Giraut L, Falque M, Drouaud J, Pereira L, Martin OC, Mézard C. 2011. Genome-wide crossover distribution in *Arabidopsis thaliana* meiosis reveals sex-specific patterns along chromosomes. *PLoS Genet* **7**: e1002354.

Haber JE. 1974. Bisexual mating behavior in a diploid of *Saccharomyces cerevisiae*: evidence for genetically controlled non-random chromosome loss during vegetative growth. *Genetics* **78**: 843–858.

Hayashi M, Chin GM, Villeneuve AM. 2007. *C. elegans* germ cells switch between distinct modes of double-strand break repair during meiotic prophase progression. *PLoS Genet* **3**: e191.

Heger A, Holm L. 2000. Rapid automatic detection and alignment of repeats in protein sequences. *Proteins* **41**: 224–237.

Henderson KA, Kee K, Maleki S, Santini PA, Keeney S. 2006. Cyclin-dependent kinase directly regulates initiation of meiotic recombination. *Cell* **125**: 1321–1332.

Herman RK, Kari CK, Hartman PS. 1982. Dominant X-chromosome nondisjunction mutants of *Caenorhabditis elegans*. *Genetics* **102**: 379–400.

Hillers KJ, Villeneuve AM. 2003. Chromosome-wide control of meiotic crossing over in *C. elegans*. *Curr Biol CB* **13**: 1641–1647.

Hodgkin J, Horvitz HR, Brenner S. 1979. Nondisjunction mutants of the nematode *Caenorhabditis elegans*. *Genetics* **91**: 67–94.

Holliday R. 1964. A mechanism for gene conversion in fungi. *Genet Res* **5**: 282–304.

Holloway K, Lawson VE, Jeffreys AJ. 2006. Allelic recombination and *de novo* deletions in sperm in the human β-globin gene region. *Hum Mol Genet* **15**: 1099–1111.

Holway AH, Kim S-H, La Volpe A, Michael WM. 2006. Checkpoint silencing during the DNA damage response in *Caenorhabditis elegans* embryos. *J Cell Biol* **172**: 999–1008.

Howell AM, Gilmour SG, Mancebo RA, Rose AM. 1987. Genetic analysis of a large autosomal region in *Caenorhabditis elegans* by the use of a free duplication. *Genet Res* **49**: 207–213.

Hyppa RW, Smith GR. 2010. Crossover invariance determined by partner choice for meiotic DNA break repair. *Cell* **142**: 243–255.

Inoue A, Li T, Roby SK, Valentine MB, Inoue M, Boyd K, Kidd VJ, Lahti JM. 2007. Loss of ChlR1 helicase in mouse causes lethality due to the accumulation of aneuploid cells generated by cohesion defects and placental malformation. *Cell Cycle Georget Tex* **6**: 1646–1654.

Janssens FA. 1909. La théorie de la Chiasmatypie. Nouvelle interprétation des cinèses de maturation. *Cellule* **22**: 387–411.

Jantsch V, Pasierbek P, Mueller MM, Schweizer D, Jantsch M, Loidl J. 2004. Targeted gene knockout reveals a role in meiotic recombination for ZHP-3, a Zip3-related protein in *Caenorhabditis elegans*. *Mol Cell Biol* **24**: 7998–8006.

Jones DT, Taylor WR, Thornton JM. 1992. The rapid generation of mutation data matrices from protein sequences. *Comput Appl Biosci CABIOS* **8**: 275–282.

Jones M, Rose A. 2012. A DOG's view of Fanconi anemia: Insights from *C. elegans*. *Anemia* **2012**. http://www.ncbi.nlm.nih.gov/pmc/articles/PMC3368526/ (Accessed September 14, 2015).

Kaback DB, Steensma HY, Jonge P de. 1989. Enhanced meiotic recombination on the smallest chromosome of *Saccharomyces cerevisiae*. *Proc Natl Acad Sci* **86**: 3694–3698.

Kadandale P, Chatterjee I, Singson A. 2009. Germline transformation of *Caenorhabditis elegans* by injection. *Methods Mol Biol Clifton NJ* **518**: 123–133.

Kaur T, Rockman MV. 2014. Crossover heterogeneity in the absence of hotspots in *Caenorhabditis elegans*. *Genetics* **196**: 137–148.

Keeney S. 2001. Mechanism and control of meiotic recombination initiation. *Curr Top Dev Biol* **52**: 1–53.

Keeney S. 2008. Spo11 and the formation of DNA double-strand breaks in meiosis. *Genome Dyn Stab* **2**: 81–123.

Keeney S, Giroux CN, Kleckner N. 1997. Meiosis-specific DNA double-strand breaks are catalyzed by Spo11, a member of a widely conserved protein family. *Cell* **88**: 375–384.

Keeney S, Lange J, Mohibullah N. 2014. Self-organization of meiotic recombination initiation: general principles and molecular pathways. *Annu Rev Genet* **48**: 187–214.

Kelly KO, Dernburg AF, Stanfield GM, Villeneuve AM. 2000. *Caenorhabditis elegans msh-5* is required for both normal and radiation-induced meiotic crossing over but not for completion of meiosis. *Genetics* **156**: 617–630.

Khil PP, Smagulova F, Brick KM, Camerini-Otero RD, Petukhova GV. 2012. Sensitive mapping of recombination hotspots using sequencing-based detection of ssDNA. *Genome Res* **22**: 957–965.

Kliman RM, Hey J. 1993. Reduced natural selection associated with low recombination in *Drosophila melanogaster*. *Mol Biol Evol* **10**: 1239–1258.

Koole W, van Schendel R, Karambelas AE, van Heteren JT, Okihara KL, Tijsterman M. 2014. A polymerase theta-dependent repair pathway suppresses extensive genomic instability at endogenous G4 DNA sites. *Nat Commun* **5**: 3216.

Kruisselbrink E, Guryev V, Brouwer K, Pontier DB, Cuppen E, Tijsterman M. 2008. Mutagenic capacity of endogenous G4 DNA underlies genome instability in FANCJ-defective *C. elegans*. *Curr Biol CB* **18**: 900–905.

Laha S, Das SP, Hajra S, Sau S, Sinha P. 2006. The budding yeast protein Chl1p is required to preserve genome integrity upon DNA damage in S-phase. *Nucleic Acids Res* **34**: 5880–5891.

Lans H, Vermeulen W. 2015. Tissue specific response to DNA damage: *C. elegans* as role model. *DNA Repair* **32**: 141–148.

Leman AR, Noguchi C, Lee CY, Noguchi E. 2010. Human Timeless and Tipin stabilize replication forks and facilitate sister-chromatid cohesion. *J Cell Sci* **123**: 660–670.

Levitus M, Waisfisz Q, Godthelp BC, de Vries Y, Hussain S, Wiegant WW, Elghalbzouri-Maghrani E, Steltenpool J, Rooimans MA, Pals G, et al. 2005. The DNA helicase BRIP1 is defective in Fanconi anemia complementation group J. *Nat Genet* **37**: 934–935.

Levran O, Attwooll C, Henry RT, Milton KL, Neveling K, Rio P, Batish SD, Kalb R, Velleuer E, Barral S, et al. 2005. The BRCA1-interacting helicase BRIP1 is deficient in Fanconi anemia. *Nat Genet* **37**: 931–933.

Libuda DE, Uzawa S, Meyer BJ, Villeneuve AM. 2013. Meiotic chromosome structures constrain and respond to designation of crossover sites. *Nature* **502**: 703–706.

Lim JGY, Stine RRW, Yanowitz JL. 2008. Domain-specific regulation of recombination in *Caenorhabditis elegans* in response to temperature, age and sex. *Genetics* **180**: 715–726.

Litman R, Peng M, Jin Z, Zhang F, Zhang J, Powell S, Andreassen PR, Cantor SB. 2005. BACH1 is critical for homologous recombination and appears to be the Fanconi anemia gene product FANCJ. *Cancer Cell* **8**: 255–265.

Liu T, Rechtsteiner A, Egelhofer TA, Vielle A, Latorre I, Cheung M-S, Ercan S, Ikegami K, Jensen M, Kolasinska-Zwierz P, et al. 2011. Broad chromosomal domains of histone modification patterns in *C. elegans*. *Genome Res* **21**: 227–236.

London TBC, Barber LJ, Mosedale G, Kelly GP, Balasubramanian S, Hickson ID, Boulton SJ, Hiom K. 2008. FANCJ is a structure-specific DNA helicase associated with the maintenance of genomic G/C tracts. *J Biol Chem* **283**: 36132–36139.

Lui DY, Colaiácovo MP. 2013. Meiotic development in *Caenorhabditis elegans*. *Adv Exp Med Biol* **757**: 133–170.

Lundin C, North M, Erixon K, Walters K, Jenssen D, Goldman ASH, Helleday T. 2005. Methyl methanesulfonate (MMS) produces heat-labile DNA damage but no detectable *in vivo* DNA double-strand breaks. *Nucleic Acids Res* **33**: 3799–3811.

Mayer ML, Pot I, Chang M, Xu H, Aneliunas V, Kwok T, Newitt R, Aebersold R, Boone C, Brown GW, et al. 2004. Identification of protein complexes required for efficient sister chromatid cohesion. *Mol Biol Cell* **15**: 1736–1745.

McIntire SL, Jorgensen E, Horvitz HR. 1993a. Genes required for GABA function in *Caenorhabditis elegans*. *Nature* **364**: 334–337.

McIntire SL, Jorgensen E, Kaplan J, Horvitz HR. 1993b. The GABAergic nervous system of *Caenorhabditis elegans*. *Nature* **364**: 337–341.

McKim KS, Howell AM, Rose AM. 1988. The effects of translocations on recombination frequency in *Caenorhabditis elegans*. *Genetics* **120**: 987–1001.

McKim KS, Peters K, Rose AM. 1993. Two types of sites required for meiotic chromosome pairing in *Caenorhabditis elegans*. *Genetics* **134**: 749–768.

Meneely PM, Farago AF, Kauffman TM. 2002. Crossover distribution and high interference for both the X chromosome and an autosome during oogenesis and spermatogenesis in *Caenorhabditis elegans*. *Genetics* **162**: 1169–1177.

Meneely PM, McGovern OL, Heinis FI, Yanowitz JL. 2012. Crossover distribution and frequency are regulated by *him-5* in *Caenorhabditis elegans*. *Genetics* **190**: 1251–1266.

Mets DG, Meyer BJ. 2009. Condensins regulate meiotic DNA break distribution, thus crossover frequency, by controlling chromosome structure. *Cell* **139**: 73–86.

Mohaghegh P, Karow JK, Brosh RM, Bohr VA, Hickson ID. 2001. The Bloom's and Werner's syndrome proteins are DNA structure-specific helicases. *Nucleic Acids Res* **29**: 2843–2849.

Mojica FJM, Díez-Villaseñor C, García-Martínez J, Almendros C. 2009. Short motif sequences determine the targets of the prokaryotic CRISPR defence system. *Microbiology* **155**: 733–740.

Murakami H, Keeney S. 2014. Temporospatial coordination of meiotic DNA replication and recombination via DDK recruitment to replisomes. *Cell* **158**: 861–873.

Nabeshima K, Villeneuve AM, Hillers KJ. 2004. Chromosome-wide regulation of meiotic crossover formation in *Caenorhabditis elegans* requires properly assembled chromosome axes. *Genetics* **168**: 1275–1292.

Nachman MW, Churchill GA. 1996. Heterogeneity in rates of recombination across the mouse genome. *Genetics* **142**: 537–548.

Needleman SB, Wunsch CD. 1970. A general method applicable to the search for similarities in the amino acid sequence of two proteins. *J Mol Biol* **48**: 443–453.

Nottke AC, Beese-Sims SE, Pantalena LF, Reinke V, Shi Y, Colaiácovo MP. 2011. SPR-5 is a histone H3K4 demethylase with a role in meiotic double-strand break repair. *Proc Natl Acad Sci U S A* **108**: 12805–12810.

Ogiwara H, Ui A, Lai MS, Enomoto T, Seki M. 2007. Chl1 and Ctf4 are required for damage-induced recombinations. *Biochem Biophys Res Commun* **354**: 222–226.

Oliver SG, van der Aart QJ, Agostoni-Carbone ML, Aigle M, Alberghina L, Alexandraki D, Antoine G, Anwar R, Ballesta JP, Benit P. 1992. The complete DNA sequence of yeast chromosome III. *Nature* **357**: 38–46.

O'Neil NJ, Martin JS, Youds JL, Ward JD, Petalcorin MIR, Rose AM, Boulton SJ. 2013. Joint molecule resolution requires the redundant activities of MUS-81 and XPF-1 during *Caenorhabditis elegans* meiosis. *PLoS Genet* **9**: e1003582.

Page SL, Hawley RS. 2003. Chromosome choreography: the meiotic ballet. *Science* **301**: 785–789.

Pan J, Sasaki M, Kniewel R, Murakami H, Blitzblau HG, Tischfield SE, Zhu X, Neale MJ, Jasin M, Socci ND, et al. 2011. A hierarchical combination of factors shapes the genome-wide topography of yeast meiotic recombination initiation. *Cell* **144**: 719–731.

Pannunzio NR, Li S, Watanabe G, Lieber MR. 2014. Non-homologous end joining often uses microhomology: Implications for alternative end joining. *DNA Repair* **17**: 74–80.

Parish JL, Rosa J, Wang X, Lahti JM, Doxsey SJ, Androphy EJ. 2006. The DNA helicase ChlR1 is required for sister chromatid cohesion in mammalian cells. *J Cell Sci* **119**: 4857–4865.

Pasierbek P, Födermayr M, Jantsch V, Jantsch M, Schweizer D, Loidl J. 2003. The *Caenorhabditis elegans* SCC-3 homologue is required for meiotic synapsis and for proper chromosome disjunction in mitosis and meiosis. *Exp Cell Res* **289**: 245–255.

Pasierbek P, Jantsch M, Melcher M, Schleiffer A, Schweizer D, Loidl J. 2001. A *Caenorhabditis elegans* cohesion protein with functions in meiotic chromosome pairing and disjunction. *Genes Dev* **15**: 1349–1360.

Penkner A, Portik-Dobos Z, Tang L, Schnabel R, Novatchkova M, Jantsch V, Loidl J. 2007. A conserved function for a *Caenorhabditis elegans* Com1/Sae2/CtIP protein homolog in meiotic recombination. *EMBO J* **26**: 5071–5082.

Petalcorin MIR, Galkin VE, Yu X, Egelman EH, Boulton SJ. 2007. Stabilization of RAD-51-DNA filaments via an interaction domain in *Caenorhabditis elegans* BRCA2. *Proc Natl Acad Sci U S A* **104**: 8299–8304.

Petalcorin MIR, Sandall J, Wigley DB, Boulton SJ. 2006. CeBRC-2 stimulates D-loop formation by RAD-51 and promotes DNA single-strand annealing. *J Mol Biol* **361**: 231–242.

Petronczki M, Chwalla B, Siomos MF, Yokobayashi S, Helmhart W, Deutschbauer AM, Davis RW, Watanabe Y, Nasmyth K. 2004. Sister-chromatid cohesion mediated by the alternative RF-CCtf18/Dcc1/Ctf8, the helicase Chl1 and the polymerase-alpha-associated protein Ctf4 is essential for chromatid disjunction during meiosis II. *J Cell Sci* **117**: 3547–3559.

Phillips CM, Dernburg AF. 2006. A family of zinc-finger proteins is required for chromosome-specific pairing and synapsis during meiosis in *C. elegans*. *Dev Cell* **11**: 817–829.

Phillips CM, Wong C, Bhalla N, Carlton PM, Weiser P, Meneely PM, Dernburg AF. 2005. HIM-8 binds to the X chromosome pairing center and mediates chromosome-specific meiotic synapsis. *Cell* **123**: 1051–1063.

Piano F, Schetter AJ, Morton DG, Gunsalus KC, Reinke V, Kim SK, Kemphues KJ. 2002. Gene clustering based on RNAi phenotypes of ovary-enriched genes in *C. elegans*. *Curr Biol CB* **12**: 1959–1964.

Rattray B, Rose AM. 1988. Increased intragenic recombination and non-disjunction in the Rec-1 strain of *Caenorhabditis elegans*. *Genet Res* **51**: 89–93.

Reinke V, Cutter AD. 2009. Germline expression influences operon organization in the *Caenorhabditis elegans* genome. *Genetics* **181**: 1219–1228.

Richard G-F, Kerrest A, Lafontaine I, Dujon B. 2005. Comparative genomics of hemiascomycete yeasts: genes involved in DNA replication, repair, and recombination. *Mol Biol Evol* **22**: 1011–1023.

Rinaldo C, Bazzicalupo P, Ederle S, Hilliard M, La Volpe A. 2002. Roles for *Caenorhabditis elegans rad-51* in meiosis and in resistance to ionizing radiation during development. *Genetics* **160**: 471–479.

Rockman MV, Kruglyak L. 2009. Recombinational landscape and population genomics of *Caenorhabditis elegans*. *PLoS Genet* **5**: e1000419.

Rose AM, Baillie DL. 1979. A mutation in *Caenorhabditis elegans* that increases recombination frequency more than threefold. *Nature* **281**: 599–600.

Rose AM, Baillie DL, Curran J. 1984. Meiotic pairing behavior of two free duplications of linkage group I in *Caenorhabditis elegans. Mol Gen Genet MGG* **195**: 52–56.

Rose AM, O'Neil NJ, Bilenky M, Butterfield YS, Malhis N, Flibotte S, Jones MR, Marra M, Baillie DL, Jones SJM. 2010. Genomic sequence of a mutant strain of *Caenorhabditis elegans* with an altered recombination pattern. *BMC Genomics* **11**: 131.

Rosenbluth RE, Baillie DL. 1981. The genetic analysis of a reciprocal translocation, *eT1(III; V)*, in *Caenorhabditis elegans. Genetics* **99**: 415–428.

Ross JA, Koboldt DC, Staisch JE, Chamberlin HM, Gupta BP, Miller RD, Baird SE, Haag ES. 2011. *Caenorhabditis briggsae* recombinant inbred line genotypes reveal inter-strain incompatibility and the evolution of recombination. *PLoS Genet* **7**: e1002174.

Rosu S, Libuda DE, Villeneuve AM. 2011. Robust crossover assurance and regulated interhomolog access maintain meiotic crossover number. *Science* **334**: 1286–1289.

Rudra S, Skibbens RV. 2013. Chl1 DNA helicase regulates Scc2 deposition specifically during DNA-replication in *Saccharomyces cerevisiae*. *PloS One* **8**: e75435.

Saito TT, Lui DY, Kim H-M, Meyer K, Colaiácovo MP. 2013. Interplay between structure-specific endonucleases for crossover control during *Caenorhabditis elegans* meiosis. *PLoS Genet* **9**: e1003586.

Saito TT, Mohideen F, Meyer K, Harper JW, Colaiácovo MP. 2012. SLX-1 is required for maintaining genomic integrity and promoting meiotic noncrossovers in the *Caenorhabditis elegans* germline. *PLoS Genet* **8**: e1002888.

Sanford C, Perry MD. 2001. Asymmetrically distributed oligonucleotide repeats in the *Caenorhabditis elegans* genome sequence that map to regions important for meiotic chromosome segregation. *Nucleic Acids Res* **29**: 2920–2926.

Schvarzstein M, Pattabiraman D, Libuda DE, Ramadugu A, Tam A, Martinez-Perez E, Roelens B, Zawadzki KA, Yokoo R, Rosu S, et al. 2014. DNA helicase HIM-6/BLM both promotes MutSγ-dependent crossovers and antagonizes MutSγ-independent interhomolog associations during *Caenorhabditis elegans* meiosis. *Genetics* **198**: 193–207.

Schwacha A, Kleckner N. 1995. Identification of double Holliday junctions as intermediates in meiotic recombination. *Cell* **83**: 783–791.

Schwacha A, Kleckner N. 1994. Identification of joint molecules that form frequently between homologs but rarely between sister chromatids during yeast meiosis. *Cell* **76**: 51–63.

Sen D, Gilbert W. 1988. Formation of parallel four-stranded complexes by guanine-rich motifs in DNA and its implications for meiosis. *Nature* **334**: 364–366.

Severson AF, Ling L, van Zuylen V, Meyer BJ. 2009. The axial element protein HTP-3 promotes cohesin loading and meiotic axis assembly in *C. elegans* to implement the meiotic program of chromosome segregation. *Genes Dev* **23**: 1763 –1778.

Skibbens RV. 2004. Chl1p, a DNA helicase-like protein in budding yeast, functions in sister-chromatid cohesion. *Genetics* **166**: 33–42.

Smolikov S, Eizinger A, Hurlburt A, Rogers E, Villeneuve AM, Colaiácovo MP. 2007a. Synapsis-defective mutants reveal a correlation between chromosome conformation and the mode of double-strand break repair during *Caenorhabditis elegans* meiosis. *Genetics* **176**: 2027–2033.

Smolikov S, Eizinger A, Schild-Prufert K, Hurlburt A, McDonald K, Engebrecht J, Villeneuve AM, Colaiácovo MP. 2007b. SYP-3 restricts synaptonemal complex assembly to bridge paired chromosome axes during meiosis in *Caenorhabditis elegans*. *Genetics* **176**: 2015–2025.

Smolikov S, Schild-Prüfert K, Colaiácovo MP. 2008. CRA-1 uncovers a double-strand break-dependent pathway promoting the assembly of central region proteins on chromosome axes during *C. elegans* meiosis. *PLoS Genet* **4**: e1000088.

Solignac M, Mougel F, Vautrin D, Monnerot M, Cornuet J-M. 2007. A third-generation microsatellite-based linkage map of the honey bee, *Apis mellifera*, and its comparison with the sequence-based physical map. *Genome Biol* **8**: R66.

Sommermeyer V, Béneut C, Chaplais E, Serrentino ME, Borde V. 2013. Spp1, a member of the Set1 Complex, promotes meiotic DSB formation in promoters by tethering histone H3K4 methylation sites to chromosome axes. *Mol Cell* **49**: 43–54.

Sonnhammer ELL, Hollich V. 2005. Scoredist: a simple and robust protein sequence distance estimator. *BMC Bioinformatics* **6**: 108.

Stergiou L, Eberhard R, Doukoumetzidis K, Hengartner MO. 2011. NER and HR pathways act sequentially to promote UV-C-induced germ cell apoptosis in *Caenorhabditis elegans*. *Cell Death Differ* **18**: 897–906.

Sturtevant AH. 1913a. A third group of linked genes in *Drosophila ampelophila*. *Science* **37**: 990–992.

Sturtevant AH. 1913b. The linear arrangement of six sex-linked factors in *Drosophila*, as shown by their mode of association. *J Exp Zool* **14**: 43–59.

Sulston JE, Horvitz HR. 1977. Post-embryonic cell lineages of the nematode, *Caenorhabditis elegans*. *Dev Biol* **56**: 110–156.

Sulston JE, Schierenberg E, White JG, Thomson JN. 1983. The embryonic cell lineage of the nematode *Caenorhabditis elegans*. *Dev Biol* **100**: 64–119.

Sun H, Treco D, Schultes NP, Szostak JW. 1989. Double-strand breaks at an initiation site for meiotic gene conversion. *Nature* **338**: 87–90.

Surzycki SA, Belknap WR. 2000. Repetitive-DNA elements are similarly distributed on *Caenorhabditis elegans* autosomes. *Proc Natl Acad Sci U S A* **97**: 245–249.

Suzek BE, Huang H, McGarvey P, Mazumder R, Wu CH. 2007. UniRef: comprehensive and non-redundant UniProt reference clusters. *Bioinforma Oxf Engl* **23**: 1282–1288.

Swanson WJ, Vacquier VD. 2002. The rapid evolution of reproductive proteins. *Nat Rev Genet* **3**: 137–144.

Szostak JW, Orr-Weaver TL, Rothstein RJ, Stahl FW. 1983. The double-strand-break repair model for recombination. *Cell* **33**: 25–35.

Tamura K, Peterson D, Peterson N, Stecher G, Nei M, Kumar S. 2011. MEGA5: molecular evolutionary genetics analysis using maximum likelihood, evolutionary distance, and maximum parsimony methods. *Mol Biol Evol* **28**: 2731–2739.

Uringa E-J, Youds JL, Lisaingo K, Lansdorp PM, Boulton SJ. 2011. RTEL1: an essential helicase for telomere maintenance and the regulation of homologous recombination. *Nucleic Acids Res* **39**: 1647–1655.

Van der Lelij P, Chrzanowska KH, Godthelp BC, Rooimans MA, Oostra AB, Stumm M, Zdzienicka MZ, Joenje H, de Winter JP. 2010. Warsaw breakage syndrome, a cohesinopathy associated with mutations in the XPD helicase family member *DDX11/ChlR1*. *Am J Hum Genet* **86**: 262–266.

Van Kregten M, Tijsterman M. 2014. The repair of G-quadruplex-induced DNA damage. *Exp Cell Res* **329**: 178–183.

Van Schendel R, Roerink SF, Portegijs V, van den Heuvel S, Tijsterman M. 2015. Polymerase Θ is a key driver of genome evolution and of CRISPR/Cas9-mediated mutagenesis. *Nat Commun* **6**: 7394.

Villeneuve AM. 1994. A *cis*-acting locus that promotes crossing over between X chromosomes in *Caenorhabditis elegans*. *Genetics* **136**: 887–902.

Wagner CR, Kuervers L, Baillie DL, Yanowitz JL. 2010. *xnd-1* regulates the global recombination landscape in *Caenorhabditis elegans*. *Nature* **467**: 839–843.

Wan L, Niu H, Futcher B, Zhang C, Shokat KM, Boulton SJ, Hollingsworth NM. 2008. Cdc28-Clb5 (CDK-S) and Cdc7-Dbf4 (DDK) collaborate to initiate meiotic recombination in yeast. *Genes Dev* **22**: 386–397.

Ward JD. 2015. Rapid and precise engineering of the *Caenorhabditis elegans* genome with lethal mutation co-conversion and inactivation of NHEJ repair. *Genetics* **199**: 363–377.

Ward JD, Barber LJ, Petalcorin MI, Yanowitz J, Boulton SJ. 2007. Replication blocking lesions present a unique substrate for homologous recombination. *EMBO J* **26**: 3384–3396.

Watson JD, Crick FH. 1953. Molecular structure of nucleic acids; a structure for deoxyribose nucleic acid. *Nature* **171**: 737–738.

Wicks SR, Yeh RT, Gish WR, Waterston RH, Plasterk RH. 2001. Rapid gene mapping in *Caenorhabditis elegans* using a high density polymorphism map. *Nat Genet* **28**: 160–164.

Wu Y, Shin-ya K, Brosh RM Jr. 2008. FANCJ helicase defective in Fanconia anemia and breast cancer unwinds G-quadruplex DNA to defend genomic stability. *Mol Cell Biol* **28**: 4116–4128.

Xu H, Boone C, Brown GW. 2007. Genetic dissection of parallel sister-chromatid cohesion pathways. *Genetics* **176**: 1417–1429.

Yokoo R, Zawadzki KA, Nabeshima K, Drake M, Arur S, Villeneuve AM. 2012. COSA-1 reveals robust homeostasis and separable licensing and reinforcement steps governing meiotic crossovers. *Cell* **149**: 75–87.

Youds JL, Barber LJ, Ward JD, Collis SJ, O'Neil NJ, Boulton SJ, Rose AM. 2008. DOG-1 is the *Caenorhabditis elegans* BRIP1/FANCJ homologue and functions in interstrand cross-link repair. *Mol Cell Biol* **28**: 1470–1479.

Youds JL, Mets DG, McIlwraith MJ, Martin JS, Ward JD, ONeil NJ, Rose AM, West SC, Meyer BJ, Boulton SJ. 2010. RTEL-1 enforces meiotic crossover interference and homeostasis. *Science* **327**: 1254–1258.

Youds JL, O'Neil NJ, Rose AM. 2006. Homologous recombination is required for genome stability in the absence of DOG-1 in *Caenorhabditis elegans*. *Genetics* **173**: 697–708.

Young JA, Schreckhise RW, Steiner WW, Smith GR. 2002. Meiotic recombination remote from prominent DNA break sites in *S. pombe*. *Mol Cell* **9**: 253–263.

Yu A, Zhao C, Fan Y, Jang W, Mungall AJ, Deloukas P, Olsen A, Doggett NA, Ghebranious N, Broman KW, et al. 2001. Comparison of human genetic and sequence-based physical maps. *Nature* **409**: 951–953.

Zalevsky J, MacQueen AJ, Duffy JB, Kemphues KJ, Villeneuve AM. 1999. Crossing over during *Caenorhabditis elegans* meiosis requires a conserved MutS-based pathway that is partially dispensable in budding yeast. *Genetics* **153**: 1271–1283.

Zetka MC, Kawasaki I, Strome S, Müller F. 1999. Synapsis and chiasma formation in *Caenorhabditis elegans* require HIM-3, a meiotic chromosome core component that functions in chromosome segregation. *Genes Dev* **13**: 2258–2270.

Zetka MC, Rose AM. 1995. Mutant *rec-1* eliminates the meiotic pattern of crossing over in *Caenorhabditis elegans*. *Genetics* **141**: 1339–1349.

Zhao P, Zhang Z, Ke H, Yue Y, Xue D. 2014. Oligonucleotide-based targeted gene editing in *C. elegans* via the CRISPR/Cas9 system. *Cell Res* **24**: 247–250.

Zhao Y, Tarailo-Graovac M, O'Neil NJ, Rose AM. 2008. Spectrum of mutational events in the absence of DOG-1/FANCJ in *Caenorhabditis elegans*. *DNA Repair* **7**: 1846–1854.

Appendices

Appendix A

List of additional *C. elegans* strains used in this work

Strain name	Genotype	Description	Context
VC2010	+, Bristol	Bristol N2 wild type sub-culture kept at the Moerman Gene Knockout Lab at the University of British Columbia.	Ch. 2-4
KR4676	*chl-1(tm2188)/eT1* III; *+/eT1* V	*chl-1(tm2188),* which confers a recessive sterile and uncoordinated phenotype, balanced by translocation *eT1*	Ch. 2
KR4677	*chl-1(tm2188)/eT1* III; *+/eT1* V; *oxIs12* X	D-neuron GFP marker (*oxIs12*) in a *chl-1* genetic background	Ch. 2
KR4681	*dog-1(gk10)* I*; chl-1(tm2188)/eT1* III; *+/eT1* V	*dog-1 chl-1* double mutant	Ch. 2
KR5345	*+/hT2* I*; chl-1(h2877)/hT2* III	The *h2877* rearrangement allele of *chl-1* generated by CRISPR-Cas9 treatment	Ch. 3
CB4865	+, Hawaiian	Hawaiian wild type sub-culture archived at the Caenorhabditis Genetics Center.	Ch. 4
BC313	*rec-1(s180)* I	*rec-1(s180)* mutation (Q29 > STOP)	Ch. 4
KR5301	*rec-1(h2872)* I	*rec-1(h2875)* mutation, a 1-bp deletion in exon 2. Not outcrossed after CRISPR-Cas9 mutagenesis.	Ch. 4
KR5305	*rec-1(h2875)* I	*rec-1(h2875)* mutation, a 64-bp deletion in exon 2. 6 × outcrossed to VC2010 after CRISPR-Cas9 mutagenesis	Ch. 4
KR5306	*rec-1(h2875)* I, Hawaiian	*rec-1(h2875)* mutation, a 64-bp deletion in exon 2. 6 × outcrossed to CB4865 after CRISPR-Cas9 mutagenesis	Ch. 4
EG6699	*ttTi5605* II; *unc-119(ed3)* III; *oxEx1578*	*Mos*I insertion on Chromosome II (*ttTi5605*) with the *unc-119* mutation balanced by *oxEx1578*. Unc-119 segregants used for *Mos*SCI experiments	Ch. 4
DW687	*dwSi4[rec-1(+) Cbr-unc-119(+)]* II; *unc-119(ed3)* III	Wild type *rec-1*, with its endogenous promoter and 3' region, inserted at the *ttTi5605* site.	Ch. 4
KR5326	*rec-1(h2875)* I; *dwSi4[rec-1(+) Cbr-unc-119(+)]* II	Derived from KR5305 and DW687	Ch. 4
DW688	*dwSi5[rec-1(8S/T>E) Cbr-unc-119(+)]* II; *unc-*	*rec-1(8S/T>E),* with the *rec-1* endogenous promoter and 3' region, inserted at the	Ch. 4

	119(ed3) III	*ttTi5605* site.	
KR5327	*rec-1(h2875)* I; *dwSi5[rec-1(8S/T>E) Cbr-unc-119(+)]* II	Derived from KR5305 and DW688.	Ch. 4
DW690	*dwSi6[rec-1(8S/T>A) Cbr-unc-119(+)]* II; *unc-119(ed3)* III	*rec-1(8S/T>A),* with the *rec-1* endogenous promoter and 3' region, inserted at the *ttTi5605* site.	Ch. 4
KR5328	*rec-1(h2875)* I; *dwSi6[rec-1(8S/T>A) Cbr-unc-119(+)]* II	Derived from KR5305 and DW690	Ch. 4
CB4088	*him-5(e1490)* V	*him-5(e1490)* mutation	Ch. 4
RB1562	*him-5(ok1896)* V	*him-5(ok1896)* mutation	Ch. 4
QP833	*rec-1(s180)* I; *him-5(ok1896)* V	Derived from BC313 and RB1562	Ch. 4
QP856	*rec-1(h2875)* I; *him-5(ok1896)* V	Derived from KR5305 and RB1562	Ch. 4
QP857	*rec-1(h2875)* I; *him-5(e1490)* V	Derived from KR5305 and CB4088	Ch. 4
QP962	*rec-1(s180)* I; *him-5(e1490)* V	Derived from BC313 and CB4088	Ch. 4

Appendix B

List of primers used in this work

Primer name	Sequence	Use	Context
chl1-R	TAACCCTCGCACTGCGTCTA	Genotyping *tm2188* and WT *chl-1*	Ch. 2
chl1-i	GAATTGACGTGGCCAACG	Genotyping *tm2188* and WT *chl-1*	Ch. 2
chl1-F	CCTTCATCCGTTCCCTCAAC	Genotyping *tm2188* and WT *chl-1*	Ch. 2
gsp4	AAGAAGCGGAGCCTGAGC	Amplifying cDNA of *chl-1*	Ch. 2
gsp5	CTTGACTTGAGTGCGATCTCC	Amplifying cDNA of *chl-1*	Ch. 2
C1+	GAATGCATCGCGCGCACCGTACGTCTCG AGACTTGTTGCTTGGAATCTTCTGAAAA TTCG	Generation of HA-tagged *chl-1* template	Ch. 3
C2-	AGCGTAATCTGGAACATCGTATGGGTAC ATTCTGCTGGGATAGAGTGAGAGATCAT TTAT	Generation of HA-tagged *chl-1* template	Ch. 3
C3	ATGTACCCATACGATGTTCCAGATTACG CTATGGACGAATTCTCATTTCCATTTCA ACC	Generation of HA-tagged *chl-1* template	Ch. 3
C6-	GCCCGGGCTACGTAATACGACTCACTTA AGCCGCGTGTATGTCAAGCAAAAAAGA AGAGC	Generation of HA-tagged *chl-1* template	Ch. 3
chl-5'-sgRNA+	GAGAATTCGTCCATTCTGCTGTTTTAGA GCTAGAAATAGCAAGTTAAAATAAGG	Construction of plasmid for production of sgRNA targeting *chl-1*	Ch. 3
chl-5'-sgRNA-	AGCAGAATGGACGAATTCTCAAACATTT AGATTTGCAATTCAATTATATAGGGACC	Construction of plasmid for production of sgRNA targeting *chl-1*	Ch. 3
AmpR1(+)	GGAAGCTAGAGTAAGTAGTTCGCCAG	Construction of plasmid for production of sgRNA targeting *chl-1*	Ch. 3
AmpR1(-)	CTGGCGAACTACTTACTCTAGCTTCC	Construction of plasmid for production of sgRNA targeting *chl-1*	Ch. 3
C1+(trunc)	ACTTGTTGCTTGGAATCTTCTGAAAATT CG	Genotyping for targeted insertion of HA at *chl-1*	Ch. 3
geno1	TTCTTGTCGAACGCTCATGC	Genotyping for targeted insertion of HA at *chl-1*	Ch. 3
geno2	GTCCATAGCGTAATCTGGAACATCGTAT GG	Genotyping for targeted insertion of HA at *chl-1*	Ch. 3
geno3	TCAGCCACATGTGAATTTCC		Ch. 3
chl-del-1	GTTTGCAATTTCCATGATGCAAACC	Determining breakpoints of *h2877*	Ch. 3
chl-del-2	TGATTTTTCTCGCGTTTTCCATGTC	Determining breakpoints of *h2877*	Ch. 3
chl-del-3	TGGTACGGTAGGTGGGTACG	Determining breakpoints of *h2877*	Ch. 3
chl-del-4	AACCGCTGGAACACAATAGCTC	Determining breakpoints of *h2877*	Ch. 3
chl-del-5	CGCCTTTTCTCAATTCTCTCCTCG	Determining breakpoints of *h2877*	Ch. 3
chl-del-6	TGCAGGAGAATGTCATCTGGAGAC	Determining breakpoints of *h2877*	Ch. 3
chl-del-7	GTTGGAACACCGACAGACGTC	Determining breakpoints of *h2877*	Ch. 3
chl-del-8	CATGAGCGTTCGACAAGAACAGG	Determining breakpoints of *h2877*	Ch. 3
chl-del-a	AAATTCGTTTAAAATTTTGCCTATTTTCC A	Determining breakpoints of *h2877*	Ch. 3
chl-del-b	AATAAACAAACACTGGCATTTAATTTGG	Determining breakpoints of *h2877*	Ch. 3
chl-del-c	AAAGTTCAAAACCAAATTAAATGCCAGT G	Determining breakpoints of *h2877*	Ch. 3
chl-del-d	ACAAGCGTCTCACAGTTTGGATG	Determining breakpoints of *h2877*	Ch. 3
chl-del-e	TTCTGGAAAAACCTTGAAATACGCA	Determining breakpoints of *h2877*	Ch. 3
chl-del-f	TTGCCCGTAAATCGACACAAGC	Determining breakpoints of *h2877*	Ch. 3

chl-del-g	TAGCGCTTGTGTCGATTTACGG	Determining breakpoints of *h2877*	Ch. 3
chl-del-h	ATTCAATTCCCCATGCTTTTCGTG	Determining breakpoints of *h2877*	Ch. 3
chl-del-i	AAGTTTTGCTTCATGATGGAACACG	Determining breakpoints of *h2877*	Ch. 3
chl-del-j	AGCTTGTAGTGAGCATTGTATTCTCG	Determining breakpoints of *h2877*	Ch. 3
seqFa	TGCCGTTATTACCCATACGC	Determining breakpoints of *h2877*	Ch. 3
seqFc	GAAAAACGAAAACGGACTGG	Determining breakpoints of *h2877*	Ch. 3
seqRc	ATTGAGAATGTGTTCGTGATGC	Determining breakpoints of *h2877*	Ch. 3
Y18 CRISPR seqFi	CGCCATGTGCCTTTAGTACC	Sequencing/genotyping after CRISPR-Cas9 at *y18h1a7*	Ch. 4
Y18 CRISPR seqFi	GCAGTTTCTGGTGATTTTCG	Sequencing/genotyping after CRISPR-Cas9 at *y18h1a7*	Ch. 4
IIIA-F	GCATAAACCGGCTAAAAATCG	Chrom III genotype site A* (use *Aat*II to digest Hawaiian allele)	Ch. 4
IIIA-R	TTGCAGGGTATATGACTTCTGG	Chrom III genotype site A* (use *Aat*II to digest Hawaiian allele)	Ch. 4
IIIB-F(new)	CATCATTTTCCACTTCTGAAACC	Chrom III genotype site B (use *Spe*I to digest Hawaiian allele)	Ch. 4
IIIB-F(new)	CTCCTCCGAGAAGCTCAAGG	Chrom III genotype site B (use *Spe*I to digest Hawaiian allele)	Ch. 4
IIIC-F(new)	AAATCTTGCTGTTCCTTGTCC	Chrom III genotype site C (use *Acc*I to digest Bristol allele)	Ch. 4
IIIC-F(new)	CACCTTAATCCCTTCAAAACG	Chrom III genotype site C (use *Acc*I to digest Bristol allele)	Ch. 4
IIID-F(new)	CACCAATGTTTTCCGCACAGC	Chrom III genotype site D (use *Dra*I to digest Hawaiian allele)	Ch. 4
IIID-F(new)	TTGATGATGCATTTGATTATTGG	Chrom III genotype site D (use *Dra*I to digest Hawaiian allele)	Ch. 4
IIIE*-F	TGGGAGAAAATCGAAAATCG	Chrom III genotype site E (use *Hind*III to digest Hawaiian allele)	Ch. 4
IIIE*-R	GCCTAAGCCTATGCCTATGCCTAAACCT AAGCCTAAGCCCGAGCTTTAGC	Chrom III genotype site E (use *Hind*III to digest Hawaiian allele)	Ch. 4